# Evaluation of the Effects of Climate Change on Hurricane-Induced Losses for Residential Buildings

By

MIRSARDAR ESMAEILI

DISSERTATION

Submitted in partial satisfaction of the requirements for the degree of

DOCTOR OF PHILOSOPHY

in

Civil and Environmental Engineering

in the

OFFICE OF GRADUATE STUDIES

of the

UNIVERSITY OF CALIFORNIA

DAVIS

Approved:

---

Michele Barbato, Chair

---

John Bolander

---

Sashi Kunnath

Committee in Charge

2022

# Abstract

Hurricanes are among the most destructive and costliest extreme weather events. The intensity of future hurricanes is generally expected to increase due to climate change effects. In this work, the potential effects of climate change on hurricanes and associated changes of the risks for residential buildings located on the coastal areas of the United States is investigated. A simulation method based on a comprehensive statistical analysis of historical data is developed to account for the changes in climatological conditions and their effects on the frequency and intensity of hurricanes. This method is applied to simulate the hurricane wind speed distributions under different climatological conditions in the US Atlantic Basin from Texas to Maine, which is one of the most vulnerable regions of the world to hurricane hazards. To this end, regression models for several different hurricane parameters are fit to the historical hurricane data. The proposed model is validated by comparing its predicted hurricane-induced wind speeds with available historical data and other existing models based on physics-based hurricane path simulation. This new model is found to reproduce very well historical wind speed distributions, and to provide wind speed projection results that are consistent with those of more computationally expensive models based on the simulation of hurricane tracks. The statistical characteristics of future potential hurricanes are simulated using the proposed model along with the climate projections presented in the 5th Assessment Report of the Intergovernmental Panel for Climate Change. The results of this study indicate that, by year 2060 and depending on the considered projection scenario, the design wind speeds along the US Gulf and Atlantic Coast corresponding to the different mean return intervals considered by ASCE 7 are expected to increase in average between 14% and 26%, which correspond to an average increase of the design wind-induced loads contained between 30% and 59%.

To account for the effects of climate change on hurricane risk for structures, an appropriate methodology is presented, which extends the performance-based hurricane engineering (PBHE) framework to account for the nonstationarity of both hazard, induced by climate change effects, and vulnerability, produced by structural aging. The newly developed general nonstationary PBHE framework is implemented

by performing a loss analysis on a benchmark low-rise single-family house over a 50-year design service life, for which climate change effects are accounted for by using the predictive model for the changes in the hurricane wind hazards, whereas structural aging is neglected. The effects of different modeling assumptions and solution approaches (including approximate estimates, time discretization, interpolation techniques, and models for annual discount rates), different locations, and different climate change scenarios on the means and standard deviations of the total losses are investigated. The performance comparison of different storm mitigation strategies is also performed as an application example. In general, the proposed methodology provides consistent results under different modeling assumptions; however, the modeling assumptions for the annual discount rates can affect the results significantly. Climate change effects are generally significant, with increases contained between 13.2% and 38.1% for the total loss means, and between 2.5% and 12.4% for the standard deviations of the total losses for the benchmark structure at the reference location of Pinellas Park, FL. The extended nonstationary PBHE framework is able to identify the optimal retrofit strategy in terms of costs and benefits for any given combination of structures, residential developments, locations, and climate scenarios. The proposed nonstationary PBHE framework represents an advancement in performance-based engineering, as it provides a rigorous approach to account for climate change effects and structural aging.

The extended PBHE methodology is also used to investigate the combined effects of structural aging and increase in the hurricane hazard level on the hurricane risk for wooden single-family houses. To this end, a time series for the climatological condition variables during the lifetime of the structure is simulated and is used along with decay models for wood, adhesive, and nails to investigate the effects of aging and how different limit states of components are being modified. The changes in hurricane-induced losses due to the separate and combined effects of climate change and structural aging are investigated for a single-family residential building located in Miami, FL. It is found that the combined effects of climate change and aging can increase the total expected losses for the structure to more than 108% compared to the case where no climate change or aging is considered during the lifetime of the structure.

The research presented in this dissertation represents an advancement not only in performance-based hurricane engineering, but generally in performance-based engineering, as it provides a rigorous framework that can be adapted to other single and multiple hazards to account for the effects (individually or simultaneously) of climate change and structural aging.

# Acknowledgement

First and foremost, I would like to thank my supervisor, Professor Michele Barbato, whose expertise was invaluable in formulating the research questions and methodology. His insightful feedback pushed me to sharpen my thinking and brought my work to a higher level. It would have been impossible to finish this dissertation without his care and dedication not only to my research, but also to me personally. It was an honor to have him as my advisor.

I am also grateful to my doctoral committee members, Prof. John Bolander, and Prof. Sashi Kunnath for their insightful knowledge, interest in my research work, and thoughtful comments. I would also like to thank Ms. Lauren Worrell for her kind support and consideration throughout my graduate life at the University of California, Davis.

I would also like to thank to my parents, Roya and Saeed, and my sister, Dordaneh, who supported me through this journey and gave me the opportunity to pursue my education to this level. Finally, I would like to thank my wife, Kahila, for her love, support, and understanding toward the completion of my research work.

# Table of Contents

Abstract ..... ii

Acknowledgement ..... v

Table of Contents ..... vi

List of Tables ..... ix

List of Figures ..... xi

Chapter 1. Introduction ..... 1

1.1. Objectives and Motivation ..... 2

1.2. Scope ..... 3

1.3. Organization of the dissertation ..... 3

1.4. Journal publications derived from this dissertation ..... 5

Chapter 2. A predictive model for hurricane wind hazard under changing climate conditions ..... 6

2.1. Introduction ..... 6

2.2. Research significance ..... 8

2.3. Modeling of IMs as functions of SST ..... 9

2.3.1. Hurricane frequency model ..... 10

2.3.2. Model for SST at time and location of hurricane ..... 12

2.3.3. Peak wind speed model ..... 13

2.3.4. Radius to maximum wind speed model ..... 13

2.3.5. Translational wind speed model ..... 14

2.4. Development of hurricane wind speed distributions for the US Gulf and Atlantic Coast as function of climatological conditions ..... 15

2.5. Validation of the proposed model with historical data ..... 23

2.6. Hurricane wind speed projections considering climate change: comparison with other existing models and design implications ..... 29

2.7. Conclusions ..... 32

Chapter 3. Performance-Based Hurricane Engineering under Changing Climate Conditions: General Framework and Performance of Single-Family Houses in the US ..... 34

3.1. Introduction ..... 34

3.2. Research Significance and Novelty ..... 36

3.3. Extended PBHE Framework: Methodology ..... 37

3.3.1. Simulation approach using Multi-layer Monte-Carlo simulation (MMCS) ..... 39

3.3.2. Loss analysis and cost-benefit analysis ..... 40

3.4. Extended PBHE Framework: Benchmark Structure and Sensitivity Analysis ..... 42

3.4.1. Loss analysis results for reference conditions ..... 44

3.4.2. Sensitivity of loss analysis results to time discretization and interpolation ..... 45

3.4.3. Sensitivity of loss analysis results to variability of discount rate ..... 48

3.4.4. Sensitivity of loss analysis results to different locations ..... 51

3.4.5. Sensitivity of loss analysis results to different climate change scenarios ..... 52

3.5. Application Example: Cost-Benefit Analysis of Different Storm Mitigation Strategies ..... 54

3.6. Conclusions ..... 58

Chapter 4. Hurricane performance assessment of single-family houses considering the combined effects of climate change and structural aging ..... 60

4.1. Introduction ..... 60

4.2. Novelty and Relevance ..... 65

4.3. Extended PBHE framework ..... 65

.4.4 Modeling of structural aging ..... 66

4.4.1. Strength degradation for asphalt shingles due to sealant aging ..... 67

4.4.2. rength degradation due to wood decay ..... 68

4.4.3. Strength degradation due to nail pull-out strength decay ..... 70

4.5. Multilayer Monte Carlo simulation procedure for aging structures ..... 72

4.6. Case study ..... 73

4.6.1. Results on the expected annual losses ..... 77

4.7. Conclusions ..... 79

Chapter 5. Research Summary and Conclusion ..... 80

5.1. Conclusions ..... 80

5.2. Future research work ..... 82

References ..... 83

Appendix: Simulation procedure for wood mass loss ..... 96

A.1. Simulation of temperature and relative humidity time series ..... 96

A.2. Development of the wood mass loss probability distribution as a function of time ..... 104

# List of Tables

Table 2-1. Location depedent parameters for mileposts at intervals of 185.2 km (100 nautical miles) along the US Gulf and Atlantic Coast: hurricane annual frequency, $\nu_{\mathrm{h}}$; radius of influence, $r_{\mathrm{inf}}$; location parameter, $\lambda$; scale parameter, $\kappa$; and shape parameter, $\xi$ ..... 11

Table 2-2. Regression parameters for mean and standard deviations of hurricane IMs for the US Gulf and Atlantic Coast..... 14

Table 2-3. Random variables and corresponding probability distributions used in the proposed sampling procedure..... 23

Table 2-4. Comparison of hurricane gradient wind speed (fastest 1-minute hurricane speed at 10 m above ground over open terrain) means and standard deviations at different mileposts estimated using NIST data and the proposed simulation procedure ..... 26

Table 2-5. Comparison of design wind speeds (base wind speeds corresponding to 3-second gust wind speeds at 10 m above ground over open terrain) from ASCE 7-16 and proposed simulation procedure along the US Gulf and Atlantic Coast ..... 28

Table 2-6. Projected increases in design wind speeds (basic wind speeds corresponding to 3-second gust wind speeds at 10 m above ground over open terrain) for year 2060 and scenario RCP 8.5 along the US Gulf and Atlantic Coast ..... 31

Table 3-1. Statistical description of limit state capacities for different components in the base structure. 44

Table 3-2. Sensitivity of loss analysis results to time discretization and interpolation scheme for reference conditions by using accurate equations and $d_t = 3\%$. ..... 48

Table 3-3. Sensitivity of loss analysis results to annual discount rate modeling for reference conditions by using accurate estimations and $\Delta t = 1$ year..... 50

Table 3-4. Sensitivity of total loss analysis results to climate change scenarios for the unretrofitted benchmark house in Pinellas Park, FL, with $d_t = 3\%$ and $\Delta t = 1$ year over the period of 2015-2065..... 54

Table 3-5. Statistics of different retrofit scenarios and their limit states ..... 55

Table 3-6. Cost-benefit analysis results for the benchmark structure located in Pinellas Park, FL, for RCP 8.5, with $d_t = 3\%$ and $\Delta t = 1$ year over the period of 2015-2065, assuming constant initial retrofit costs. ..... 56

Table 3-7. Effects of retrofit cost variability on cost-benefit analysis performed for retrofit scenario $r = 9$. ..... 57

Table 4-1. Limit states and corresponding structural aging effects considered in this study ..... 66

Table 4-2. Statistical description of limit state capacities for as-built structure ..... 74

Table 4-3. Mean and standard deviation of total losses under different assumptions ..... 78

Table A-1. Probability distributions for monthly temperature deviations (°C) for Pinellas Park, FL, based on historical data corresponding to the period 2000-2020 ..... 100

Table A-2. Probability distributions for daily temperature deviations (°C) for Pinellas Park, FL, based on historical data corresponding to the period 2000-2020 ..... 101

Table A-3. Probability distributions for hourly temperature deviations (°C) for Pinellas Park, FL, based on historical data corresponding to the period 2000-2020 ..... 102

Table A-4. Parameters describing the relationship between temperature and dew point temperature ..... 103

Table A-5. Wood mass loss probability distributions for Pinellas Park, FL, during the period 2015-2065 ..... 104

# List of Figures

Figure 2-1. US Gulf and Atlantic Coast hurricane-prone region: (a) yearly number of hurricanes in the 1851-2018 period as a function of $T_y$ , and (b) location of mileposts at intervals of 185.2 km (100 nautical miles) considered in this study ..... 11

Figure 2-2. Historical data for US Gulf and Atlantic Coast between 1988-2018 and linear regression lines for: (a) $T$ vs. $T_y$, (b) $V_{max}$ vs. $T$, (c) $R_{max}$ vs. $T$, and (d) $V_t$ vs. $T$ ..... 15

Figure 2-3. Flowchart of the proposed hurricane wind speed simulation methodology ..... 16

Figure 2-4. IPCC AR5 Projections for increases in average yearly sea surface temperature ..... 18

Figure 2-5. Description of Willoughby's hurricane profile model ..... 21

Figure 2-6. Comparison of statistics for hurricane wind speed (gradient wind speed corresponding to fastest 1-minute hurricane speeds at 10 meters above ground over open terrain) obtained from the NIST database and from the proposed simulation procedure along the US Gulf and Atlantic Coast: (a) means and (b) standard deviations ..... 24

Figure 2-7. Comparison of projected hurricane wind speeds (gradient wind speeds corresponding to 3-second gust wind speeds at 10 m above ground over open terrain) for year 2100 in Miami, FL, from proposed model, Cui and Caracoglia (2016), and Pant and Cha (2019) ..... 30

Figure 3-1. Multi-layer Monte Carlo Simulation (MCS) flowchart for extended PBHE framework accounting for hazard nonstationarity due to climate change. ..... 40

Figure 3-2. Plan view of the residential development with benchmark building identified by a red unfilled circular marker (map data © 2020 Google). ..... 43

Figure 3-3. Unfolded view of the benchmark building. ..... 43

Figure 3-4. Annual loss exceedance probability curves for reference conditions ..... 45

Figure 3-5. Comparison of sampled annual probabilities of exceedance for years 2035, 2040, and 2045, and interpolated annual probability of exceedance based on Eq. (3.9) for year 2040 corresponding to the benchmark structure at reference conditions with $d_t = 3\%$ and $\Delta t = 10$ years . ..... 47

Figure 3-6. Variability of annual discount rate: (a) historical annual discount rates for the United States during the period 1950-2020, and (b) fitting of different probability distributions to the historical data… 49

Figure 3-7. Loss analysis results for the unretrofitted benchmark house under RCP 8.5 with $d_t = 3\%$ and $\Delta t = 1$ year: (a) considered locations along the US Gulf and Atlantic coasts, and (b) means and standard deviations of the total losses. ..... 51

Figure 3-8. Sensitivity of loss analysis results to climate change scenarios for the unretrofitted benchmark house in Pinellas Park, FL: (a) expected annual losses and (b) standard deviation of annual losses..... 53

Figure 4-1. Benchmark building's location: (a) Pinellas Park, FL, and (b) plan view of the residential development with benchmark building identified by a red circle (map data © 2021 Google). ..... 73

Figure 4-2. Unfolded view of the benchmark building..... 73

Figure 4-3. Historical records and sample realization of time histories corresponding to year 2015 for: (a) temperature and (b) relative humidity (with insets providing a zoomed view for a three-day interval. ..... 75

Figure 4-4. The average percentage of wooden mass loss for future climatological conditions along with 95% confidence intervals ..... 76

Figure A-1. IPCC AR5 projections for increases in the average yearly temperature ..... 98

Figure A-2. Flowchart to generate the temperature time series. ..... 99

# Chapter 1. Introduction

Severe tropical storms often cause extensive social and financial losses all around the world. The US Gulf and Atlantic Coast regions are often struck by these extreme weather events, which are locally known as hurricanes (Huang et al. 2001). The increasing trend in the number of residents (Crossett et al. 2013) and centralization of the US energy production (Adams et al. 2004) increase the vulnerability of the region. Hurricane Katrina (2005) with $172.5 billion, Hurricane Harvey (2017) with $133.8 billion, and Hurricane Maria (2017) with $96.3 billion of estimated losses (in 2021 Consumer Price Index-adjusted dollars) are among the costliest hurricanes since weather-related billion dollar disaster have been recorded (National Hurricane Center 2020). The observed pattern of data from 1900-2005 shows that the hurricane-induced losses in the US Gulf Coast region are doubling every 10 years (Pielke et al. 2008). Scientists believe that the global warming phenomenon, commonly referred to as climate change, is highly correlated with the intensification of hurricane actions and, thus, very likely to increase the hurricane-induced losses for coastal communities (Bjarnadottir et al. 2014; Hallegatte 2007). This dissertation is a collection of published research works, where each chapter (from chapter 2 to chapter 4) represents a published, submitted, or in-preparation journal article. The general goal of this research work is to formulate and evaluate the effects of climate change on hurricane wind hazards and the induced losses of residential buildings located along the US Gulf and Atlantic coasts.

Many research studies have been devoted to modeling the intensification of hurricane actions due to climate change, mostly based on the projections for future climatological conditions by the Intergovernmental Panel on Climate Change (IPCC) (Stocker et al. 2013). A majority of these research works utilize complicated and computationally expensive models to simulate the full track path of a hurricane (Cui and Caracoglia 2016; Lee and Ellingwood 2017; Mudd et al. 2014; Pant et al. 2018; Pant and Cha 2019). The present study aims to achieve a balance between accuracy and computational cost within a performance-based engineering framework for practical applications.

## 1.1. Objectives and Motivation

The first objective for this work is to provide researchers and practicing engineers with a simple, yet accurate methodology to account for different climatological assumptions without the need to simulate the full track path of hurricanes that is being used traditionally in the literature (Cui and Caracoglia 2016; Lee and Ellingwood 2017; Mudd et al. 2014; Pant and Cha 2018, 2019), which is a computationally expensive and time-consuming process. The specific outcomes of this research are: (1) development of climate-dependent wind speed distributions at different locations along the US Gulf and Atlantic coasts, (2) quantification of climate change effects on hurricane wind hazard for coastal areas under different assumptions for climate change in the future years, and (3) provide engineers, designers, and decision makers with appropriate changes in the minimum design wind speeds for structures of different risk categories in future years.

Many recent studies have tried to develop methodologies to account for non-stationarities of hazards in evaluation of the risk for structure (Decò and Frangopol 2011; Liang and Lee 2012; Bisadi and Padgett 2015; Dong et al. 2016), but none of them have used a performance-based engineering approach. The second objective of this research is to extend the existing performance-based hurricane engineering framework to account for non-stationarity in both hazard levels, induced by climate change and structural vulnerability, induced by structural aging. In particular, this research's outcomes are: (1) quantification of total losses for a given structure under different assumptions of location, climate change, and discount rate; and (2) performance comparison of different mitigation techniques when considering the effects of climate change.

Finally, the third objective of this research is to model and quantify the individual and joint effects of climate change and structural aging on the performance of structures subject to hurricane hazard. This methodological development is applied to the loss analysis for low-rise single-family houses located in hurricane-prone regions. The sensitivity of the total losses for a given structure under different assumptions for aging, effect of climate change on aging process is also investigated.

## 1.2. Scope

The scope of this research work is limited to study the effects of climate change on hurricane wind-related hazards and does not account for the climate change effects on the other hurricane related hazards (i.e., rain and flood). The effects of climate change for hurricane hazards are also not considered for the locations far away from the coastal area. Although the extended performance-based methodology is general, the scope of the case-studies presented in this research is single-family residential buildings.

## 1.3. Organization of the dissertation

In chapter 2 of this dissertation, an efficient and robust statistical model for wind hazard in coastal areas is developed, which can account for the non-stationary climatological conditions produced by climate change by using a simple and efficient indirect statistics approach (Unnikrishnan and Barbato 2017), where the statistics of the different intensity measures for hurricane wind hazard are indirectly obtained from site-specific statistics of basic hurricane parameters. The model is evaluated by comparing the results with the historical data (ASCE 2016; NIST 2016). The source of the projections for future climatological conditions is the fifth assessment report (IPCC AR5), which is by the time of writing this dissertation, is the latest version of the projections. The influence of all climate change scenarios on the hurricane-wind speed is investigated and the changes in the mean hurricane wind speed and design wind speed for selected milepost along the US/Gulf Coast regions are reported.

The development of risk assessment methodologies for structures subject to hurricane hazard has been the subject of several studies (Huang et al. 2001; Stewart et al. 2003). Barbato et al. (2013) proposed a performance-based hurricane engineering (PBHE) framework based on the total probability theorem to evaluate the risk for structures. Most of the existing hurricane risk/loss assessment methodologies do not account for non-stationarity in the hurricane wind hazard caused by climate change (Sutter et al. 2009). As the hurricane wind hazards are increasing, the associated damage and losses are expected to increase (Bjarnadottir et al. 2011; Estrada et al. 2015; Cui and Caracoglia 2016). Several recent studies have tried to develop methodologies to account for non-stationarities of hazards (Decò and Frangopol 2011; Liang and

Lee 2012; Bisadi and Padgett 2015; Dong et al. 2016) but to the best of the author's knowledge, no performance-based engineering framework is available in the literature to account for structural aging and non-stationary hazards.

In chapter 3 of this dissertation, the proposed PBHE framework (Barbato et al. 2013) is extended to account for the non-stationarities in the hazard level due to the effects of climate change during the lifetime of the structure. The variability of the total expected losses for a target residential building based on the selection of different climate change scenarios, different locations, different storm mitigation scenarios, and different discount rates, and different repair costs, and different techniques for integrating over the lifetime of the structure is investigated.

In a more realistic scenario, not only the hurricane hazard level is affected by climate change actions, but also the integrity and strength of different structural components may deteriorate over time. The aging phenomenon is referred to as the irreversible changes in the mechanical, physical, and chemical properties of the material due to applied environmental stresses. Environmental and biological stresses may cause deterioration of the wooden components (Kránitz et al. 2016). Aging can also affect the non-wooden structural components like nails in the connections (Takanashi et al. 2017) or roof covers (Dixon et al. 2013a). Hence, the strength deterioration due to the aging of these materials is also needed to be taken into account to evaluate the hurricane-induced losses to the structure in a more realistic manner. The proposed extended version of the PBHE framework can capture the effects of aging by modifying the structural parameters.

In chapter 4, the objective is to consider the changes in the vulnerability of structural components due to aging along with the climate change-induced changes in hazard levels. In this chapter, aging models for structural components are derived from the literature. The time series of data for future years are generated based on different assumptions for climate change. The sensitivity of the results to different assumptions for different climate change scenarios and different assumptions for the extend of aging is investigated. In addition to that, the results are compared for two assumptions for aging, in which in the first case, the aging of the structural component is dependent on climate change, and in the second case, the aging is an independent phenomenon.

Finally, Chapter 5 provides a summary of the research performed, identifies the conclusions achieved in this study, and suggests some future research directions.

## 1.4. Journal publications derived from this dissertation

Journal article based on chapter 2 (published):

- Esmaeili, M.[1], and Barbato, M.[2] (2021). "Predictive model for hurricane wind hazard under changing climate conditions." *Natural Hazards Review*, 22(3), 04021011.

Journal article based on chapter 3 (submitted):

- Esmaeili, M., and Barbato, M. "Performance-Based Hurricane Engineering under Changing Climate Conditions: General Framework and Performance of Single-Family Houses in the US".

Journal article based on chapter 4 (in preparation):

- Esmaeili, M., and Barbato, M. "Hurricane performance assessment of single-family houses considering the combined effects of climate change and structural aging".

[1] Ph.D student, Department of Civil & Environmental Engineering, University of California, Davis, One Shields Avenue, 2209 Academic Surge, Davis, Califonia 95616, USA; Email: mesmaeili@ucdavis.edu

[2] Professor, Department of Civil & Environemental Engineering, University of California Davis, One Shields Avenue, 3149 Ghausi Hall, Davis, California 95616, USA; E-mail: mbarbato@ucdavis.edu

# Chapter 2. A predictive model for hurricane wind hazard under changing climate conditions

## 2.1. Introduction

Tropical cyclones are extreme weather events that often cause extensive social and economic losses worldwide (Huang et al. 2001). The US Gulf and Atlantic Coast regions are frequently struck by these natural events, which are locally referred to as hurricanes. The growing number of resident population (Crossett et al. 2013) and the concentration of US energy production (Adams et al. 2004) contribute to increasing the hurricane vulnerability of this region. This fact is reflected by the massive losses (normalized to 2017 US dollar) caused by recent hurricanes, e.g., $160 billion losses by Hurricane Katrina in 2005, $125 billion losses by Hurricane Harvey in 2017, and $50 billion losses by Hurricane Irma in 2017 (National Hurricane Center 2018). The observed trend based on 1900-2005 data indicates that hurricane losses in the US Gulf Coast region are doubling every 10 years (Pielke et al. 2008).

The phenomena commonly known as climate change are responsible for changes in the sea water level, sea water temperature, and intensity of extreme weather events, including hurricanes (Stocker et al. 2013). The current consensus among climate scientists is that climate change will very likely produce an intensification of future hurricanes, resulting in potential increases of hurricane-induced losses (Bjarnadottir et al. 2014; Elsner et al. 2011; Hallegatte 2007). By analyzing the data from high-resolution dynamic models, Knutson et al. (2010) concluded that the intensity of hurricanes will increase between 2-11% by 2100 due to global warming. Grinsted et al. (2013) observed that the most extreme weather events are very sensitive to changes in temperature and estimated that the frequency of Katrina-like events could double due to the global warming produced during the 20$^{th}$ century. Significant research has been devoted to modeling the intensification of hurricanes due to climate change (Bjarnadottir et al. 2011, 2014; Emanuel 2011; Knutson et al. 2007, 2013; Manuel et al. 2008), often based on the climate projection scenarios proposed by the Intergovernmental Panel on Climate Change (IPCC) (Stocker et al. 2013). Some studies

approached the problem of estimating future hurricane intensities and corresponding expected induced losses from a statistical point of view based on the abundant available data (Elsner et al. 2011; Jagger et al. 2001; Malmstadt et al. 2010). More recently, hurricane path simulation has been used to predict future hurricane damages to structures and infrastructure systems in a warmer climate. Mudd et al. (2014) developed a framework for assessing climate change effects on the US East Coast hurricane hazards by modeling hurricane paths and decay by combining the Georgiou's hurricane wind speed model (Georgiou et al. 1983), an empirical hurricane track model (Vickery et al. 2000), and a hurricane genesis model depending on the sea surface temperature (SST) changes predicted by different climate scenarios (Stocker et al. 2013). Considering the worst-case climate change scenario, they found that the design wind speeds given by ASCE 7-10 for the US Northeast region should be increased by up to 15m/s for structures of risk category I and II, and up to 30m/s for structures of risk category III and IV to ensure that structures designed today will achieve appropriate target safety and expected performance levels in year 2100 (Mudd et al. 2014). Cui and Caracoglia (2016) developed a framework for estimating lifetime costs of tall buildings subject to hurricane-induced damages under different climate change scenarios by means of a statistical hurricane track path model. Under the worst-case scenario, they estimated that the hurricane-induced losses on tall buildings could increase up to 30% from 2015 to 2115. Lee and Ellingwood (2017) developed a framework for risk assessment of infrastructures with long expected service periods accounting for the effects of climate change by adopting the model by Vickery et al. (2000). Pant and Cha (2018) developed a framework to account for the effects of climate change on hurricane wind-induced damage and losses for residential buildings in the Miami-Dade County, FL. They used Georgiou's model (Georgiou et al. 1983) in conjunction with a transition matrix to simulate the hurricane track, and developed relationships between average yearly SST and hurricane parameters used for hurricane genesis. They found that, for each 1°C increase, the 3-second averaged wind speed for 700 years return period is expected to increase by about 6.7-8.9 m/s for the county, and the accumulated hurricane-induced losses in 2016 to 2055 period are expected to increase by 1.4 to 1.7 times the expected losses predicted for the 2006 climatological conditions.

Climate change affects all hazards associated with hurricane events, i.e., wind, windborne debris, storm surge, and rain hazards (Barbato et al. 2013; Unnikrishnan and Barbato 2017). This investigation focuses

only on hurricane wind hazard. The objective is to develop an accurate and efficient statistical model for wind hazard in coastal areas, which can account for the non-stationary climatological conditions produced by climate change. A simulation procedure based on the indirect statistics approach is proposed in this study.

This study is organized as follows: (1) the vector of parameters necessary to describe the hurricane wind hazard, referred to as intensity measure (IM) vector, is identified and a statistical model is developed for its components as functions of climatological conditions, synthetically described by SST; (2) using a multi-layer Monte Carlo simulation approach and an existing hurricane wind profile model, a wind distribution simulation procedure for coastal sites and given SST is developed; (3) the model simulation capabilities are validated through a comparison with historical data from the National Institute of Standards and Technology (NIST 2016) and the design wind speeds from ASCE 7-16 (ASCE 2016); and (4) the results of the developed simulation approach are compared with those of other existing models based on simulation of hurricane tracks, i.e., the models developed by Cui and Caracoglia (2016) and Pant and Cha (2019), and the proposed models is used to develop hurricane wind speed distributions along the US Gulf and Atlantic Coast based on the climate scenarios presented in the IPCC 5$^{th}$ Assessment Report (AR5) (Stocker et al. 2013).

## 2.2. Research significance

This research proposes a predictive simulation approach to quantify the non-stationary effects of climate change on hurricane wind speeds along the US Gulf and Atlantic Coast. This simulation procedure innovatively uses a simple and efficient indirect statistics approach (Unnikrishnan and Barbato 2017), in which the statistics of the different IMs are indirectly obtained from site-specific statistics of fundamental hurricane parameters. The major contribution of this method is the lower computational cost when compared to full track approaches existing in the literature (Cui and Caracoglia 2016; Lee and Ellingwood 2017; Mudd et al. 2014; Pant and Cha 2018, 2019), which can allow researchers and practicing engineers to consider a significantly higher number of scenarios at only a fraction of the computational cost of a single

scenario for a full track approach. The proposed methodology is specialized in this investigation for the US Gulf and Atlantic Coast; however, it can be easily extended to other regions worldwide, by using appropriate statistical data from pertinent historical records.

## 2.3. Modeling of IMs as functions of SST

This study uses the SST at the location and time of a given hurricane, $T$, as the main indicator of climate change effects on hurricane properties. This selection is consistent with the high correlation between hurricane intensity and SST (Bjarnadottir et al. 2011; Elsner et al. 2012; Emanuel 2011, 1999; Vickery et al. 2000, 2009; Webster et al. 2005), explained by the increase in warm water evaporation that fuels hurricanes as SST increases. Consistently with an indirect statistics approach, the following subset of IM components were selected as the primary IMs affected by climate change: hurricane annual frequency, $\nu_{\mathrm{h}}$; peak hurricane wind speed (here defined as the maximum 1-minute average speed measured at 10 m height over open terrain), $V_{\max}$; radius to maximum wind speed, $R_{\max}$; and translational wind speed, $V_{\mathrm{t}}$. These IM components were selected because they are consistent with the hurricane radial wind profile model proposed by Willoughby et al. (2006) to describe the pressure gradient component, $V_{\mathrm{r}}(r)$, of the hurricane wind speed at a given distance, $r$, from the hurricane eye.

All IMs except $\nu_{\mathrm{h}}$ are modeled as functions of $T$ to account for the non-stationary climatic conditions produced by climate change. In particular, means and standard deviations are defined by a linear regression model, the parameters of which are based on historical data, as follows:

$$\mu_p(T) = a_{p0} + a_{p1} \cdot T \tag{2.1}$$

$$\sigma_p(T) = b_{p0} + b_{p1} \cdot T \tag{2.2}$$

in which $p = V_{\max}, R_{\max}, V_{\mathrm{t}}$. For each IM, a modified Kolmogorov-Smirnov statistical test (Soong 2004) was used to identify an appropriate probability distribution. Note that this approach is different from that adopted in Pant and Cha (2018), in which the linear regression models of the hurricane parameters were developed as function of the average yearly SST, $T_y$.

### 2.3.1. Hurricane frequency model

Existing literature indicates a significant level of disagreement among different researchers regarding the variation in hurricane frequency and the development of an appropriate hurricane frequency model under changing climate conditions (Lombardo and Ayyub 2015). In this work, climate change-induced modifications of the hurricane annual frequency were investigated by analyzing the yearly number of hurricanes in the US Gulf and Atlantic Coast during the 1851-2018 period as a function of the yearly global $T_y$, which is plotted in Figure 2-1(a) based on the hurricane records in the HURDAT2 database (Landsea et al. 2015). The slope of the linear regression model used to fit the historical data is almost equal to zero, i.e., the annual frequency for Atlantic hurricanes is independent of $T_y$ (p-value = 0.95). The same methodology was followed to investigate the climate change effects on the hurricane annual frequency at different marine mileposts at intervals of 185.2 km (100 nautical miles) along the US Gulf and Atlantic Coast regions (shown in Figure 2-1(b)), based on the hurricane annual frequencies given in the NIST database (NIST 2016). For all considered mileposts, the slope of the linear regression was found to be statistically equal to zero, with p-values ranging between 0.74 and 0.86. Based on the existing literature, two distributions were considered to model the hurricane annual occurrences: the Poisson distribution (Batts et al. 1980, Mudd et al. 2014) and the negative binomial distribution (Cui and Caracoglia 2016, Jagger and Elsner 2012, Oxenyuk et al. 2017, Vickery et al. 2000). A chi-squared goodness-of-fit test (Soong 2004) failed to reject the null hypothesis at a 5% significance level in 24 out of 27 locations for the Poisson distribution (i.e., the fitting of the available data with a Poisson distribution was acceptable for 24 out of 27 locations), and in 10 out of 27 locations for the negative binomial distribution (i.e., the fitting of the available data with a negative binomial distribution was acceptable for 10 out of 27 locations). It was also observed that, for the 17 locations where the negative binomial distribution was rejected, the sample mean of the number of hurricane annual occurrences was higher than the corresponding sample variance, confirming that the use of a negative binomial distribution was not appropriate for those locations.

Based on these results, the yearly number of hurricanes affecting a given location is modeled as a Poisson random variable with constant (i.e., not dependent on $T_y$) annual frequency, $\nu_{\mathrm{h}}$, equal at each

location to the annual hurricane frequency given in the NIST database (NIST 2016). The values of $\nu_h$ corresponding to the considered mileposts along the US Gulf and Atlantic Coast are given in Table 2-1.

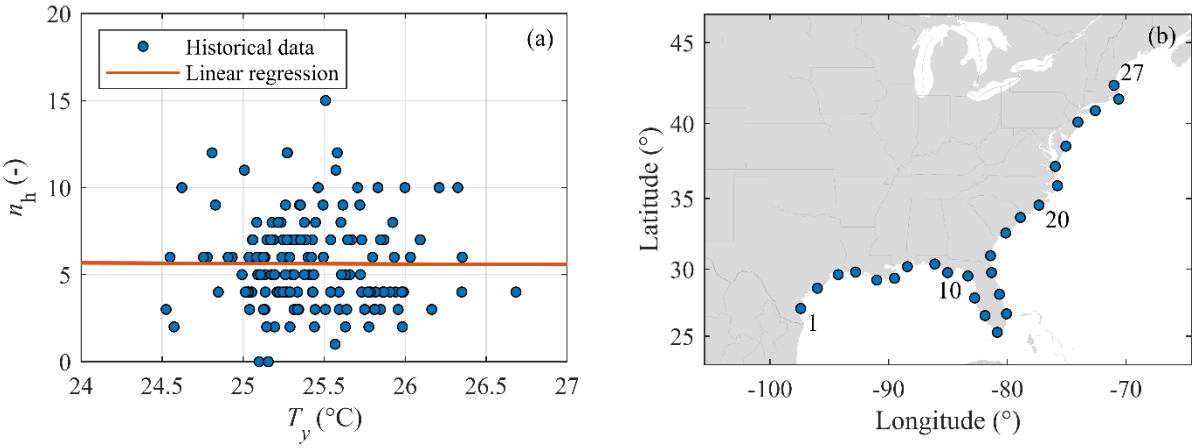


Figure 2-1. US Gulf and Atlantic Coast hurricane-prone region: (a) yearly number of hurricanes in the 1851-2018 period as a function of $T_y$, and (b) location of mileposts at intervals of 185.2 km (100 nautical miles) considered in this study

Table 2-1. Location depedent parameters for mileposts at intervals of 185.2 km (100 nautical miles) along the US Gulf and Atlantic Coast: hurricane annual frequency, $\nu_h$; radius of influence, $r_{inf}$; location parameter, $\lambda$; scale parameter, $\kappa$; and shape parameter, $\xi$

| Milepost # | $\nu_h$ (-) | $r_{inf}$ (km) | $\lambda$ (km) | $\kappa$ (km) | $\xi$ (-) |
|---|---|---|---|---|---|
| 1 | 0.37 | 275 | 215 | 39.96 | -0.71 |
| 2 | 0.44 | 285 | 208 | 41.74 | -0.10 |
| 3 | 0.48 | 270 | 212 | 39.13 | -0.75 |
| 4 | 0.51 | 295 | 223 | 43.66 | -0.36 |
| 5 | 0.50 | 290 | 225 | 42.67 | -0.60 |
| 6 | 0.50 | 295 | 230 | 43.56 | -0.67 |
| 7 | 0.50 | 285 | 220 | 41.83 | -0.56 |
| 8 | 0.51 | 285 | 225 | 41.73 | -0.83 |
| 9 | 0.50 | 295 | 230 | 43.96 | -0.87 |
| 10 | 0.51 | 295 | 235 | 43.76 | -0.92 |

| | | | | | |
|---|---|---|---|---|---|
| 11 | 0.51 | 290 | 229 | 37.58 | -0.87 |
| 12 | 0.53 | 225 | 178 | 30.99 | -0.84 |
| 13 | 0.57 | 255 | 192 | 42.29 | -0.40 |
| 14 | 0.55 | 215 | 171 | 42.03 | -1.04 |
| 15 | 0.63 | 300 | 224 | 54.67 | -0.37 |
| 16 | 0.57 | 345 | 268 | 62.58 | -0.69 |
| 17 | 0.53 | 345 | 274 | 62.53 | -0.98 |
| 18 | 0.55 | 320 | 252 | 58.66 | -0.74 |
| 19 | 0.61 | 280 | 221 | 51.57 | -0.46 |
| 20 | 0.68 | 285 | 225 | 51.44 | -0.89 |
| 21 | 0.63 | 268 | 212 | 48.29 | -0.17 |
| 22 | 0.56 | 297 | 234 | 54.33 | -0.65 |
| 23 | 0.45 | 325 | 257 | 58.53 | -0.26 |
| 24 | 0.32 | 307 | 243 | 55.48 | -0.84 |
| 25 | 0.29 | 270 | 213 | 48.93 | -1.01 |
| 26 | 0.29 | 270 | 214 | 48.96 | -0.79 |
| 27 | 0.26 | 292 | 231 | 52.85 | -0.45 |

### 2.3.2. Model for SST at time and location of hurricane

This study proposes a model for the SST at the place and location of the hurricane, $T$, as a function of climatic conditions, which are synthetically represented by the average yearly SST, $T_y$. The SST $T$ is assumed to follow a probability distribution with mean and standard deviation described as linear functions of $T_y$. The linear regression models were developed using the National Oceanic and Atmospheric Administration (NOAA) datasets for $T$ and $T_y$ corresponding to years 1988-2018 (NOAA/OAR/ESRL-PSD 2015). The obtained relation for the mean SST, $\mu_T$, is plotted in Figure 2-2(a) with the historical data and is given by:

$$\mu_T\left(T_y\right) = a_{T0} + a_{T1} \cdot T_y \tag{2.3}$$

in which $a_{T0} = -27.38\ ^{\circ}\mathrm{C}$ and $a_{T1} = 2.19$. Eq. (2.3) is valid for $T_y \geq 24.0\ ^{\circ}\mathrm{C}$. The standard deviation was found to be almost independent of $T_y$, with the slope of the regression line statistically equal to zero (p-value = 0.33). Thus, the SST standard deviation is assumed constant and equal to $\sigma_T = 1.23\ ^{\circ}\mathrm{C}$. Based on the results of a modified Kolmogorov-Smirnov test (Soong 2004), a normal distribution with mean given by Eq. (2.3) and $\sigma_T = 1.23\ ^{\circ}\mathrm{C}$ is selected to describe $T$.

### 2.3.3. Peak wind speed model

A statistical model for $V_{\max}$ as a function of $T$ was developed based on the historical peak hurricane wind speeds collected from the HURDAT2 database (Landsea et al. 2015) and the maximum temperature at the time and location of the hurricane obtained from the NOAA database (NOAA/OAR/ESRL-PSD 2015) for hurricanes in the Atlantic Basin during the period 1988-2018. The historical data of $V_{\max}$ are plotted as a function of $T$ in Figure 2-2(b) together with the linear regression model used to describe $\mu_{V_{\max}}(T)$. The regression parameters for the mean and standard deviation of $V_{\max}$ according to Eqs. (2.1) and (2.2) (as well as the p-values of the slopes of the regressions) are given in Table 2-2 and are valid for $T \geq 24^{0}\mathrm{C}$. Based on the results of a two-sided Kolmogorov-Smirnov test (Soong 2004), the Weibull distribution provides the best fit to the collected data and is adopted here, consistently with other research works available in the literature (e.g., Li and Ellingwood 2006).

### 2.3.4. Radius to maximum wind speed model

The statistical model for $R_{\max}$ was developed using the same approach and the same data sources used for $V_{\max}$. The historical data of $R_{\max}$ are plotted as a function of $T$ in Figure 2-2(c) together with the linear regression model used to describe $\mu_{R_{\max}}(T)$. The regression parameters for the mean and standard deviation of $R_{\max}$ according to Eqs. (2.1) and (2.2) (as well as the p-values of the slopes of the regressions) are given in Table 2-2 and are valid for $T \geq 24^{0}\mathrm{C}$. Based on the results of a two-sided Kolmogorov-Smirnov test (Soong 2004), the truncated normal distribution with lower tail truncation $R_{\max} > 0$ provides the best fit to the collected data and is adopted here, consistently with other research works available in the literature (Bjarnadottir et al. 2011; Unnikrishnan and Barbato 2017). A weak but not negligible inverse correlation between $V_{\max}$ and $R_{\max}$ was also found, with a correlation coefficient $\rho_{V_{\max}R_{\max}} = -0.301$.

### 2.3.5. Translational wind speed model

The statistical model for $V_t$ was developed following a similar approach and the same data sources used for $V_{max}$ and $R_{max}$. Because the values of $V_t$ are not directly available in the HURDAT2 database (Landsea et al. 2015), they were calculated as the maximum values of the translational speed along each hurricane track by assuming a constant translational speed between subsequent recorded positions of the tropical cyclone center. Figure 2-2(d) shows the historical data for $V_t$ and the linear regression fit for the mean of $V_t$ as a function of $T$. The slopes of the linear regressions for mean and standard deviation of $V_t$ are not statistically different than zero (see Table 2-2); thus, both mean and standard deviation of $V_t$ are assumed to be independent of $T$. Based on the results of a two-sided Kolmogorov-Smirnov test (Soong 2004), a log-normal distribution with $\mu_{V_t} = 6.02$ m/s and $\sigma_{V_t} = 2.45$ m/s provides the best fit to the collected data and is adopted here. It is noteworthy that $V_t$ is a variable that is location-dependent, with hurricanes generally moving faster north along the Atlantic Coast region and moving slower inside the Gulf Coast region (Vickery and Twinsdale 1995; Vickery et al. 2000). However, a single random variable is used here to describe the hurricane translation wind speed over the entire US Gulf and Atlantic Coast region. In fact, this quantity has a small effect on the peak wind speeds, which represent the focus of this study. This modeling assumption is not appropriate when modeling other hazards such as storm surge and rainfall, which are strongly dependent on the translational wind speed of tropical cyclones. For these applications, it is recommended to use multiple location-dependent random variables to describe $V_t$.

Table 2-2. Regression parameters for mean and standard deviations of hurricane IMs for the US Gulf and Atlantic Coast

| $p$ | Unit | $a_{p0}$ | $a_{p1} \cdot °C$ | p-value | $b_{p0}$ | $b_{p1} \cdot °C$ | p-value |
|---|---|---|---|---|---|---|---|
| $V_{max}$ | m/s | -29.31 | 2.93 | 0.01 | -20.05 | 1.06 | < 0.01 |
| $R_{max}$ | km | 105.8 | -2.57 | 0.05 | 29.0 | -0.48 | < 0.01 |
| $V_t$ | m/s | 6.66 (6.02)* | -0.02 (0)* | 0.91 | -3.52 (2.45)* | 0.21 (0)* | 0.37 |

* values in parentheses are those used in the proposed sampling procedure

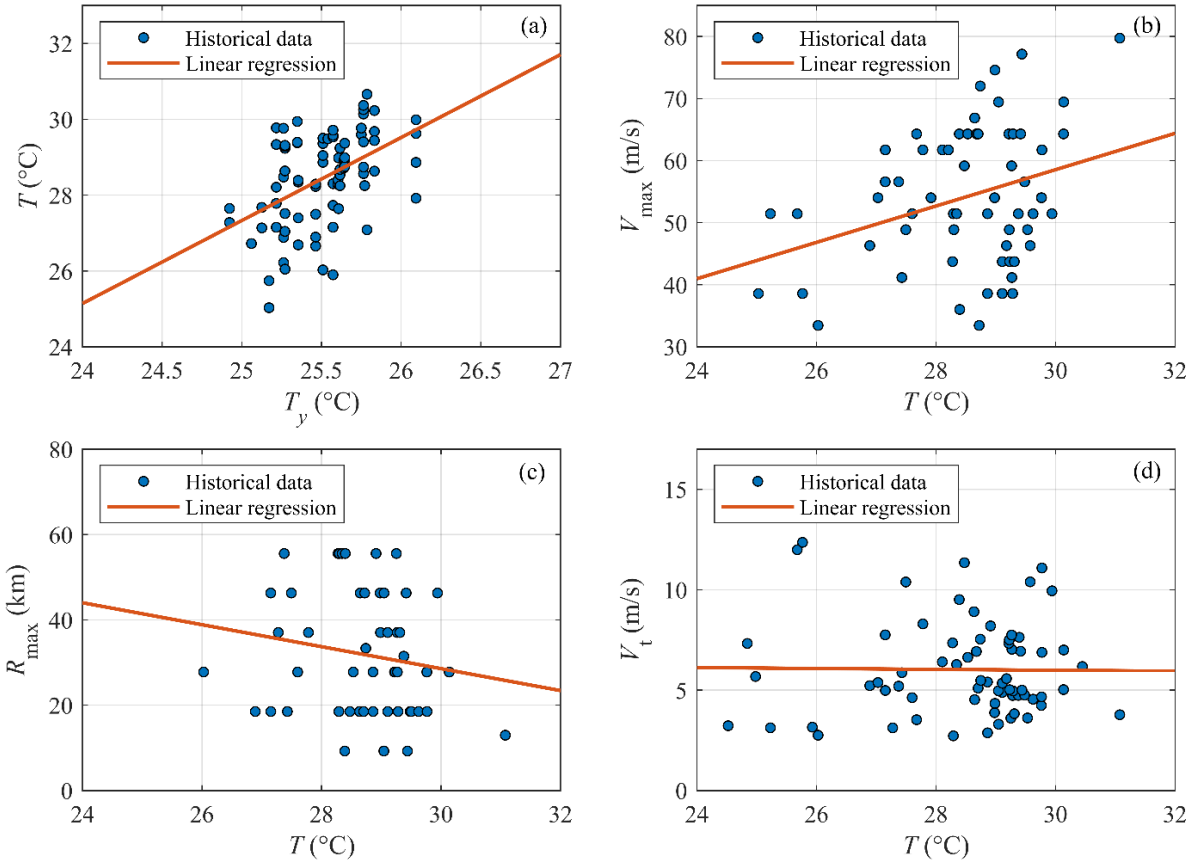


Figure 2-2. Historical data for US Gulf and Atlantic Coast between 1988-2018 and linear regression lines for: (a) $T$ vs. $T_y$, (b) $V_{max}$ vs. $T$, (c) $R_{max}$ vs. $T$, and (d) $V_t$ vs. $T$

## 2.4. Development of hurricane wind speed distributions for the US Gulf and Atlantic Coast as function of climatological conditions

A simulation approach based on a multi-layered Monte Carlo simulation (Barbato et al. 2013; Unnikrishnan and Barbato 2017) is proposed here to develop the hurricane wind speed distributions at different locations as functions of climatological conditions described by changes in the SST. A flowchart of the simulation algorithm is provided in Figure 2-3. The random parameters used in the sampling procedure and their probability distributions are described in Table 2-3.

- Select the site of interest by setting: latitude, longitude, $\nu_h$, and $r_{inf}$.
- Select the number of samples: $n_s$.
- Select the year of interest: $y$.
- For $i = 1 : n_s$
  - If $y \le 2005$:
    - Set $T_y^{(i)}$ equal to historical value corresponding to year $y$.
  - Else
    - Select projection scenario.
    - Sample $\Delta T_y^{(i)}$ from a normal distribution based on IPCC AR5 projections.
    - Calculate $T_y^{(i)}$ from Eq. (4).
  - End if.
  - Sample number of yearly hurricanes, $n_h^{(i)}$, from a Poisson distribution with event rate = $\nu_h$.
  - If $n_h^{(i)} = 0$:
    - Set: $V^{(i)} = 0$ m/s
  - Else
    - For $j = 1 : n_h^{(i)}$
      - Sample the hurricane eye location, i.e., bearing angle $\theta^{(i,j)}$, and distance $r^{(i,j)}$ using the distributions given in Table 3. If hurricane eye location is on land, resample until hurricane eye location is on water.
      - Calculate $\mu_T\left(T_y^{(i)}\right)$ from Eq. (3) and sample $T^{(i,j)}$.
      - Calculate $\mu_{V_{max}}\left(T^{(i,j)}\right)$ and $\mu_{R_{max}}\left(T^{(i,j)}\right)$ from Eq. (1), and $\sigma_{V_{max}}\left(T^{(i,j)}\right)$ and $\sigma_{R_{max}}\left(T^{(i,j)}\right)$ from Eq. (2). Set $\mu_{V_t} = 6.02$ m/s and $\sigma_{V_t} = 2.45$m/s.
      - Sample $V_{max}^{(i,j)}$, $R_{max}^{(i,j)}$, and $V_t^{(i,j)}$ from the distributions given in Table 3.
      - Sample $A^{(i,j)}$, $n^{(i,j)}$, and $X_1^{(i,j)}$ using a Nataf's model based on the probability distributions given in Table 3.
      - Calculate $V_r^{(i,j)}$ from Eq. (5).
      - Sample $\beta^{(i,j)}$ from the distribution given in Table 3 and calculate $\alpha^{(i,j)}$.
      - Calculate $V^{(i,j)}$ at the site from Eq. (6).
  - End if

End for

Figure 2-3. Flowchart of the proposed hurricane wind speed simulation methodology

The methodology is initialized by selecting the location (latitude and longitude) of the site of interest, the number of samples, $n_s$, and the year of interest, $y$. Once the locations is selected, the corresponding value of $\nu_h$ is obtained from the NIST database (NIST 2016). The sampling procedures is started by finding the average yearly SST, $T_y^{(i)}$, for sample *i*. If the simulation is done to validate historical data (in this study,

when $y \leq 2005$), $T_y^{(i)}$ is set deterministically equal to the measured average yearly SST for the year under consideration, e.g., by using data from NOAA's records (NOAA/OAR/ESRL-PSD 2015). If the simulation is performed to predict future wind speed distributions for a given scenario, the temperature increment $\Delta T_y^{(i)}$ is sampled based on the data reported in the IPCC AR5 (Stocker et al. 2013). These data correspond to the mean and the 90% confidence intervals for the predicted global annual SST changes during the 2010-2060 period with respect to 2005, which are reported in Figure 2-4. In particular, the filled markers represent the mean estimates, whereas the empty markers correspond to the lower and upper bounds of the 90% confidence intervals. This figure also shows the estimated global annual SST change for years 2010 and 2015 with respect to year 2005. The lower and upper bounds of the 90% confidence intervals for the measured $\Delta T_y$ in 2010 and 2015 are not visible at the scale used in Figure 2-4 and are equal to [0.25, 0.29] °C for 2010 and [0.38, 0.42] °C for 2015. The IPCC AR5 projections do not provide the probability distribution for the average yearly SST increase. In the present study, the average yearly SST change in any given year is assumed to follow a truncated normal distribution (with the lower bound equal to -1.73 °C) fitted to data corresponding to the different IPCC AR5 projections (Stocker et al. 2013). The *i*-th sample value of $T_y$ for the year and scenario of interest is finally obtained as:

$$T_y^{(i)} = T_{2005} + \Delta T_y^{(i)} \tag{2.4}$$

in which, $T_{2005} = 25.73\ ^{\circ}\text{C}$ is the average yearly SST for the reference year 2005 used by the IPCC AR5 projection scenarios. The lower bound of the $\Delta T_y$ distribution was selected so that $T_y \geq 24\ ^{\circ}\text{C}$, consistently with the validity range for Eq. (2.3).

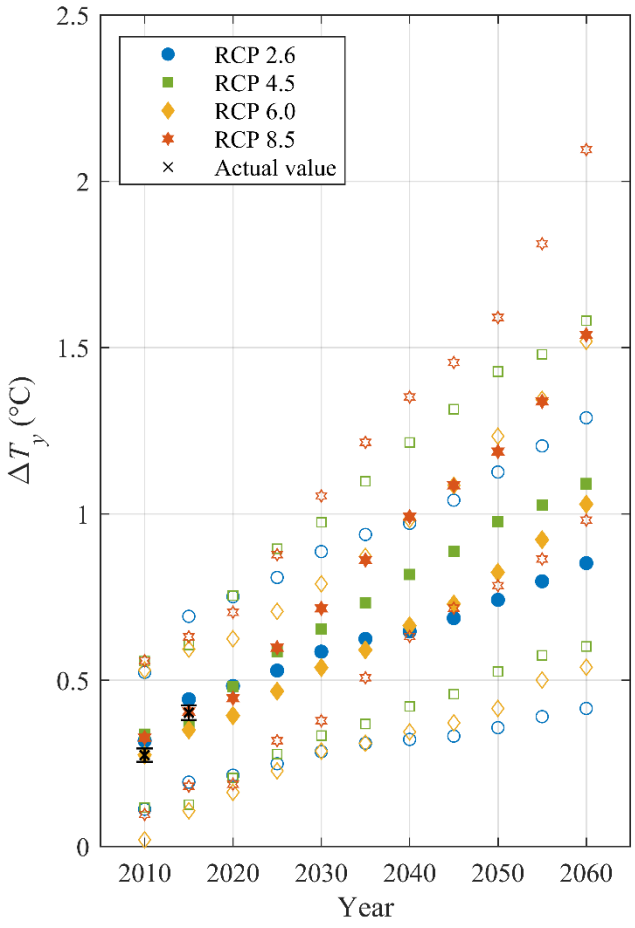


Figure 2-4. IPCC AR5 Projections for increases in average yearly sea surface temperature

The next step of the sampling procedure requires sampling the number of hurricanes in a year for the *i*-th sample, $n_{\mathrm{h}}^{(i)}$, from a Poisson distribution with an event rate equal to $\nu_{\mathrm{h}}$ for the location of interest. If $n_{\mathrm{h}}^{(i)} = 0$, the yearly maximum wind speed for the *i*-th sample is set equal to zero, i.e., $V^{(i)} = 0$ m/s. Otherwise, an inner loop is initiated to obtain the maximum wind speeds for each of the sampled hurricanes in a year corresponding to the *i*-th sample.

For the *j*-th hurricane of this inner loop (where $j = 1, 2, \ldots, n_{\mathrm{h}}^{(i)}$), the sampling procedure requires to sample the position of the hurricane eye closest to the location of interest, conditional to this position being on water. More specifically, a bearing angle, $\theta^{(i,j)}$, and a distance, $r^{(i,j)}$, are sampled from a uniform distribution and a truncated generalized extreme value distribution (tGEV) respectively, as described in

Table 2-3. The values of the parameters defining the tGEV distribution (i.e., radius of influence $r_{\text{inf}}$, location parameter $\lambda$, scale parameter $\kappa$, and shape parameter $\xi$) are given in for the different locations considered in this study (see Figure 2-1(b)). The values of $r_{\text{inf}}$ were calculated using historical hurricane tracks for mileposts along the US Gulf and Atlantic Coast at intervals of 185.2 km (100 nautical miles) by using the HURDAT2 database (Landsea et al. 2015) and considering all the hurricanes in the Atlantic basin during the period 1871-1963, i.e., the period for which the NIST database was developed (Batts et al. 1980). In particular, the values of $r_{\text{inf}}$ were obtained by rounding to the next 10 km the distance within which the hurricane frequency obtained from historical data coincides with the hurricane annual frequency provided by the NIST database, $\nu_{\text{h}}$. The values of the other parameters were obtained by fitting a tGEV distribution to the historical data from the HURDAT2 database (Landsea et al. 2015). Only hurricane location samples positioned on water are accepted by digitizing the map of the region and rejecting the location samples on land until the condition is satisfied. The procedure to identify the hurricane eye's position from the latitude and longitude of the site on interest and the sampled values of $r$ and $\theta$ is described in Todhunter (2006).

Once the hurricane eye's position is determined, the temperature $T^{(i,j)}$ at the time and location of the hurricane is sampled from a truncated normal distribution with lower limit equal to 24 °C, mean $\mu_T\left(T_y^{(i)}\right)$ obtained from Eq. (2.3), and standard deviation $\sigma_T = 1.23\ ^{\text{o}}\text{C}$. The probability distributions shown in Table 2-3 are used in combination with the Nataf's model (Liu and Der Kiureghian 1986) to sample the remaining IM components $V_{\text{max}}^{(i,j)}$, $R_{\text{max}}^{(i,j)}$, and $V_{\text{t}}^{(i,j)}$, with correlation coefficients $\rho_{R_{\text{max}},V_{\text{max}}} = -0.301$ and $\rho_{V_{\text{max}},V_{\text{t}}} = \rho_{R_{\text{max}},V_{\text{t}}} = 0$. The parameter values given in Table 2-2 are used in conjunction with Eq. (2.1) to determine $\mu_{V_{\text{max}}}\left(T^{(i,j)}\right)$ and $\mu_{R_{\text{max}}}\left(T^{(i,j)}\right)$, and with Eq. (2.2) to determine to determine $\sigma_{V_{\text{max}}}\left(T^{(i,j)}\right)$ and $\sigma_{R_{\text{max}}}\left(T^{(i,j)}\right)$.

The next step of the sampling procedure requires to calculate the pressure gradient component of the wind speed, $V_{\text{r}}^{(i,j)}$, which in this study is based on the Willoughby's model for dual-exponential hurricane

profile (Willoughby et al. 2006). This model is a piecewise continuous profile for the pressure gradient component of the hurricane wind speed defined as follows (Figure 2-5):

$$V_{\mathrm{r}}(r)=\begin{cases} V_1 = V_{\max}\cdot\left(\dfrac{r}{R_{\max}}\right)^n & 0\le r\le R_1 \\ V_1\cdot(1-w)+V_2\cdot w & R_1<r<R_2 \\ V_2 = V_{\max}\cdot\left[(1-A)\cdot e^{\left(-\frac{r-R_{\max}}{X_1}\right)}+A\cdot e^{\left(-\frac{r-R_{\max}}{X_2}\right)}\right] & r\ge R_2 \end{cases} \tag{2.5}$$

where *n* is the exponent controlling the wind speed increase inside the hurricane eye, $w$ denotes a weighting function described by a smooth 9th order polynomial that monotonically increases from zero to one in the transition zone defined by $R_1 \le R_{\max} \le R_2$, $X_1$ and $X_2$ denote the e-folding lengths, and *A* is a parameter determining the proportion of the two exponentials in the profile outside the transition zone. Based on Willoughby et al. (2006), $R_2 = R_1 + 10$ km, $X_2 = 25$ km, whereas $n$, $X_1$, and *A* are correlated random variables described by the probability distributions given in Table 2-3 with correlation coefficients $\rho_{X_1 n} = -0.143$, $\rho_{X_1 A} = 0.165$, and $\rho_{nA} = 0.391$. These distributions were obtained by fitting to the data provided for the dual-exponential model in Willoughby et al. (2006). Also in this case, the statistical sampling of the correlated random variables *n*, $X_1$, and *A* is performed using the Nataf's model (Liu and Der Kiureghian 1986). Parameter $R_1$ is a function of $n, A, X_1, X_2$, and $R_{\max}$ and is found by numerical inversion of the 9th order polynomial defining $w$ after calculating the value of $w$ corresponding to $V_{\max}$ (Willoughby et al. 2006).

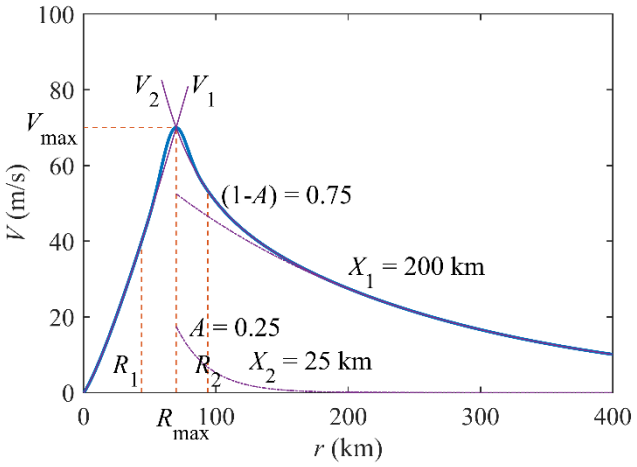


Figure 2-5. Description of Willoughby's hurricane profile model

Finally, the heading angle $\beta^{(i,j)}$ is sampled from a normal distribution with mean and standard deviation derived from historical data (Vickery et al. 2000). Using the Georgiou's model (Georgiou et al. 1983), the sampled pressure gradient and translational wind speeds, $V_{\mathrm{r}}^{(i,j)}$ and $V_{\mathrm{t}}^{(i,j)}$, are combined to obtain the maximum gradient wind speed at the site of interest, $V^{(i,j)}$:

$$V^{(i,j)} = \frac{1}{2}\cdot\left[V_{\mathrm{t}}^{(i,j)}\cdot\sin\left(\alpha^{(i,j)}\right) - f\cdot r^{(i,j)}\right] + \sqrt{\frac{1}{4}\cdot\left[V_{\mathrm{t}}^{(i,j)}\cdot\sin\left(\alpha^{(i,j)}\right) - f\cdot r^{(i,j)}\right]^2 + \left(V_{\mathrm{r}}^{(i,j)}\right)^2} \qquad (2.6)$$

in which $\alpha^{(i,j)}$ is the relative angle between the translational direction of the hurricane (defined by the heading angle $\beta^{(i,j)}$) and the direction defined by connecting the site of interest with the hurricane eye position, and $f$ is the Coriolis parameter.

The simulated hurricane wind speeds obtained using the proposed sampling procedure can then be post-processed depending on the statistics of interest. For example, if the statistics of interest is the annual peak wind speed distribution at the site, the experimental cumulative distribution function can be obtained by using only the yearly maxima, i.e., $V^{(i)} = \max_{1\le j\le n_{\mathrm{h}}^{(i)}}\left(V^{(i,j)}\right)$. It is also noted that the hurricane wind speed obtained from the proposed sampling procedure correspond to the fastest 1-minute hurricane speed at 10 m

above ground over open terrain, i.e., equivalent to Exposure Category C in ASCE 7-16 (ASCE 2016). The simulated hurricane wind speeds $V$ can then be converted to different gust averaging times, exposures, and elevations as follows:

$$V_{t,e,z} = c_t \cdot c_e \cdot c_z \cdot V \tag{2.7}$$

where $c_t$ = conversion factor for different wind time averages (ESDU 1993, ASCE 2016) with $c_t = 1$ for the fastest 1-minute hurricane speed, $c_e$ = conversion factor for different terrain exposure categories (ASCE 2016) with $c_e = 1$ over open terrain (Exposure Category C), and $c_z$ = conversion factor for different elevations $z$ above ground (ASCE 2016) with $c_z = 1$ at $z$ = 10 m above ground.

Table 2-3. Random variables and corresponding probability distributions used in the proposed sampling procedure

| Variable | Unit | Distribution | Distribution description | Range |
|---|---|---|---|---|
| $\Delta T_y$ | °C | Truncated Normal | Based on IPCC AR5 (Stocker et al. 2013) projections | $-1.73 \le \Delta T_y \le +\infty$ |
| $n_{\mathrm{h}}$ | - | Poisson | $\nu_{\mathrm{h}}$ at each location from NIST database (2016) | $n_{\mathrm{h}} \ge 0$ |
| $\theta$ | rad | Uniform | $\mu_\theta = \pi, \quad \sigma_\theta = \pi^2/3$ | $0 \le \theta \le 2\pi$ |
| $r$ | km | tGEV | Parameters $r_{\mathrm{inf}}, \lambda, \kappa, \xi$ at each location given in Table 2-1 | $0.0 \le r \le r_{\mathrm{inf}}$ |
| $T$ | °C | Truncated Normal | $\mu_T$ calculated from Eq. (2.3), $\sigma_T = 1.23\ ^{\circ}\mathrm{C}$ | $T \ge 24\ ^{\circ}\mathrm{C}$ |
| $V_{\max}$ | m/s | Translated Weibull | $\mu_{V_{\max}}$ calculated from Eq. (2.1), $\sigma_{V_{\max}}$ calculated from Eq. (2.2) | $V_{\max} \ge 33.4$ m/s |
| $R_{\max}$ | km | Truncated Normal | $\mu_{R_{\max}}$ calculated from Eq. (2.1), $\sigma_{R_{\max}}$ calculated from Eq. (2.2) | $R_{\max} \ge 0.0$ km |
| $V_{\mathrm{t}}$ | m/s | Lognormal | $\mu_{V_{\mathrm{t}}} = 6.02$ m/s , $\sigma_{V_{\mathrm{t}}} = 2.45$ m/s | $V_{\mathrm{t}} \ge 0.0$ m/s |
| $A$ | - | Mixed GEV | $0.61 + 0.39 \cdot \mathrm{tGEV}(\xi, \kappa, \lambda)$ $\xi = 0.1392, \quad \kappa = 0.1517, \quad \lambda = 0.2044$ | $0.0 \le A \le 1.0$ |
| $X_1$ | km | Weighted GEV | $0.82 \cdot \mathrm{tGEV}(\xi_1, \kappa_1, \lambda_1) + 0.18 \cdot \mathrm{tGEV}(\xi_2, \kappa_2, \lambda_2)$ $\xi_1 = -0.0023, \quad \kappa_1 = 65.40, \quad \lambda_1 = 210.55$ $\xi_2 = 0.6519, \quad \kappa_2 = 2.4885, \quad \lambda_2 = 452.41$ | $100 \le X_1 \le 500$ km |
| $n$ | - | Truncated Lognormal | $\mu_n = 0.8808, \quad \sigma_n = 0.4252$ | $0.0 \le n \le 2.5$ |
| $\beta$ | rad | Normal | From Vickery et al. (2000). | $0 \le \beta \le 2\pi$ |

## 2.5. Validation of the proposed model with historical data

The proposed simulation procedure for the hurricane wind speed at a given location along the US Gulf and Atlantic Coast is validated by comparing the statistics of the simulation results with two sets of historical data: hurricane wind speeds from the NIST database (NIST 2016), and design wind speeds from ASCE 7-16 (ASCE 2016). The first set of data from the NIST database (NIST 2016) is used to validate the means

and the standard deviations (i.e., the body region of the corresponding distribution) of historical hurricane wind speeds during the 1871-1963 period for the considered mileposts. The simulation procedure was performed using as $T_y$ the average value of the annual temperature for this period, i.e., $T_{1871\text{-}1963} = 25.41\,^{\circ}\text{C}$. The NIST data corresponds to fastest 1-minute hurricane speeds at 10 meters above ground over open terrain; thus, for this comparison, the coefficients in Eq. (2.7) assume the values $c_t = c_e = c_z = 1.0$. The results from the proposed simulation method are based on 1,000,000 samples and are compared with the means and standard deviations obtained from the 999 data points available at each location from the NIST database. These means and standard deviations are conditional to the occurrence of a hurricane event. Figure 2-6 (a) and (b) compare the means and standard deviations, respectively, obtained from the NIST data and the proposed model at each considered milepost from the coast of Texas to that of Maine. The 95% confidence intervals for the estimates of the means and standard deviations are also shown, even though those corresponding to the simulated data from the proposed simulation method are not visible at the scale presented in Figure 2-6.

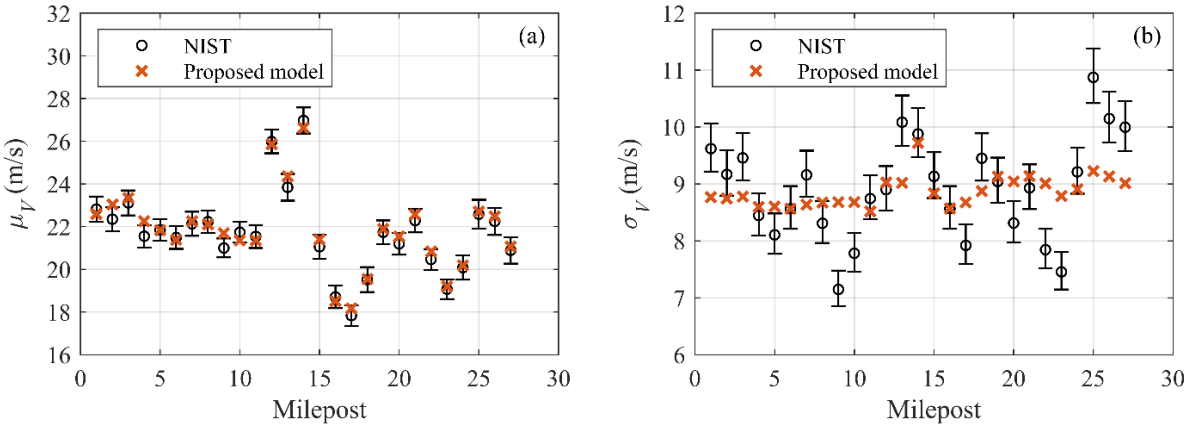


Figure 2-6. Comparison of statistics for hurricane wind speed (gradient wind speed corresponding to fastest 1-minute hurricane speeds at 10 meters above ground over open terrain) obtained from the NIST database and from the proposed simulation procedure along the US Gulf and Atlantic Coast: (a) means and (b) standard deviations

Table 2-4 reports the hurricane wind speed means and standard deviations estimated using the NIST data and the simulated data obtained from the proposed method, as well as the corresponding percent relative errors, for all the considered mileposts along the US Gulf and Atlantic Coast. The average relative difference between the simulated and NIST estimates of the hurricane wind speed means is +0.68%, with individual relative differences contained between $-1.79\%$ and $3.33\%$. The corresponding root mean square error (RMSE) and the modified root mean square error (mRMSE) (Peng et al. 2014; Rizzo et al. 2018) for the hurricane wind speed means are equal to $0.33\,\text{m/s}$ and $0.00\,\text{m/s}$, respectively. These results indicate that the proposed simulation procedure is able to reproduce very accurately historical data corresponding to hurricane wind speed means along the entire US Gulf and Atlantic Coast. In fact, the mRMSE value of zero indicates that the simulation estimates of the hurricane wind speed means is always contained within ± 2 standard errors from the NIST-based estimates of the means. The difference between the simulated and NIST estimates of the hurricane wind speed standard deviations is +0.07%, with individual relative errors contained between $-21.65\%$ and $21.58\%$. The corresponding RMSE and mRMSE are equal to $0.83\,\text{m/s}$ and $0.57\,\text{m/s}$, respectively. The proposed simulation procedure generates estimates of hurricane wind speed standard deviations that are globally representative of the US Gulf and Atlantic Coast; however, it can capture well the effects of geographical differences for the hurricane wind speed means, but not for the hurricane wind speed standard deviations, as observed from Figure 2-6.

Table 2-4. Comparison of hurricane gradient wind speed (fastest 1-minute hurricane speed at 10 m above ground over open terrain) means and standard deviations at different mileposts estimated using NIST data and the proposed simulation procedure

| Milepost | NIST (m/s) | | Proposed model (m/s) | | Relative difference (%) | |
|---|---|---|---|---|---|---|
| # | $\mu_V$ | $\sigma_V$ | $\mu_V$ | $\sigma_V$ | $\varepsilon_{\mu_V}$ | $\varepsilon_{\sigma_V}$ |
| 1 | 22.82 | 9.62 | 22.60 | 8.76 | -0.97 | -8.92 |
| 2 | 22.35 | 9.17 | 23.04 | 8.66 | 3.10 | -5.52 |
| 3 | 23.11 | 9.46 | 23.33 | 8.79 | 0.95 | -7.08 |
| 4 | 21.55 | 8.44 | 22.26 | 8.53 | 3.30 | 1.09 |
| 5 | 21.85 | 8.11 | 21.81 | 8.53 | -0.18 | 5.16 |
| 6 | 21.49 | 8.56 | 21.39 | 8.57 | -0.48 | 0.07 |
| 7 | 22.13 | 9.16 | 22.27 | 8.60 | 0.62 | -6.15 |
| 8 | 22.23 | 8.31 | 22.10 | 8.68 | -0.59 | 4.39 |
| 9 | 21.00 | 7.15 | 21.70 | 8.69 | 3.33 | 21.58 |
| 10 | 21.74 | 7.78 | 21.35 | 8.70 | -1.79 | 11.80 |
| 11 | 21.54 | 8.74 | 21.34 | 8.49 | -0.94 | -2.81 |
| 12 | 25.99 | 8.9 | 25.86 | 9.04 | -0.49 | 1.53 |
| 13 | 23.84 | 10.08 | 24.36 | 9.02 | 2.20 | -10.55 |
| 14 | 26.97 | 9.88 | 26.63 | 9.74 | -1.24 | -1.45 |
| 15 | 21.06 | 9.13 | 21.40 | 8.85 | 1.60 | -3.08 |
| 16 | 18.71 | 8.57 | 18.52 | 8.59 | -1.00 | 0.22 |
| 17 | 17.83 | 7.92 | 18.13 | 8.66 | 1.70 | 9.34 |
| 18 | 19.52 | 9.45 | 19.57 | 8.87 | 0.28 | -6.14 |
| 19 | 21.73 | 9.04 | 21.90 | 9.15 | 0.79 | 1.24 |
| 20 | 21.19 | 8.31 | 21.54 | 8.97 | 1.65 | 7.99 |
| 21 | 22.28 | 8.93 | 22.55 | 9.12 | 1.21 | 2.12 |
| 22 | 20.46 | 7.84 | 20.83 | 8.97 | 1.82 | 14.38 |
| 23 | 19.07 | 7.45 | 19.19 | 8.77 | 0.61 | 17.76 |
| 24 | 20.08 | 9.21 | 20.19 | 8.92 | 0.57 | -3.13 |
| 25 | 22.58 | 10.87 | 22.68 | 8.52 | 0.44 | -21.65 |
| 26 | 22.25 | 10.15 | 22.47 | 9.10 | 1.01 | -10.30 |
| 27 | 20.89 | 10.00 | 21.05 | 8.99 | 0.79 | -10.10 |
| Average | 21.71 | 8.90 | 21.85 | 8.82 | 0.68 | 0.07 |
| Minimum | 17.83 | 7.15 | 18.13 | 8.49 | -1.79 | -21.65 |
| Maximum | 26.97 | 10.87 | 26.63 | 9.74 | 3.33 | 21.58 |

The second set of data from the design wind speeds given in ASCE 7-16 (ASCE 2016) is used to validate the tail of the hurricane wind speed distributions. In particular, the ASCE 7-16 design wind speeds (also referred to as basic wind speeds) correspond to the 3-second gust wind speeds over open terrain at 10 m above ground at any given location with mean return intervals (MRIs) of 300, 700, 1700, and 3000 years,

which are used for the design of structures of risk category I through IV, respectively. Thus, the coefficients in Eq. (2.7) assume the values $c_e = c_z = 1.0$ and $c_t = 1.25$. The design wind speeds in ASCE 7-16 are based on data corresponding to the 1886-1983 period, for which the average yearly SST was calculated as $T_{1886\text{-}1983} = 25.30^{\circ}\text{C}$. It is noted here that the design wind speed in ASCE 7-16 are obtained from the wind speed distributions including both hurricane and non-hurricane wind speeds, whereas the wind speeds obtained from the proposed simulation procedure correspond to the hurricane wind speeds only. However, it was also observed that the differences between the two distributions in all the locations considered in this study are negligible for MRI larger than or equal to 100 years. The design wind speeds obtained from the proposed sampling methodology are based on 1,000,000 simulations and are obtained as:

$$V_{MRI} = \text{CDF}^{-1}\left(\frac{MRI - 1}{MRI}\right) \tag{2.8}$$

in which, *MRI* = 300, 700, 1700, and 3000 years denotes the MRI of interest, and $\text{CDF}^{-1}$ denotes the inverse of the empirical cumulative distribution function (CDF) of the generated wind speed data. Table 2-5 reports the wind speeds corresponding to MRIs of 300, 700, 1700, and 3000 years obtained from ASCE 7-16 and from the proposed simulation procedure at each considered milepost from the coast of Texas to that of Maine, as well as the relative differences between the two sets of values. As shown in Table 2-5, the average relative differences in the design wind speeds over all mileposts are smaller than 1% in absolute value for all four risk categories, with minimum and maximum relative differences slightly increasing in absolute values for increasing MRIs. The RMSEs over all considered mileposts for structures corresponding to risk categories I through IV are equal to 1.80 m/s, 2.55 m/s, 2.84 m/s and 3.07 m/s, respectively. It is observed that the proposed simulation procedure can match very well the design wind speeds overall, with only a few locations out of the 27 considered along the US Gulf and Atlantic Coast where the simulated design wind speeds differ from the ASCE 7-16 design wind speeds by more than 5% (i.e., in 5, 7, 3, and 4 locations for MRIs of 300, 700, 1700, and 3000 years, respectively). These locations correspond almost exactly to the locations where higher differences were observed between the NIST-based and the simulated estimates of the hurricane wind speed standard deviations. It is also observed that the average relative

differences and the RMSEs of the simulated design wind speed tend to slightly increase for increasing MRIs. Based on the results presented here, it is shown that the proposed simulation approach can capture well both the body and the tail of the hurricane wind speed distributions obtained from historical data for different locations along the US Gulf and Atlantic Coast.

Table 2-5. Comparison of design wind speeds (base wind speeds corresponding to 3-second gust wind speeds at 10 m above ground over open terrain) from ASCE 7-16 and proposed simulation procedure along the US Gulf and Atlantic Coast

| Milepost # | ASCE (m/s) | | | | Proposed model (m/s) | | | | Relative difference (%) | | | |
|---|---|---|---|---|---|---|---|---|---|---|---|---|
| | 300 | 700 | 1700 | 3000 | 300 | 700 | 1700 | 3000 | 300 | 700 | 1700 | 3000 |
| 1 | 61.24 | 66.16 | 69.74 | 72.42 | 58.05 | 62.73 | 67.60 | 70.42 | -5.20 | -5.18 | -3.07 | -2.76 |
| 2 | 61.69 | 66.61 | 70.63 | 72.87 | 58.89 | 63.19 | 67.66 | 70.34 | -4.53 | -5.13 | -4.21 | -3.47 |
| 3 | 59.9 | 64.37 | 68.4 | 70.19 | 60.35 | 64.92 | 69.65 | 72.57 | 0.75 | 0.85 | 1.82 | 3.39 |
| 4 | 58.12 | 63.48 | 68.4 | 70.19 | 57.87 | 62.29 | 66.54 | 69.53 | -0.43 | -1.87 | -2.72 | -0.93 |
| 5 | 67.06 | 75.1 | 80.02 | 82.7 | 64.04 | 68.81 | 73.85 | 76.89 | -4.50 | -8.38 | -7.71 | -7.02 |
| 6 | 66.61 | 74.21 | 80.02 | 81.81 | 66.46 | 71.76 | 76.86 | 80.24 | -0.23 | -3.31 | -3.95 | -1.92 |
| 7 | 65.27 | 71.53 | 78.68 | 81.81 | 61.70 | 66.48 | 71.06 | 74.22 | -5.47 | -7.07 | -9.69 | -9.27 |
| 8 | 56.77 | 61.24 | 66.16 | 68.4 | 57.63 | 62.18 | 66.87 | 69.51 | 1.52 | 1.54 | 1.08 | 1.62 |
| 9 | 52.75 | 58.56 | 63.48 | 62.14 | 53.79 | 57.99 | 62.37 | 65.10 | 1.97 | -0.98 | -1.74 | 4.77 |
| 10 | 50.52 | 54.54 | 60.8 | 62.14 | 53.13 | 57.46 | 61.61 | 64.60 | 5.17 | 5.35 | 1.34 | 3.96 |
| 11 | 59.9 | 64.82 | 68.4 | 70.19 | 57.44 | 61.86 | 66.20 | 69.07 | -4.10 | -4.56 | -3.21 | -1.60 |
| 12 | 64.37 | 69.29 | 75.1 | 78.68 | 64.66 | 69.59 | 74.32 | 77.27 | 0.45 | 0.44 | -1.04 | -1.79 |
| 13 | 71.53 | 77.34 | 82.26 | 85.83 | 69.66 | 74.68 | 79.61 | 82.83 | -2.62 | -3.44 | -3.22 | -3.50 |
| 14 | 69.29 | 75.55 | 80.47 | 83.6 | 67.92 | 73.34 | 78.82 | 82.39 | -1.98 | -2.92 | -2.05 | -1.45 |
| 15 | 61.24 | 66.61 | 71.08 | 75.55 | 60.24 | 64.83 | 69.28 | 72.35 | -1.63 | -2.67 | -2.53 | -4.24 |
| 16 | 53.64 | 58.12 | 62.59 | 66.61 | 54.21 | 58.95 | 63.62 | 66.97 | 1.06 | 1.43 | 1.64 | 0.54 |
| 17 | 52.75 | 58.12 | 63.93 | 67.5 | 53.03 | 58.04 | 63.22 | 66.54 | 0.53 | -0.14 | -1.10 | -1.42 |
| 18 | 58.56 | 65.71 | 70.19 | 73.76 | 57.84 | 63.00 | 67.99 | 71.28 | -1.22 | -4.13 | -3.14 | -3.36 |
| 19 | 60.35 | 66.16 | 69.74 | 72.87 | 60.43 | 65.40 | 70.27 | 73.69 | 0.12 | -1.14 | 0.77 | 1.12 |
| 20 | 59.9 | 64.82 | 67.95 | 70.19 | 59.94 | 64.57 | 69.52 | 72.75 | 0.06 | -0.38 | 2.31 | 3.65 |
| 21 | 55.43 | 59.01 | 63.03 | 66.16 | 55.88 | 60.27 | 64.50 | 67.01 | 0.81 | 2.13 | 2.34 | 1.29 |
| 22 | 49.62 | 54.09 | 58.56 | 60.8 | 52.34 | 56.59 | 61.03 | 63.72 | 5.49 | 4.63 | 4.22 | 4.81 |
| 23 | 50.96 | 55.88 | 59.9 | 62.59 | 51.81 | 56.28 | 60.83 | 63.85 | 1.68 | 0.72 | 1.56 | 2.02 |
| 24 | 49.62 | 54.09 | 58.56 | 61.24 | 50.86 | 55.77 | 60.03 | 63.03 | 2.51 | 3.11 | 2.50 | 2.93 |
| 25 | 54.09 | 58.12 | 62.14 | 64.37 | 54.67 | 58.84 | 63.13 | 65.67 | 1.07 | 1.24 | 1.60 | 2.03 |
| 26 | 54.99 | 59.01 | 62.59 | 64.82 | 57.16 | 62.36 | 67.81 | 70.94 | 3.94 | 5.67 | 8.35 | 9.44 |
| 27 | 49.17 | 53.64 | 57.22 | 59.46 | 52.35 | 57.43 | 62.10 | 65.50 | 6.46 | 7.06 | 8.52 | 10.15 |
| Average | 58.35 | 63.56 | 68.15 | 70.7 | 58.24 | 62.95 | 67.64 | 70.68 | 0.06 | -0.63 | -0.42 | 0.33 |

| | | | | | | | | | | | | |
|---|---|---|---|---|---|---|---|---|---|---|---|---|
| Minimum | 49.17 | 53.64 | 57.22 | 59.46 | 50.86 | 55.77 | 60.03 | 63.03 | -5.47 | -8.38 | -9.69 | -9.27 |
| Maximum | 71.53 | 77.34 | 82.26 | 85.83 | 69.66 | 74.68 | 79.61 | 82.83 | 6.46 | 7.06 | 8.52 | 10.15 |

## 2.6. Hurricane wind speed projections considering climate change: comparison with other existing models and design implications

The proposed simulation procedure is used to develop projected hurricane wind speed distributions under different climate change projections along the US Gulf and Atlantic Coast. As a further validation of this methodology, its projection results are compared with those obtained from existing methodologies based on a rigorous simulation of the hurricane tracks from their formation in the Atlantic Ocean to their landfall on the US Gulf and Atlantic Coast based on downscaled climate change projections. Specifically, the wind speed projections for year 2100 in Miami, FL, corresponding to the models developed by Cui and Caracoglia (2016) and Pant and Cha (2019) are compared in Figure 2-7 to those obtained using the proposed model for the climate change scenarios defined by the Representative Concentration Pathways (RCP) in the best-case scenario RCP 2.6 and the worst-case scenario RCP 8.5. The predicted changes in design wind speeds obtained by using the proposed model are very close to those provided by the other two models, with a maximum absolute value of the relative differences smaller than 3.0% for the RCP 2.6 scenario (corresponding to a wind speed difference of approximately 2.3 m/s) and smaller than 2.4% for the RCP 8.5 scenario (corresponding to a wind speed difference of approximately 2.2 m/s). It is concluded that the proposed simulation procedure provides projections of wind speed distributions that are consistent with other existing methodologies based on hurricane tracks at a small fraction of their computational cost. For example, the proposed methodology allows to derive the hurricane wind speed distributions based on 1,000,000 simulation at the 27 different locations and for all four climate change scenarios considered in this study in little less than 2 minutes on an ordinary personal computer (Intel® Core i7-8700 processor, 3.2 GHz, 16 GB RAM).

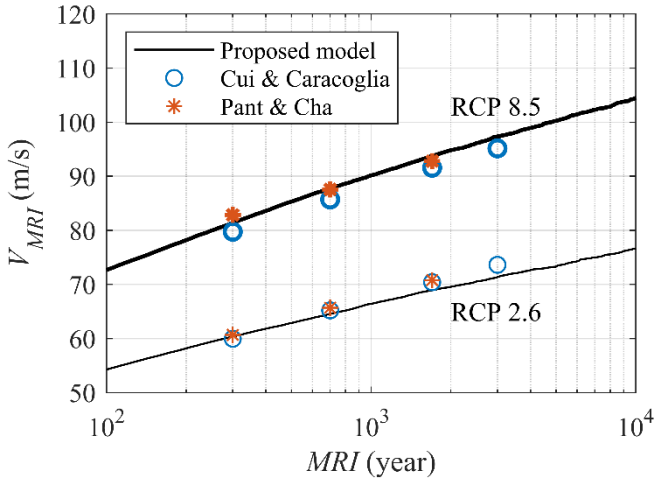


Figure 2-7. Comparison of projected hurricane wind speeds (gradient wind speeds corresponding to 3-second gust wind speeds at 10 m above ground over open terrain) for year 2100 in Miami, FL, from proposed model, Cui and Caracoglia (2016), and Pant and Cha (2019)

Finally, the proposed simulation approach is used to estimate the projected wind design speeds under different climate change scenarios at different locations along the US Gulf and Atlantic Coast. Table 2-6 reports the projected absolute and relative increases in design wind speeds by year 2060 at each considered milepost from the coast of Texas to that of Maine when considering the RCP 8.5 climate change scenario. These average relative increases in design wind speeds are equal to 25.01%, 24.52%, 25.13%, and 26.05% for structures in risk categories I through IV, respectively, with peak relative increases as high as 39.70% near the coast of Maine, where the largest relative increases are expected for all risk categories.

Table 2-6. Projected increases in design wind speeds (basic wind speeds corresponding to 3-second gust wind speeds at 10 m above ground over open terrain) for year 2060 and scenario RCP 8.5 along the US Gulf and Atlantic Coast

| Milepost | 300 years | | 700 years | | 1700 years | | 3000 years | |
|---|---|---|---|---|---|---|---|---|
| # | (m/s) | (%) | (m/s) | (%) | (m/s) | (%) | (m/s) | (%) |
| 1 | 11.15 | 18.21 | 12.22 | 18.47 | 14.35 | 20.58 | 15.18 | 20.97 |
| 2 | 12.25 | 19.86 | 13.08 | 19.64 | 14.36 | 20.33 | 15.62 | 21.43 |
| 3 | 15.62 | 26.08 | 17.04 | 26.46 | 19.15 | 28.00 | 21.00 | 29.91 |
| 4 | 14.56 | 25.06 | 14.75 | 23.23 | 15.45 | 22.58 | 17.33 | 24.69 |
| 5 | 11.61 | 17.31 | 9.87 | 13.14 | 11.48 | 14.35 | 12.90 | 15.60 |
| 6 | 13.93 | 20.91 | 12.69 | 17.11 | 13.33 | 16.66 | 15.89 | 19.42 |
| 7 | 11.31 | 17.33 | 11.09 | 15.51 | 9.74 | 12.38 | 10.25 | 12.53 |
| 8 | 15.35 | 27.03 | 16.84 | 27.49 | 18.02 | 27.23 | 19.33 | 28.26 |
| 9 | 15.44 | 29.28 | 15.30 | 26.13 | 15.81 | 24.91 | 20.28 | 32.64 |
| 10 | 16.66 | 32.97 | 18.18 | 33.33 | 17.67 | 29.06 | 19.43 | 31.27 |
| 11 | 12.24 | 20.44 | 13.01 | 20.07 | 15.15 | 22.15 | 17.11 | 24.37 |
| 12 | 16.91 | 26.28 | 18.15 | 26.19 | 18.55 | 24.70 | 18.51 | 23.53 |
| 13 | 13.87 | 19.39 | 14.76 | 19.08 | 16.37 | 19.90 | 16.55 | 19.28 |
| 14 | 16.76 | 24.19 | 17.60 | 23.30 | 19.83 | 24.64 | 21.04 | 25.17 |
| 15 | 14.46 | 23.62 | 15.15 | 22.74 | 16.76 | 23.58 | 15.52 | 20.54 |
| 16 | 14.60 | 27.22 | 16.09 | 27.69 | 18.00 | 28.76 | 17.44 | 26.18 |
| 17 | 13.77 | 26.11 | 14.81 | 25.48 | 15.66 | 24.49 | 16.20 | 24.00 |
| 18 | 13.90 | 23.74 | 13.38 | 20.36 | 15.52 | 22.11 | 16.21 | 21.97 |
| 19 | 16.12 | 26.71 | 16.71 | 25.25 | 19.43 | 27.86 | 20.40 | 28.00 |
| 20 | 15.60 | 26.04 | 16.94 | 26.14 | 20.30 | 29.87 | 22.07 | 31.45 |
| 21 | 14.85 | 26.80 | 16.87 | 28.59 | 18.83 | 29.87 | 19.50 | 29.47 |
| 22 | 11.21 | 22.60 | 12.15 | 22.45 | 12.77 | 21.80 | 14.15 | 23.28 |
| 23 | 14.36 | 28.18 | 15.52 | 27.78 | 17.24 | 28.77 | 18.44 | 29.46 |
| 24 | 14.30 | 28.82 | 16.00 | 29.58 | 17.94 | 30.64 | 19.41 | 31.70 |
| 25 | 14.89 | 27.53 | 16.63 | 28.62 | 18.37 | 29.57 | 19.51 | 30.30 |
| 26 | 16.39 | 29.81 | 19.53 | 33.09 | 22.36 | 35.72 | 24.81 | 38.28 |
| 27 | 16.62 | 33.81 | 18.83 | 35.10 | 21.81 | 38.12 | 23.60 | 39.70 |
| Average | 14.40 | 25.01 | 15.30 | 24.52 | 16.82 | 25.13 | 18.06 | 26.05 |
| Minimum | 11.15 | 17.31 | 9.87 | 13.14 | 9.74 | 12.38 | 10.25 | 12.53 |
| Maximum | 16.91 | 33.81 | 19.53 | 35.10 | 22.36 | 38.12 | 24.81 | 39.70 |

Similar results for other climate change scenarios are not reported here due to space constraints, but the following average relative increases in the design wind speeds are obtained for the four risk categories considered in ASCE 7-16: (1) 14.52%, 14.00%, 14.47%, and 15.27% for RCP 2.6; (2) 18.87%, 18.32%,

18.96%, and 19.82% for RCP 4.5; and (3) 17.87%, 17.39%, 17.97%, and 18.87% for RCP 6.0. Because the design wind force applied on a structure increases quadratically with the design wind speed, these results suggest that, in order to maintain the same reliability required by the current ASCE 7-16 design code under wind loads, structures with a design life longer than 50 years and located along the US Gulf and Atlantic Coast should be designed for a larger wind force than that used today, with an increase of at least 30% for RCP 2.6, at least 40% for RCP 4.5 and RCP 6.0, and between 55% and 59% for RCP 8.5.

## 2.7. Conclusions

This study proposes a novel and efficient simulation methodology based on historical records to predict hurricane wind speed statistics under different climatological conditions. The developed procedure allows to simulate hurricane wind speeds at any given location along the US Gulf and Atlantic Coast by considering the effects of climate change. The newly developed simulation procedure was validated versus historical data from NIST and the design wind speeds provided in ASCE 7-16. In addition, the results of the proposed simulation approach were compared with those obtained using other existing procedures requiring the simulation of the full tracks of hurricanes. The obtained hurricane wind speed projections were found to be consistent (i.e., less than 3.5% absolute relative differences) with those of these other methods, while being significantly less computationally expensive (i.e., with a computational time of the order of minutes on an ordinary personal computer). The simulation procedure was used in conjunction with the projection scenarios given in the Intergovernmental Panel on Climate Change's 5$^{th}$ Assessment Report to simulate hurricane wind speeds corresponding to mean return intervals of 300, 700, 1700, and 3000 years (i.e., corresponding to the design wind speeds for buildings belonging to risk category I, II, III, and IV in ASCE 7-16) under possible future climatological conditions. The simulation results indicate that climate change could produce significant changes in the design wind speeds in the next 40-100 years. In particular, by 2060, the design wind speeds along the US Gulf and Atlantic Coast are projected to increase between approximately 14% (for risk category II under scenario RCP 2.6) and 26% (for risk category IV under scenario RCP 8.5), which correspond to an average increase of the wind force acting on a structure

between approximately 30% and 59%. Therefore, it is suggested to include climate change effects in the development of design wind maps for structures with extended design life in future version of ASCE 7. Finally, whereas the model presented in this study is specifically developed for the US Gulf and Atlantic Coast, the same methodology can be employed for other hurricane-prone regions worldwide, by using the appropriate historical records to fit the numerical values of the parameters used in the present model.

The wind speed model developed in this study provides an invaluable tool for further investigation of climate change effects on the performance of the US built environment and national infrastructure systems. An important aspect that needs to be quantified in future studies is the effect of epistemic uncertainties, e.g., through a sensitivity analysis and/or a probability bounds analysis of the wind speed estimates with respect to the adopted probability distributions, the statistics used to describe such distributions, and the likelihood of different climate scenarios. Another essential research need is the quantification of the effects of the predicted wind force increases on the performance of structural and infrastructural systems, with the resulting implications on future design and building codes for different types of structures ranging from single-family houses and residential/non-residential buildings to critical infrastructure components such as bridges, dams, levees, communication towers, and power plants. Finally, the proposed wind model, used in conjunction with the results of the suggested structural performance studies, could inform the next generation of catastrophe models to predict the effects of climate change in terms of economic and life losses, to assess the resilience of our infrastructure, to quantify the potential societal impact, and above all to propose feasible mitigation and adaptation strategies that could be implemented in both the short- and long-term.

# Chapter 3. Performance-Based Hurricane Engineering under Changing Climate Conditions: General Framework and Performance of Single-Family Houses in the US

## 3.1. Introduction

The US Gulf and Atlantic coasts are frequently struck by severe tropical storms, locally known as hurricanes. The hurricane-induced losses in the US Gulf and Atlantic coasts are usually in the range of several billion dollars for each major event. Since the National Oceanic and Atmospheric Administration (NOAA) started tracking weather and climate disasters with losses exceeding $1 billion, the US has sustained 291 of such events, for a total cost exceeding $1.9 trillion and more than 14,600 deaths (NOAA 2021). Among these disasters, hurricanes have caused the most damage, exceeding $1 trillion, and the highest number of deaths (more than 6,500). The costliest hurricanes since 1980 are Hurricane Katrina (2005) with $172.5 billion, Hurricane Harvey (2017) with $133.8 billion, and Hurricane Maria (2017) with $96.3 billion of estimated losses (in 2021 Consumer Price Index-adjusted dollars).

Many studies have shown a direct relationship between the global warming phenomena, which is usually referred to as climate change, and intensified hurricanes. Emanuel (2005) concluded that, since 1970, hurricane destructiveness has increased drastically due to an increase in the sea surface temperature (SST). He also concluded that for every 1°C increase in SST, the peak wind speed of hurricanes is expected to increase by about 5%. Pant and Cha (2018) investigated the effect of climate change on hurricane winds in Miami-Dade County, FL, and concluded that an increase of 6.7 to 8.9 m/s is expected for 700-year return period wind speeds with each 1°C increase in SST. Esmaeili and Barbato (2021a) developed a model to predict the climate change effects on hurricane wind hazard for locations along the US Gulf and Atlantic coasts. The SST projections for future years were taken from the fifth assessment report (AR5) from the Intergovernmental Panel on Climate Change (IPCC) (Stocker et al. 2013). The simulation results indicated that climate change could produce significant changes in the design wind speeds in the future decades. In

particular, their study showed that, by year 2060, the design wind speeds corresponding to the different mean return intervals considered by ASCE 7 are expected to increase on average between 14% and 26%, with a corresponding average increase in the design wind-induced loads between 30% and 59%.

The development of risk assessment methodologies for structures subject to hurricane hazard has been the subject of several studies. Huang et al. (2001) proposed an event-based simulation technique for long-term risk assessment for residential buildings. This methodology was also adopted by Stewart et al. (2003) to study the economic viability of different retrofit scenarios. Barbato et al. (2013) proposed a performance-based hurricane engineering (PBHE) framework based on the total probability theorem to evaluate the risk for structures. This general framework was used to compare the performance of different storm mitigation techniques for low-rise residential buildings (Unnikrishnan and Barbato 2016) and to investigate the multi-hazard interaction effects on the performance of low-rise single-family houses subject to hurricane hazard (Unnikrishnan and Barbato 2017).

Many of the existing hurricane risk/loss assessment methodologies assume that the wind speed distribution at a given location is stationary over time (Sutter et al. 2009; Unnikrishnan and Barbato 2016). Hence, they do not account for climate change effects on the hurricane wind hazard. However, in warming climate conditions, the hurricane wind speeds and the corresponding damage and losses are expected to increase (Li and Stewart 2011; Cui and Caracoglia 2016). Several recent studies have addressed this issue (Decò and Frangopol 2011; Bisadi and Padgett 2015; Dong et al. 2016). Bjarnadottir et al. (2011) developed a probabilistic framework to account for the effects of climate change on hurricane risk and losses for residential constructions, in which the damages were calculated based on an experimental damage model for residential buildings. Their model was applied to assess the expected losses for a single-family unit in Miami-Dade County, leading to an increase in expected hurricane-induced losses of up to 37% between 2010 and 2060. Li et al. (2015) developed an approach to estimate the time-dependent reliability of structures while accounting for non-stationary loads and degradation. Wang et al. (2016) proposed a probability-based model of hurricane damage assessment for coastal structures, in which the non-stationarity in hurricane intensity and frequency was explicitly considered. However, to the best of the

authors' knowledge, no performance-based engineering framework is available in the literature to account for structural aging and non-stationary hazards.

This work extends the general PBHE framework proposed by Barbato et al. (2013) to account for non-stationarity in hurricane hazard (i.e., climate change) and vulnerability (i.e., aging of structural components) during the lifetime of a given structure. This study focuses on hurricane-induced losses for single-family houses located along the US Gulf and Atlantic coasts. The presented application example considers wind hazard non-stationarity only, i.e., it explicitly models the effects of climate change on the predicted loss distribution and performance of different storm mitigation strategies; however, it does not include the effects of structural aging. This investigation quantifies the sensitivity of the proposed methodology's numerical results to different time discretization, time integration techniques, and discount rate assumptions. This study also investigates the effects of location, future climate scenarios, and storm mitigation techniques on the life-cycle cost-benefit analysis for single-family houses subject to hurricane wind hazard.

## 3.2. Research Significance and Novelty

This study presents for the first time the extension of a performance-based engineering framework to account for non-stationary loading and structural properties. In particular, the proposed extended PBHE framework can accommodate the effects of climate change on hurricane hazard, structural aging, and the interaction between changing climate and structural aging. In contrast with the framework developed in this study, previous studies available in the literature focused on the non-stationarity of loading or of the structural properties and were not developed to be explicitly consistent with a performance-based engineering approach based on the total probability theorem. Even though the formulation developed in this study is specialized for the PBHE framework, the same formulation and methodology can be used to extend other existing performance-based engineering frameworks (e.g., performance-based earthquake engineering, performance-based wind engineering, performance-based tsunami engineering, performance-based fire engineering, and performance-based blast engineering) to include the effects of the non-stationarity of loading and/or structural properties. The proposed methodology provides a rigorous

framework to assess the performance of structural systems under non-stationary intensity measures, structural properties, and damage measures. This methodology is applied here to low-rise single-family houses in the US Gulf and Atlantic coasts, which constitute over 80% of the total building stock in the US and represent the structures most vulnerable to wind damage (van de Lindt and Dao 2009). However, the proposed framework is general and can be applied to any structural system worldwide, as long as proper models to describe the non-stationarity of the hazards and the structural properties are available.

## 3.3. Extended PBHE Framework: Methodology

The methodology developed in this study is based on the original PBHE framework proposed by Barbato et al. (2013). The performance of a target structure is described by a decision variable $(DV)$, which depends on damage measures $(DM)$, engineering demand parameters $(EDP)$, intensity measures $(IM)$, structural parameters $(SP)$, and interaction parameters $(IP)$. This study introduces a new set of random parameters, referred to as the vector of climatological parameters $(C)$, which are used to describe in probabilistic terms the climatological conditions under which the performance analysis is performed. Examples of climatological parameters are SST, sea water level, and/or any other parameters needed to describe the climatological conditions that may affect the loading and aging of the structure of interest. The proposed methodology also introduces two different time scales: a global time scale $(t)$, which generally corresponds to the calendar year for which a performance analysis is carried out and is used to describe the non-stationarity of climate conditions; and a structural time scale $(\tau)$, which denotes the age of structure of interest and is used to describe the non-stationarity of structural properties and damage measures. In its general form, the probabilistic description of the selected $DV$ is given by:

$$\begin{aligned} G\left(DV_{t,\tau}\right) = \int\int\int\int\int\int & G\left(DV_{t,\tau}\middle|DM_{\tau}\right)\cdot f\left(DM_{\tau}\middle|EDP,C_{t}\right) \\ & \cdot f\left(EDP\middle|IM,IP,SP_{\tau}\right)\cdot f\left(IP\middle|IM,SP_{\tau}\right)\cdot f\left(IM\,|\,C_{t}\right) \\ & \cdot f\left(SP_{\tau}\,|\,C_{t}\right)\cdot f\left(C_{t}\right)\cdot \mathrm{d}DM_{\tau}\cdot \mathrm{d}EDP\cdot \mathrm{d}IM\cdot \mathrm{d}IP\cdot \mathrm{d}SP_{\tau}\cdot \mathrm{d}C_{t} \end{aligned} \tag{3.1}$$

where $G(\bullet)$ = complementary cumulative distribution function (CDF), $G(\bullet|\bullet)$ conditional

complementary CDF, $f(\bullet)$ = probability density function (PDF), and $f(\bullet|\bullet)$ = conditional PDF. The subscripts $t$ and $\tau$ indicate explicit dependency of a given parameter on global and structural time scales, respectively.

In this framework, climatological conditions $C_t$ are considered to be explicitly dependent on the global time scale in order to account for climate change effects; whereas structural parameters $SP_\tau$ and damage measures $DM_\tau$ are explicitly dependent on the structural time scale, as they may change with the aging of the structure. Finally, the decision variable $DV_{t,\tau}$ is considered explicitly dependent on both global and structural time scales, because financial items such as costs and discount rates change in time and can depend on the conditions and age of the structure under consideration. Other parameters depend on the different time scales only implicitly. For instance, the components of the $IM$ vector depend on the global time scale $t$ only through their dependence on the $C_t$ vector. Structural parameters $SP_\tau$ and damage measures $DM_\tau$ may also depend on $t$ through $C_t$, because the aging of a structure (e.g., chloride penetration for concrete, corrosion for steel, and rot for wood) may depend on the climatological conditions at the site.

This study focuses on the non-stationarity of the climate conditions, which is estimated by using historical records and climate change projection scenarios based on the 5th Assessment Report by the Intergovernmental Panel on Climate Change (Stocker et al. 2013). In particular, this study uses an existing model to predict the future wind speed distributions at different locations in the US Gulf and Atlantic coasts under different climate change scenarios (Esmaeili and Barbato 2021a). In order to better investigate the effects of climate change on the performance of single-family houses subject to hurricane wind hazard, the effect of structural aging is neglected here. The general Eq. (3.1) is then simplified as follows:

$$\begin{aligned} G(DV_t) = \int\int\int\int\int\int & G(DV_t|DM)\cdot f(DM|EDP) \\ & \cdot f(EDP|IM,IP,SP)\cdot f(IP|IM,SP)\cdot f(IM\,|\,C_t) \\ & \cdot f(SP)\cdot f(C_t)\cdot \mathrm{d}DM\cdot \mathrm{d}EDP\cdot \mathrm{d}IM\cdot \mathrm{d}IP\cdot \mathrm{d}SP\cdot \mathrm{d}C_t \end{aligned} \tag{3.2}$$

By neglecting the effects of structural aging in Eq. (3.2), any explicit dependence on the structural time scale $\tau$ is removed and the PDFs of $SP$ and $DM$ are no longer conditional on $C_t$. These seemingly minor simplifications have a significant effect on the implementation of the performance assessment framework.

In particular, if the selected $DV_t$ represents annual losses, an annual probability of outcrossing a limit state, or a quantity derived from annual losses such as total losses or total benefits of a mitigation strategy over the design life of the structure (Unnikrishnan and Barbato 2016), $G\left(DV_t\right)$ can be calculated as a function of the global time scale alone by considering each analysis year, over which the performance analysis is performed, as independent from all other years, similar to what is currently done for existing performance-based engineering frameworks (Porter 2003; Ciampoli et al. 2011; Barbato et al. 2013).

### 3.3.1. Simulation approach using Multi-layer Monte-Carlo simulation (MMCS)

Eq. (3.1) can be solved using closed-form analytical solutions (Jalayer and Cornell 2003), direct integration (Bradley et al. 2009), and stochastic techniques (Porter et al. 2001). This study adopts an MMCS approach (Conte and Zhang 2007; Barbato et al. 2013; Unnikrishnan and Barbato 2013, 2016, 2017), which can account for all uncertainties through multiple analysis phases, each including a stochastic simulation component and a deterministic analysis model (Unnikrishnan and Barbato 2015, 2016). Under the simplifying assumption of no structural aging used to derive Eq. (3.2), the only modifications to the MMCS approach presented in Unnikrishnan and Barbato (2016) consist in: (1) an additional random sampling step of the components of $C_t$ from the PDF $f\left(C_t\right)$, and (2) an additional analysis step to obtain the conditional PDF $f\left(IM \mid C_t\right)$ and the conditional hurricane annual rate at the site of interest (see Figure 3-1).

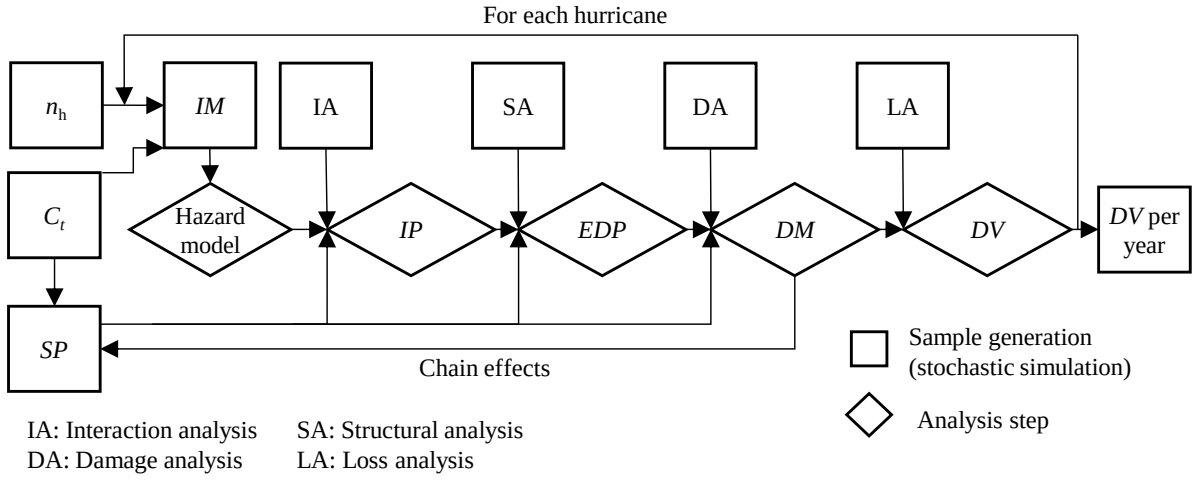

Figure 3-1. Multi-layer Monte Carlo Simulation (MCS) flowchart for extended PBHE framework accounting for hazard nonstationarity due to climate change.

This study employs the hurricane wind hazard model proposed by Esmaeili and Barbato (2021a), which uses the average yearly SST as climatological parameter with a time-dependent PDF. This model assumes that the hurricane annual rates are constant in time (thus, independent on $C_t$), whereas the peak hurricane wind speed, the radius at maximum wind speed, and the translational wind speed are intensity measures dependent on $C_t$. The output of this model is the hurricane wind speed distribution at the site of interest conditional on $C_t$.

### 3.3.2. Loss analysis and cost-benefit analysis

The results of the proposed methodology can be expressed in terms of different decision variables, e.g., total losses $L_r$ (loss analysis when considering a specific structural configuration $r$) or net benefit $B_{r_1 r_2}$ (cost-benefit analysis when comparing the performance of two different configurations $r_1$ and $r_2$) over the design life of the structure of interest. For a given sample $j$, the total losses $L_{r,j}$ for configuration $r$ are obtained as follows:

$$L_{r,j} = \sum_{i=0}^{\tau_D} \frac{L_{r,t_0+i,j}}{\left(1+d_{t_0+i,j}\right)^i} \tag{3.3}$$

in which $L_{r,t_0+i,j}$ = $j$-th sample of annual losses calculated at year $t_0+i$, which can be obtained following the flowchart in Figure 3-1; $d_{t_0+i,j}$ = $j$-th sample of discount rate at year $t_0+i$, which can be assumed as a constant (Liel and Deierlein 2013), sampled from an appropriate distribution derived from historical data (Van Dyke and Hu 1989), or forecasted using more advanced methods (Lee and Lee 2017); $t_0$ = year of construction; and $\tau_D$ = design life duration in years for the structure of interest. By using the proposed MMCS approach, different statistics of $L_r$ can be estimated; e.g., expected total losses and standard deviation of total losses can be calculated as follows:

$$m_{L_r} = \frac{1}{N}\sum_{j=1}^{N} L_{r,j} \tag{3.4}$$

$$s_{L_r} = \sqrt{\frac{1}{N-1}\sum_{j=1}^{N}\left(L_{r,j} - m_{L_r}\right)^2} \tag{3.5}$$

where $N$ = number of MMCS samples. Under the assumption of no structural aging, the annual losses at different years can be modeled as approximately statistically independent. Under the additional assumption of constant discount rates, the calculation of the expected total losses and the standard deviation of total losses can be simplified as follows:

$$m_{L_r} = \sum_{i=0}^{\tau_D} \frac{m_{L_{r,t_0+i}}}{\left(1+d_{t_0+i}\right)^i} \tag{3.6}$$

$$s_{L_r} = \sqrt{\sum_{i=0}^{\tau_D} \frac{s^2_{L_{r,t_0+i}}}{\left(1+d_{t_0+i}\right)^{2i}}} \tag{3.7}$$

respectively, in which $m_{L_{r,t_0+i}} = \frac{1}{N}\sum_{j=1}^{N} L_{r,t_0+i,j}$ and $s^2_{L_{r,t_0+i}} = \frac{1}{N-1}\sum_{j=1}^{N}\left(L_{r,t_0+i,j} - m_{L_{r,t_0+i}}\right)^2$.

Similar to the loss analysis, the *j*-th sample value of the net benefit of configuration $r_2$ over configuration $r_1$ can be calculated as follows:

$$B_{r_1,r_2,j} = L_{r_1,j} - L_{r_2,j} - C_{r_1,r_2,j} \tag{3.8}$$

in which $L_{r_1,j}$ and $L_{r_2,j}$ = *j*-th samples of total losses for configuration $r_1$ (often chosen as a baseline or unretrofitted configuration corresponding to lowest initial cost) and $r_2$, respectively; and $C_{r_1,r_2,j}$ = *j*-th sample of initial cost difference between configurations $r_2$ and $r_1$. Also in this case, several statistics can be derived, such as the expected net benefit $m_{B_{r_1,r_2}}$, and the standard deviation of net benefit $s_{B_{r_1,r_2}}$, with simplified approximate expressions similar to those in Eqs. (3.6) and (3.7) under the additional assumption that the initial cost differences are statistically independent on the corresponding total losses.

It is noted here that the most computationally expensive terms in Eqs. (3.3) and (3.8) are the total losses $L_{r,j}$, $L_{r_1,j}$, and $L_{r_2,j}$, which require to repeat all sampling and analysis steps described in Figure 3-1 for

each year during the design life duration $\tau_D$. Thus, it is useful to consider appropriate approximations to provide the best compromise between computational cost and accuracy. This study investigates the accuracy of estimating the total losses by rigorously calculating the annual losses $L_{r,t_0+i,j}$ at intervals of time larger than 1 year and using different approximations to find the intermediate values of annual losses between these time intervals.

## 3.4. Extended PBHE Framework: Benchmark Structure and Sensitivity Analysis

This study demonstrates the proposed extended PBHE framework by performing a loss analysis for a single-family house subject to hurricane wind and windborne debris hazards. This study also investigates the sensitivity of the loss analysis results to: (1) use of accurate and approximate estimates of mean and standard deviations, (2) time discretization and interpolation technique, (3) assumed model for the annual discount rate, (4) different locations, and (5) different climate change scenarios. It is noted here that the sensitivity to accurate/approximate estimates, time discretization, interpolation technique, and annual discount rate modeling is a measure of the robustness of the proposed methodology (i.e., the smaller the sensitivity, the more reliable the model). By contrast, the sensitivity to different locations and climate change scenarios is a measure of the actual variability of the loss analysis results (i.e., it provides a measure of how much location and climate change scenario affect the results of a loss analysis for a given structure). All loss analyses reported hereinafter are based on $N$ = 100,000 samples. The benchmark building is located in a residential development in Pinellas Park, FL, as shown in Figure 3-2 where the building of interest is identified by an unfilled circular marker.

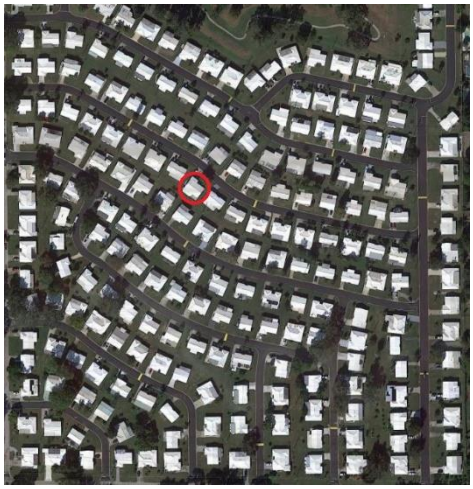

Figure 3-2. Plan view of the residential development with benchmark building identified by a red unfilled circular marker (map data © 2020 Google).

The unfolded view of the building is presented in Figure 3-3. It is assumed that the building was built in 2015, the value of the structure is $300,000, the value of its content is $150,000, and the design life is 50 years. The statistical description in terms of mean, coefficient of variation (COV), and distribution type of the different building components and corresponding limit states for the base (unretrofitted) structure is provided in Table 3-1 and is based on existing literature (Gurley et al. 2005; Datin et al. 2011; Dixon et al. 2014a; Masters et al. 2010; Stuckley and Carter 2001).

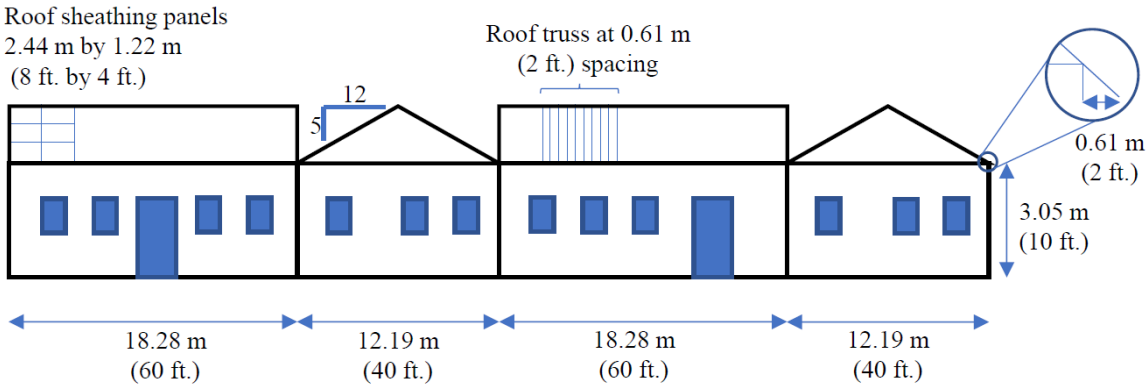


Figure 3-3. Unfolded view of the benchmark building.

Table 3-1. Statistical description of limit state capacities for different components in the base structure.

| Component | Limit state | Mean | COV | Distribution | Reference |
|---|---|---|---|---|---|
| Roof cover (shingles) | Separation | 1.96 kPa | 0.18 | Tr. Normal[(a)] | Dixon et al. (2014a) |
| Roof sheathing (6d C6/12) | Separation | 3.56 kPa | 0.22 | Lognormal | Datin et al. (2011) |
| Windows (unprotected) | Pressure failure | 3.33 kPa | 0.20 | Tr. Normal[(a)] | Gurley et al. (2005) |
| | Impact failure | 4.72 kg·m/s | 0.23 | Lognormal | Masters et al. (2010) |
| Doors (unprotected) | Pressure failure | 4.79 kPa | 0.20 | Tr. Normal[(a)] | Gurley et al. (2005) |
| Roof-to-wall connection | Tension failure | 16.68 kN | 0.20 | Lognormal | Gurley et al. (2005) |
| Wall | Uplift failure | 14.80 kN/m[(b)] | 0.25 | Tr. Normal[(a)] | Gurley et al. (2005) |
| | Lateral failure | 9.01 kN[(b)] | 0.25 | Tr. Normal[(a)] | Gurley et al. (2005) |
| Wall sheathing | Pressure failure | 6.03 kPa | 0.40 | Tr. Normal[(a)] | Gurley et al. (2005) |
| | Impact failure | 642 kg·m$^2$/s$^2$ | 0.07 | Lognormal | Stuckley & Carter (2001) |

[(a)] Truncated normal distribution with lower truncation at zero.

### 3.4.1. Loss analysis results for reference conditions

A loss analysis is performed first for reference conditions, which are defined here to correspond to the unretrofitted house located in Pinellas Park, FL, under the climate change worst-case scenario described by the representative concentration pathway (RCP) 8.5. The annual discount rate is assumed constant and equal to $d_t = 3\%$, and the total losses results are obtained using a time discretization $\Delta t = 1$ year. Figure 3-4 illustrates in semi-logarithmic scale the annual loss exceedance probability curves for years 2015 (initial climate conditions), 2040, and 2065 (end-life climate conditions). The losses reported in Figure 3-4 are not discounted. It is observed that the exceedance probabilities substantially increase for every annual loss level with the passage of time, consistently with the expected increase in hurricane wind hazard due to climate change. The loss analysis over the design life of the house is performed by estimating the mean and standard deviation of total losses by using both Eqs. (3.3) through (3.5) (accurate estimations) and Eqs. (3.6) and (3.7) (approximate estimations). The expected total losses from accurate and approximate estimations are both equal to \$72,831, with the corresponding standard deviations equal to \$61,714 and \$61,653, respectively.

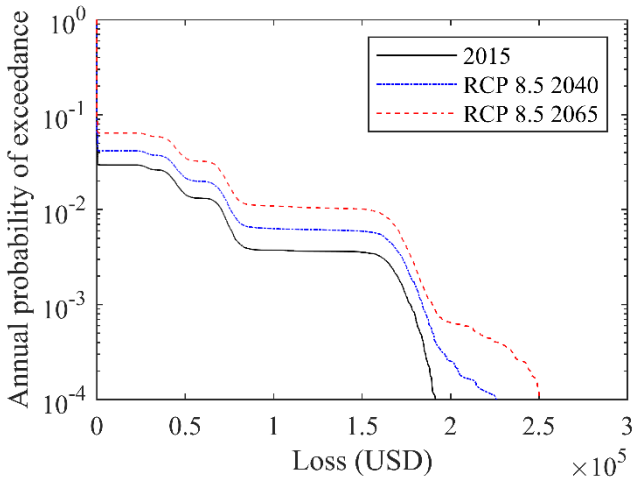


Figure 3-4. Annual loss exceedance probability curves for reference conditions.

The mean values based on the accurate and approximate estimations are identical because Eq. (3.3), which describes the total losses, is a linear function of random variables under the hypothesis of constant annual discount rate. The accurate and approximate estimations of the standard deviation of the total losses are very close (with a difference smaller than 0.1%), which indicates that neglecting the cross-correlations of the losses in different years as per Eq. (3.7) has a negligible effect on the standard deviation estimate.

### 3.4.2. Sensitivity of loss analysis results to time discretization and interpolation

The calculation of the sample annual losses $L_{r,t_0+i,j}$ is the most computationally intensive component of the proposed methodology. Therefore, it is useful to explore approaches to reduce this computational cost, e.g., by using different time discretizations of the structure's service design life, which require estimating $L_{r,t_0+i,j}$ only at time intervals longer than one year and, thus, can significantly reduce the number of times that $L_{r,t_0+i,j}$ values need to be calculated. In fact, whereas a time discretization interval $\Delta t = 1$ year requires $(\tau_D + 1)\cdot N$ annual loss samples $L_{r,t_0+i,j}$ calculated using the flowchart in Figure 3-1, a time discretization interval $1 < \Delta t \le \tau_D$ would require only $(q_{\max} + 1)\cdot N$ annual loss samples $L_{r,t_0+q\cdot\Delta t,j}$, in which $q_{\max} = \frac{\tau_D}{\Delta t} < \tau_D$ and $q = 0,1,\ldots,q_{\max}$. This study investigates the sensitivity of the loss analysis results to different time discretization intervals and to different interpolation techniques used to account for the annual

losses at intermediate years. This sensitivity analysis is performed using the accurate estimations of mean and standard deviation of the total losses for the benchmark structure at reference conditions (i.e., unretrofitted structure located in Pinellas Park, FL, under climate change scenario RCP 8.5) and assuming a constant annual discount rate $d_t = 3\%$. Two time discretization intervals are considered: (1) five years, and (2) ten years. For each of these time discretization intervals, two interpolation techniques are assessed: (1) constant annual losses equal to those calculated at the midpoint of the time interval, and (2) annual losses calculated via direct sampling from an empirical CDF (ECDF) obtained through linear interpolation of the ECDFs corresponding to the beginning and the end of each considered time interval. It is noted that the computational cost of the two interpolation techniques is comparable (with the direct sampling only marginally more computationally expensive than the assumption of constant annual losses); however, the use of larger time discretization intervals correspond to a significant (approximately proportional) reduction of the computational effort. In particular, the computational cost for $\Delta t = 5$ years and $\Delta t = 10$ years is approximately five and ten times smaller, respectively, than the computational cost for $\Delta t = 1$ year. The direct sampling from these general ECDFs is performed using the probability integral transform theorem (Angus 1994). The interpolated ECDFs, $\tilde{F}_{L_r,i_q}(l)$, for intermediate years, $i_q$, are obtained as functions of the annual loss $l$ as follows:

$$\tilde{F}_{L_r,i_q}(l) = F_{L_r,q\cdot\Delta t}(l) + \frac{F_{L_r,(q+1)\cdot\Delta t}(l) - F_{L_r,q\cdot\Delta t}(l)}{\Delta t}\cdot\left(i_q - q\cdot\Delta t\right); \quad q\cdot\Delta t \le i_q \le (q+1)\cdot\Delta t - 1 \tag{3.9}$$

in which the ECDFs $F_{L_r,q\cdot\Delta t}(l)$ and $F_{L_r,(q+1)\cdot\Delta t}(l)$ are obtained using the flowchart in Figure 3-1 and are referred to as sampled ECDFs. For the benchmark structure under reference conditions and annual discount rate $d_t = 3\%$, Figure 3-5 compares the complement of the sampled ECDFs (i.e., the annual probability of exceedance) for years 2035, 2040, and 2045, with the complement of the interpolated ECDF obtained using Eq. (3.9) and $\Delta t = 10$ years. The sampled and interpolated annual probabilities of exceedance for year 2040 are extremely close for any value of annual losses, and they are contained between the complementary ECDFs for years 2035 and 2045 for annual probabilities of exceedance higher than approximately $5\cdot10^{-4}$. For lower probabilities, the sampled annual probabilities of exceedance are not accurate, due to the limited

number of samples (i.e., 100,000 samples). The relative accuracy of the interpolated ECDF is measured by calculating the mean absolute percentage error (MAPE) (Tofallis 2015) as:

$$\text{MAPE} = \frac{100}{N}\sum_{p=1}^{N}\left|\frac{F_{L_r,i_q}\left(l_p\right)-\tilde{F}_{L_r,i_q}\left(l_p\right)}{F_{L_r,i_q}\left(l_p\right)}\right| \tag{3.10}$$

where the number of samples $N$ is equal to the number of data points for the ECDFs. The MAPE for the sampled and interpolated ECDFs corresponding to year 2040 with $\Delta t = 10$ years is equal to 0.03%, which indicates that the interpolated ECDF is a very accurate approximation of the corresponding sampled ECDF.

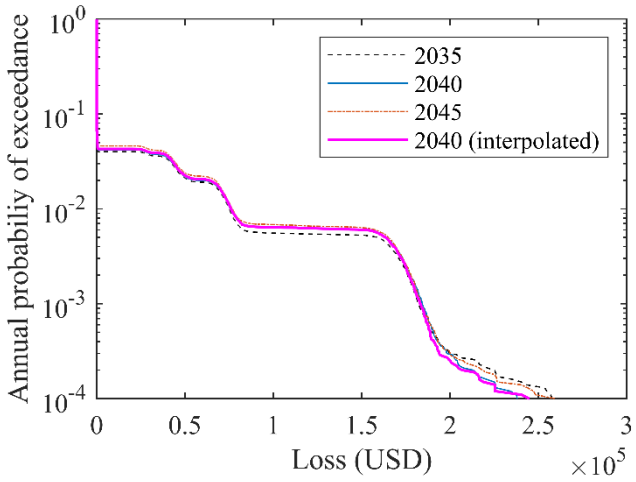


Figure 3-5. Comparison of sampled annual probabilities of exceedance for years 2035, 2040, and 2045, and interpolated annual probability of exceedance based on Eq. (3.9) for year 2040 corresponding to the benchmark structure at reference conditions with $d_t = 3\%$ and $\Delta t = 10$ years.

Table 3-2 reports the loss analysis results in terms of total loss means and standard deviations for the benchmark structure under reference conditions obtained by using accurate estimations and $d_t = 3\%$. The case with $\Delta t = 1$ year represents the reference solution without any interpolation, i.e., the sample annual losses $L_{r,t_0+i,j}$ are obtained using the flowchart in Figure 3-1 for all years.

Table 3-2. Sensitivity of loss analysis results to time discretization and interpolation scheme for reference conditions by using accurate equations and $d_t = 3\%$.

| $\Delta t$ (years) | Interpolation | Mean (USD) | Standard Deviation (USD) |
|---|---|---|---|
| **1** | None | 72,831 | 61,714 |
| **5** | Constant | 72,674 | 61,765 |
| | Sampling | 72,853 | 61,361 |
| **10** | Constant | 73,391 | 62,166 |
| | Sampling | 73,375 | 61,755 |

From Table 3-2, it is observed that the estimates of the total losses mean and standard deviation exhibit small variations (i.e., less than 0.1% differences) for increasing time discretization intervals, whereas the interpolation technique has even smaller effects on the accuracy of these estimates. Based on these results, it is concluded that accurate and computationally efficient estimates of the total losses mean and standard deviation can be obtained by using a time discretization interval $\Delta t = 5$ years and constant annual losses for intermediate years within each time discretization interval.

### 3.4.3. Sensitivity of loss analysis results to variability of discount rate

The estimates of the total losses' mean and standard deviation depend on the assumptions made on the annual discount rate during the structure design service life. This study quantifies this sensitivity of the total losses on the discount rate by considering two assumptions: (1) constant discount rate with different assumed values (which is the typical approach adopted in the literature for structural loss analysis), and (2) random annual discount rate samples based on different statistical models derived from historical values.

The statistical model of the annual discount rate was developed based on the historical data collected for the period 1950-2020, for which the sample mean and standard deviation are equal to 4.32% and 2.80%, respectively, and the minimum and maximum values are equal to 0.50% and 13.42%, respectively. Figure 3-6(a) plots the historical values of the annual discount rate versus the year in which they were measured. Different distributions were fitted to the historical data and compared by using a goodness-of-fit two-sided Kolmogrov-Smirnov test (Soong 2004). In particular, the Weibull, normal, and lognormal distributions provided the best fit to the data, with *p*-values equal to 0.94, 0.51, and 0.33, respectively, and test statistics equal to 0.06, 0.09, and 0.11, respectively. Figure 3-6(b) compares the ECDF of the annual discount rate

and the numerical CDFs for the fitted analytical distributions. Based on the results of the two-sided Kolmogorov-Smirnov test, none of these distributions can be rejected. In addition, the Weibull distribution provides the best fit to the historical data, followed by the normal and the lognormal distributions.

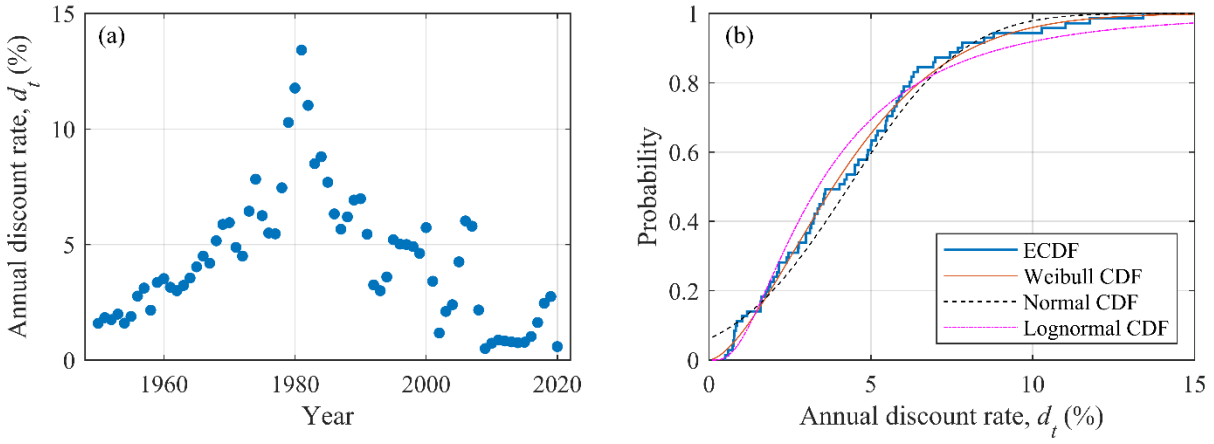


Figure 3-6. Variability of annual discount rate: (a) historical annual discount rates for the United States during the period 1950-2020, and (b) fitting of different probability distributions to the historical data.

Historical data also indicate that annual discount rates in subsequent years are highly positively correlated (as large changes of the annual discount rate between any given year and the following one are rare, with only two years out of 71 exhibiting a change in discount rate larger in absolute value than the sample standard deviation), and that this correlation decays rapidly for increasing intervals. In order to account at least in an approximate manner for this correlation, the following correlation coefficients were assumed between the annual discount rates for different years: $\rho_{\Delta t=1} = 0.75$ for consecutive years, $\rho_{\Delta t=2} = 0.50$ for years with $\Delta t = 2$ years, $\rho_{\Delta t=3} = 0.25$ for years with $\Delta t = 3$ years, and $\rho_{\Delta t>3} = 0$ for years with $\Delta t > 3$ years. This correlation structure was defined based on engineering judgement and to ensure that the correlation coefficient matrix is positive definite. More advanced statistical models to describe the time variability of annual discount rates would be beneficial; however, the development of these models is beyond the scope of the present study. By further assuming that the annual discount rate can be modeled as a stationary and ergodic stochastic process, the values of the 51 annual discount rates during the period 2015-2065 were sampled using a Nataf's model (Liu and Der Kiureghian 1986) based on each of the fitted

probability distributions and the correlation coefficient matrix previously described. The results of the loss analysis for the different cases considered in this study (constant annual discount rate $d_t =$ 1%, 3%, or 5%, and random annual discount rate based on a Weibull, normal, or lognormal distribution) are presented in Table 3-3 in terms of mean and standard deviation of the total losses. In this sensitivity analysis, the case with constant annual discount rate $d_t = 3\%$ is considered as the reference case.

Table 3-3. Sensitivity of loss analysis results to annual discount rate modeling for reference conditions by using accurate estimations and $\Delta t = 1$ year.

| Discount rate | Mean (USD) | Standard Deviation (USD) |
|---|---|---|
| Constant = 1% | 120,532 | 94,824 |
| Constant = 3% | 72,831 | 61,714 |
| Constant = 5% | 48,097 | 46,210 |
| Random (Weibull) | 66,613 | 63,087 |
| Random (Normal) | 72,781 | 86,765 |
| Random (Lognormal) | 68,209 | 63,659 |

It is observed that the assumptions made on the annual discount rates have a very large effect on the loss analysis results. In particular, when different constant values are assumed, the observed total loss changes are contained between -34.0% and +65.5% for the mean, and between -25.1% and +53.7% for the standard deviation. The variability associated with the use of different statistical models is not negligible but significantly smaller for the mean and slightly smaller for the standard deviation than that obtained by assuming different constant values for the annual discount rate. In particular, when different probability distributions are assumed, the observed total loss changes are contained between -8.5% and -0.1% for the mean, and between +2.2% and +40.6% for the standard deviation. All cases based on random annual discount rates provide expected total losses that are lower than (and relatively close to) those for constant $d_t = 3\%$, and higher than those for constant $d_t = 5\%$. This observation is consistent with the fact that the average value of the random annual discount rate, $\mu_{d_t}$, is $3\% < \mu_{d_t} = 4.32\% < 5\%$. In addition, all cases based on random annual discount rates yield standard deviations of the total losses that are higher than and relatively close to that corresponding to the reference case with $d_t = 3\%$. This observation is also consistent with the fact that modeling the annual discount rates as random quantities introduces additional variability in the estimates of the total losses. It is concluded that proper modeling of the annual discount rates is

crucial for obtaining reliable results in terms of total losses, and that further investigation of this issue in future studies is warranted.

### 3.4.4. Sensitivity of loss analysis results to different locations

The sensitivity of the loss analysis results to different locations is investigated for the unretrofitted house under the climate change scenario RCP 8.5. The annual discount rate is assumed constant and equal to $d_t = 3\%$. The mean and standard deviation of the total losses are calculated using a time discretization $\Delta t = 1$ year and the accurate estimates. The loss analysis is repeated by moving the selected residential development to different locations along the US Gulf and Atlantic coasts. These locations are selected to correspond to the coastal mileposts at 185.2 km (100 nautical miles) intervals, spanning the US Gulf and Atlantic coasts from near Port Isabel, TX, to near Portland, ME, as shown in Figure 3-7(a). The means and standard deviations of the total losses are reported in Figure 3-7(b), where the reference conditions corresponding to Pinellas Park, FL, are identified by a vertical dashed line.

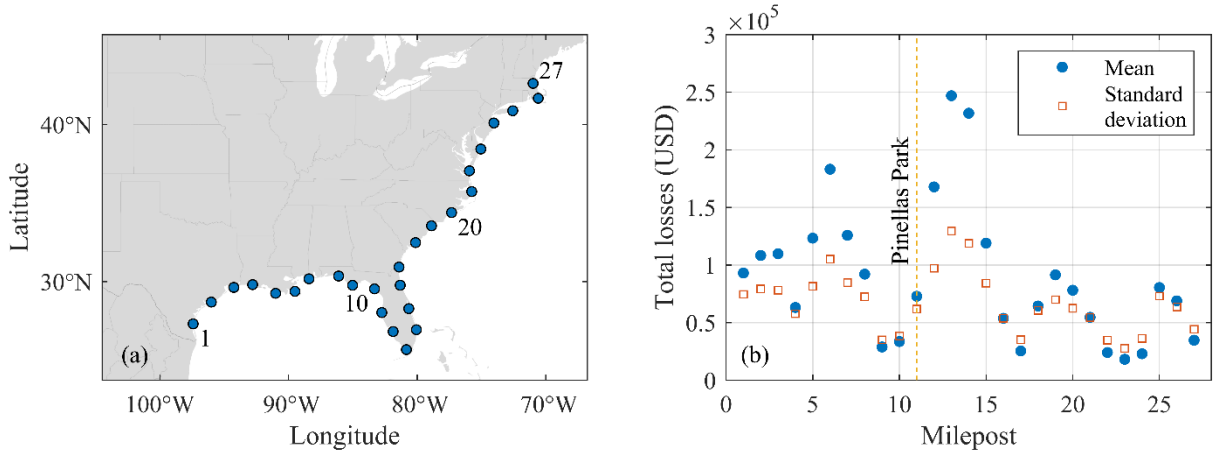


Figure 3-7. Loss analysis results for the unretrofitted benchmark house under RCP 8.5 with $d_t = 3\%$ and $\Delta t = 1$ year: (a) considered locations along the US Gulf and Atlantic coasts, and (b) means and standard deviations of the total losses.

It is observed that the total losses are significantly affected by the location, as expected based on empirical evidence and consistent with the hurricane wind speed statistics reported in Esmaeili and Barbato (2021a). In particular, locations close to New Orleans, LA, and the southernmost coast of Florida present

relatively high means (i.e., $183,079 and $246,909, respectively) and standard deviations (i.e., $105,082 and $129,495, respectively) of the total losses, when compared to other locations. The standard deviations of the total losses show a smaller variability (between $27,661 and $129,495, i.e., between -55.2% and +109.8% when compared with the reference conditions) and generally are slightly lower than and similar to the expected total losses (which vary between $18,143 and $246,909 i.e., between -75.1% and +239.0% when compared with the reference conditions), with the exception of few locations corresponding to relatively high expected total losses (for which the standard deviations are about half of the expected total losses) and relatively low expected total losses (for which the standard deviations are slightly higher than the expected total losses). It is concluded that the proposed extended PBHE framework captures the effects of different locations on the performance of low-rise single-family houses subject to hurricane hazard.

### 3.4.5. Sensitivity of loss analysis results to different climate change scenarios

The effects of different climate change scenarios on the performance of structures subject to hurricane hazard are another important component that needs to be quantified. This study investigates the sensitivity of the loss analysis results to the different climate scenarios considered in the IPCC AR5 (Stocker et al. 2013), i.e., RCP 2.6, 4.5, 6.0, and 8.5. This sensitivity is analyzed for the unretrofitted benchmark structure located in Pinellas Park, FL, by assuming $d_t = 3\%$ and $\Delta t = 1$ year, and by using the accurate estimates for the mean and standard deviation of the total losses.

Figure 3-8(a) and (b) report the undiscounted expected annual losses and the standard deviation of the annual losses, respectively, at 5-year intervals as a function of the global time for the period 2015-2065. It is observed that all climate change scenarios exhibit a gradual increase of both expected annual losses and standard deviation of the annual losses when compared to the corresponding values for year 2015 (i.e., $2,032 and $13,904 for mean and standard deviation, respectively), which corresponds to the stationary condition of no climate change. This increase is relatively small with small differences among different climate change scenarios between 2015 and 2030 (with increases contained between 5.7% and 24.0% for the mean, and between 4.3% and 11.5% for the standard deviation); however, the increase becomes more significant after 2030, with significant differences among the different climate change scenarios. In

particular, for 2065, the different climate scenarios yield increases contained between 43.5% and 137.0% for the mean annual losses, and between 22.0% and 59.7% for the standard deviations of the annual losses. This observation is consistent with the IPCC AR5 projections (Stocker et al. 2013), which suggest that the increases in average yearly sea temperature corresponding to different climate scenarios will have relatively small differences until 2030 and will diverge more significantly afterward. It is also observed that the standard deviations of the annual losses are almost an order of magnitude higher than the expected annual losses (with ratios between the standard deviations and the corresponding means contained between 4.61 and 6.84), which is consistent with the results reported in Unnikrishnan and Barbato (2016).

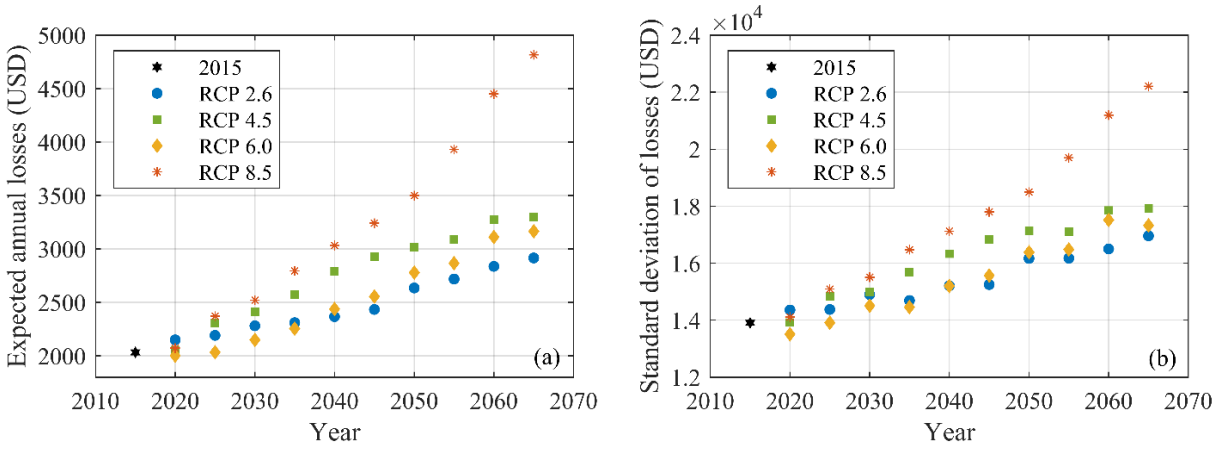


Figure 3-8. Sensitivity of loss analysis results to climate change scenarios for the unretrofitted benchmark house in Pinellas Park, FL: (a) expected annual losses and (b) standard deviation of annual losses.

Table 3-4 reports the means and standard deviations of the total losses for the different climate change scenarios considered in this study, and compares them with the corresponding results obtained by neglecting the effects of climate change. Both the mean and, in minor measure, the standard deviation of the total losses increase significantly when accounting for climate change effects. In fact, depending on the considered climate change scenario, the mean of the total losses increases between 13.2% and 38.1%, whereas the standard deviation of the total losses increases between 2.5% and 12.4%. In contrast to the results obtained for the statistics of the annual losses, the mean and standard deviation of the total losses are of the same order of magnitude, with ratios between the standard deviations and the corresponding

means contained between 0.85 and 1.04. It is concluded that the proposed extended PBHE framework is able to capture the effects of different climate change scenarios on the performance of low-rise single-family houses subject to hurricane hazard.

Table 3-4. Sensitivity of total loss analysis results to climate change scenarios for the unretrofitted benchmark house in Pinellas Park, FL, with $d_t = 3\%$ and $\Delta t = 1$ year over the period of 2015-2065.

| Climate change scenario | Mean (USD) | Standard Deviation (USD) |
|---|---|---|
| **No climate change** | 52,738 | 54,919 |
| **RCP 2.6** | 60,650 | 57,831 |
| **RCP 4.5** | 65,460 | 59,156 |
| **RCP 6.0** | 59,678 | 56,298 |
| **RCP 8.5** | 72,831 | 61,714 |

## 3.5. Application Example: Cost-Benefit Analysis of Different Storm Mitigation Strategies

The methodology proposed in this investigation is applied to perform a cost-benefit analysis of different storm mitigation strategies and design solutions considering the effects of climate change. The same benchmark structures used to perform the sensitivity analysis in previous sections is also used for this application example. The structure's site is assumed to be Pinella Park, FL, the considered climate change scenario is RCP 8.5, and the annual discount rate is assumed constant and equal to 3%. Accurate estimates are employed with a time discretization $\Delta t = 1$ year .

The retrofit scenarios are described in Table 3-5 are obtained through a combination of different storm mitigation strategies (also reported in Table 3-5), including: (1) two roof covers, i.e., asphalt shingles and clay tiles; (2) three different roof sheathing nailing solutions, i.e., 6d C6/12, 8d C6/12, and 8d C6/6; (3) two levels of protections for windows, i.e., without or with aluminum storm panels; and (4) two wall materials, i.e., light-frame wooden and masonry walls. Considering all possible combinations of the investigated storm mitigation strategies leads to a total of 24 retrofit scenarios (i.e., $r = 1, 2, \ldots, 24$). The statistical description (i.e., mean, coefficient of variation, and distribution type) of the strength for the different limit states are presented in Table 3-5 and were taken from the literature (Gurley et al. 2005; Datin et al. 2011; Shdid et al. 2011; Alphonso and Barbato 2014). The wind load parameters used in the MMCS

were adopted from Lopez et al. (2020). The full methodology for the calculation of the losses and benefits is described in Unnikrishnan and Barbato (2016); whereas the simulation of the *IM*s was performed based on predictive model presented in Esmaeili and Barbato (2021a). Finally, the cost of each different retrofit was obtained from the RSMeans national data adjusted for the specific considered location (Plotner 2017).

Table 3-5. Statistics of different retrofit scenarios and their limit states

| Component | Configuration | Limit state | Mean | COV | Distribution | Reference |
|---|---|---|---|---|---|---|
| Roof Cover | Tiles | Separation | 4.24 kPa | 0.17 | Tr. Normal[(a)] | Shdid et al. (2011) |
| Roof sheathing | 8d C6/12 | Separation | 6.20 kPa | 0.12 | Lognormal | Datin et al. (2011) |
| | 8d C6/6 | Separation | 9.83 kPa | 0.1 | Lognormal | Datin et al. (2011) |
| Windows | With panels | Impact failure | 0.496 kJ | 0.15 | Lognormal | Alphonso and Barbato (2014) |
| Roof-to-wall connection | Masonry | Tensile failure | 18.68 kN | 0.2 | Lognormal | Gurley et al. (2005) |
| Wall | Masonry | Combined uplift and bending | 18.00 kN/m | 0.2 | Tr. Normal[(a)] | Gurley et al. (2005) |
| | | | 1.31 kN | 0.2 | Tr. Normal[(a)] | Gurley et al. (2005) |

[(a)] Truncated normal distribution with lower truncation at zero.

Table 3-6 reports the retrofit costs (modeled here as a constant for each individual retrofit scenario), the mean and standard deviation of total losses, and the mean and standard deviation of the benefits associated with all 24 retrofit scenarios. Scenario #1 corresponds to the unretrofitted benchmark structure, for which the benefits are equal to zero. A positive value of the benefits corresponds to a retrofit scenario for which the reduction in losses is lower than the initial cost of the retrofit, whereas a negative value of the benefits indicates a retrofit scenario for which the initial retrofit cost is higher than the total loss reduction.

From the results reported in Table 3-6, it is observed that the costs associated with clay tiles and masonry walls (i.e., \$10,800 and \$19,000, respectively) are higher than the reduction in total losses produced by the use of each of these mitigation strategies (i.e., \$6,035 and \$1,377, respectively). The most effective standalone mitigation strategy is the use of aluminum storm panels to protect windows from windborne debris impacts, with an initial cost of \$1,600 and a total loss reduction of \$9,268. The use of stronger nailing patterns for the roof sheathing is also beneficial, with initial costs and total loss reductions equal to \$5,600 and \$7,328, respectively, for 8d C6/12, and \$5,800 and \$7,078 for 8d C6/6. As a result, the best retrofit scenario corresponds to case $r = 9$, i.e., to the combined use of the 8d C6/6 nailing pattern and

aluminum storm panels to protect windows, for which the initial cost is $7,600 and the total loss reduction is $17,502, leading to a benefit mean equal to $9,903. It is also observed that the standard deviations of the benefit, which range between $72,106 and $85,647, are always significantly higher in absolute value than the corresponding expected benefits, indicating a very large variability of the benefits associated with any retrofit mitigation strategy.

Table 3-6. Cost-benefit analysis results for the benchmark structure located in Pinellas Park, FL, for RCP 8.5, with $d_t = 3\%$ and $\Delta t = 1$ year over the period of 2015-2065, assuming constant initial retrofit costs.

| r | Material | Window protection | Roof cover | Roof nailing pattern | Retrofit cost ($) | $m_{L_r}$ ($) | $s_{L_r}$ ($) | $m_{B_{1,r}}$ ($) | $s_{B_{1,r}}$ ($) |
|---|---|---|---|---|---|---|---|---|---|
| 1 | Wood | No | Shingles | 6d C6/12 | 0 | 72,831 | 61,714 | 0 | 0 |
| 2 | | | | 8d C6/12 | 5,600 | 65,503 | 55,343 | 1,728 | 82,818 |
| 3 | | | | 8d C6/6 | 5,800 | 65,753 | 54,941 | 1,278 | 82,699 |
| 4 | | | Tiles | 6d C6/12 | 10,800 | 66,796 | 58,234 | -4,765 | 84,896 |
| 5 | | | | 8d C6/12 | 16,600 | 55,847 | 48,430 | 384 | 78,577 |
| 6 | | | | 8d C6/6 | 16,800 | 55,409 | 48,220 | 623 | 78,374 |
| 7 | | yes | Shingles | 6d C6/12 | 1,600 | 63,563 | 56,762 | 7,669 | 83,513 |
| 8 | | | | 8d C6/12 | 7,400 | 55,938 | 49,619 | 9,494 | 79,179 |
| 9 | | | | 8d C6/6 | 7,600 | 55,329 | 49,297 | 9,903 | 79,014 |
| 10 | | | Tiles | 6d C6/12 | 12,600 | 57,327 | 53,121 | 2,905 | 81,379 |
| 11 | | | | 8d C6/12 | 18,400 | 47,163 | 43,023 | 7,269 | 75,200 |
| 12 | | | | 8d C6/6 | 18,600 | 46,645 | 42,760 | 7,586 | 75,137 |
| 13 | Masonry | No | Shingles | 6d C6/12 | 19,000 | 71,454 | 59,539 | -17,623 | 85,647 |
| 14 | | | | 8d C6/12 | 24,800 | 63,828 | 52,535 | -15,797 | 80,850 |
| 15 | | | | 8d C6/6 | 25,000 | 64,067 | 52,678 | -16,236 | 80,940 |
| 16 | | | Tiles | 6d C6/12 | 30,000 | 64,108 | 55,761 | -21,277 | 83,261 |
| 17 | | | | 8d C6/12 | 35,800 | 52,217 | 43,719 | -15,186 | 75,649 |
| 18 | | | | 8d C6/6 | 36,000 | 52,188 | 43,695 | -15,356 | 75,595 |
| 19 | | yes | Shingles | 6d C6/12 | 20,800 | 60,909 | 53,119 | -8,878 | 81,384 |
| 20 | | | | 8d C6/12 | 26,600 | 53,774 | 46,573 | -7,543 | 77,400 |
| 21 | | | | 8d C6/6 | 26,800 | 53,281 | 46,530 | -7,249 | 77,301 |
| 22 | | | Tiles | 6d C6/12 | 31,800 | 54,125 | 49,194 | -13,093 | 78,975 |
| 23 | | | | 8d C6/12 | 37,600 | 43,518 | 37,483 | -8,287 | 72,108 |
| 24 | | | | 8d C6/6 | 37,800 | 43,113 | 37,402 | -8,081 | 72,106 |

These results are also consistent with those reported in Unnikrishnan and Barbato (2016) and are caused by the fact that the damage to a structure from hurricane wind and windborne debris hazard is often negligible (when the structure is not directly hit by a storm) or very large (when the structure is directly hit

by a storm). Thus, other total loss and benefit statistics beyond mean and standard deviation (e.g., different fractiles, or total losses conditional on at least one named storm hitting a given structure) may be necessary to inform homeowners' decision and/or insurance premium/deductibles calculations. It is noted here that the methodology proposed and illustrated in this study is capable of providing this additional information, which can be easily extracted from the MMCS results based on the specific application of interest. The results presented for this application example are specifically valid for the particular combination of house, residential development, location, and climate scenario. Differences in any of these items can (and most likely will) produce a different selection for the optimal retrofit scenario. However, the general methodology proposed in this study is able to account for all of these differences and identify the optimal retrofit scenario for each specific case of interest.

In order to investigate the effects of the retrofit cost variability, the cost-benefit analysis was repeated for retrofit scenario $r = 9$ by modeling the retrofit cost as a random variable with mean $\mu_{C_9} = \$7,600$, i.e., equal to the constant value used in Table 3-6 and estimated from RSMeans (Plotner 2017), and described by different probability distributions, with different support domains and different COV. The modeling assumptions and the corresponding cost-benefit analysis results are reported in Table 3-7.

Table 3-7. Effects of retrofit cost variability on cost-benefit analysis performed for retrofit scenario $r = 9$.

| Distribution | Range | COV = 10% | | COV = 20% | | COV = 30% | |
|---|---|---|---|---|---|---|---|
| | | $m_{B_{1,9}}$ (\$) | $s_{B_{1,9}}$ (\$) | $m_{B_{1,9}}$ (\$) | $s_{B_{1,9}}$ (\$) | $m_{B_{1,9}}$ (\$) | $s_{B_{1,9}}$ (\$) |
| Truncated Normal | $[0.0,\infty)$ | 9904 | 79017 | 9903 | 79032 | 9905 | 79047 |
| Truncated Normal | $[0.5,1.5]\cdot\mu_{C_9}$ | 9902 | 79016 | 9907 | 79020 | 9908 | 79035 |
| Lognormal | $(0.0,\infty)$ | 9901 | 79019 | 9901 | 79027 | 9907 | 79040 |
| Translated Beta | $[0.5,1.5]\cdot\mu_{C_9}$ | 9903 | 79015 | 9903 | 79016 | 9903 | 79022 |
| Truncated Gumbel | $[0.0,\infty)$ | 9902 | 79017 | 9909 | 79034 | 9900 | 79058 |
| Weibull | $[0.0,\infty)$ | 9904 | 79018 | 9900 | 79019 | 9903 | 79057 |

It is noted that, for the truncated distributions, the means and COVs reported in Table 3-7 are those of the corresponding parent distributions. Although extreme value distributions, such as Gumbel and Weibull distributions, are generally considered more suitable to describe cost data (Ballesteros-Pérez et al. 2020),

this sensitivity analysis included also other commonly used distributions, such as normal, lognormal, and beta distributions, in order to gain a better understanding of the relative effects of distribution type and overall variability. It is observed that retrofit cost variability has only very small effects on the cost-benefit analysis results, with relative changes contained between -0.03% and 0.06% for the expected benefits, and between 0.01% and 0.06% for the standard deviation of the benefits.

## 3.6. Conclusions

This study generalizes the performance-based hurricane engineering framework to account for nonstationarity induced by climate change effects and structural aging. The new extended framework is employed to investigate the effects of climate change on hurricane wind-induced losses for single family houses along the US Gulf and Atlantic coasts. The nonstationary wind speed model considering the effects of climate change is adopted from a previous study by the authors, which was based on the climate change scenarios considered in the 5$^{th}$ Assessment Report of the Intergovernmental Panel on Climate Change. A multi-layer Monte Carlo simulation approach is used to evaluate the mean and standard deviation of the total losses induced by hurricane wind and windborne debris hazards, for which two sets of equations are proposed: (1) a set of accurate estimates, which rigorously account for the correlation between annual losses at different years, and (2) a set of approximate estimates, which neglect the correlation between annual losses at different years. The newly proposed framework is applied for the loss analysis of a benchmark single-family house with service design life between 2015 and 2065. The sensitivity of the methodology results is investigated with respect to (1) accurate versus simplified estimates, (2) time discretization and interpolation method for intermediate years, (3) modeling assumptions for the annual discount rate, (4) location, and (5) climate change scenario. It is found that the sensitivity of the loss analysis results to accurate versus simplified estimates, time discretization, and interpolation method is negligible (i.e., changes smaller than 0.1% for both means and standard deviations), which suggests that the proposed methodology is robust with respect to different modeling assumptions. However, the loss analysis results are very sensitive (with changes between -34.0% and +65.5% for the mean, and between -25.1% and +53.7% for the standard deviation) to different modeling assumptions for the annual discount rate. Thus

further investigations to determine an appropriate model for the annual discount rate are warranted. As expected, the loss analysis results are highly sensitive to the building's location, with changes ranging between -75.1% and +239.0% for the total loss means and between -55.2% and +109.8% for the standard deviations of the total losses when compared with the reference location of Pinellas Park, FL. The sensitivity of the loss analysis results to different climate change scenarios is also significant, with increases contained between 13.2% and 38.1% for the total loss means, and between 2.5% and 12.4% for the standard deviations of the total losses. It is concluded that the proposed methodology can capture the effects of different locations and different climate change scenarios on the performance of low-rise single-family houses subject to hurricane hazard.

The proposed methodology is also used to compare the cost-benefit performance of different mitigation strategies (i.e., two roof covers, three roof sheathing nailing solutions, two levels of protection for windows, and two wall materials) and their combinations (for a total of 24 different retrofit scenarios) for the same benchmark home previously considered. It is shown that the proposed framework can be reliably employed to identify hurricane mitigation strategies that are beneficial over the design service life of the house, and in particular to select the optimal retrofit scenario for any specific combination of structures, residential developments, locations, and climate scenarios.

Whereas the general framework developed in this study is able to account for nonstationarity of both hazard (i.e., due to climate change) and vulnerability (i.e., due to structural aging), the application examples presented in this study neglect the effects of structural aging. It is recommended that future studies focus on this particular aspect of the problem, to identify and resolve specific issues that may rise when including structural aging, as well as to quantify the relative importance of climate change and structural aging on the performance of single-family homes subject to hurricane hazard in the US.

# Chapter 4. Hurricane performance assessment of single-family houses considering the combined effects of climate change and structural aging

## 4.1. Introduction

The US Gulf and Atlantic coasts are frequently affected by severe tropical storms, locally known as hurricanes, which cause severe damage to structures and infrastructure, resulting in several billion dollars of economic losses and numerous deaths every year. During the years 2018 to 2020, the National Oceanic and Atmospheric Administration (NOAA) reported about 50 hurricane events with losses exceeding $1 billion. Recent hurricanes such as Hurricane Katrina (2005) with $172.5 billion, Hurricane Harvey (2017) with $133.8 billion, and Hurricane Maria (2017) with $96.3 billion of estimated losses, expressed in 2021 Consumer Price Index-adjusted dollars, are the costliest hurricane events in US history. Since the beginning of the 20th century, hurricane-induced losses have increased significantly due to the combined effects of the population increase in hurricane-prone regions and the intensification of hurricanes (Klotzbach et al. 2018).

Climate change is responsible for several changes in the planet's climatological regime, which affect air temperature, sea surface temperature, precipitation patterns, and sea water level. Many studies have shown a direct relationship between climate change and intensified hurricane actions (Emanuel 2013; Li and Stewart 2011; Mudd et al. 2014). Esmaeili and Barbato (2021a) developed a predictive model for evaluating the effects of different climate change scenarios on hurricane wind hazards for the US Gulf and Atlantic coasts, based on the 5th assessment report (AR5) prepared by the Intergovernmental Panel on Climate Change (IPCC) (Stocker et al. 2013). They used this model to estimate the wind speeds corresponding to the return periods of different risk category structures according to ASCE 7-16 and showed that, by 2060 and along the US Gulf and Atlantic coasts, the design wind forces could experience an increase between 55% and 59% in the worst case scenario.

The performance of structures subject to hurricane hazard is also significantly affected by the degradation that structural and non-structural components can experience during their service design life (Ghosh and Padgett 2010). This issue is particularly severe for light-frame wooden houses, which represent the majority of the US housing stock (Marcin 1987) and are very vulnerable to hurricane wind and wind debris hazard (Amini and Memari 2020). This type of structures is subject to environmental stressors such as sunlight, temperature variation, wind, humidity, atmospheric pollutants, and to biological stressors due to the growth of damaging organisms (Berdahl et al. 2008; Feist 1990; Foliente et al. 2002; Liu et al. 2019; Stirling et al. 2017; Viitanen et al. 2010; Yildiz et al. 2011). The structural aging phenomena that affect the most the performance of light-frame wooden houses subject to hurricane wind hazard are sealant degradation for roof shingles (Dixon et al. 2013a, 2013b), decay of the wooden components (Viitanen et al. 2010), and nail pull-out strength decay (Alhawamdeh and Shao 2021).

Roof cover elements are subject to weathering, with asphalt shingles being the most common roofing material in Northern America (Sackey and Kim 2018). Dixon et al. (2014a) performed a set of experiments on naturally and artificially aged shingles and concluded that changes in the wind uplift resistance are not significant for fully-adhered sealant strips, as they maintained enough residual capacity to survive their expected design wind speed even after nearly a decade of aging. However, for partially-unsealed shingles, the reduction in wind uplift resistance can be significant depending on the amount of lost adhesion, as wind is forced through gaps in the unsealed sealant strip and increases the underside pressure on the affected shingle (Peterka et al. 1997). The on-site investigation of naturally aged roof shingles by Dixon et al. (2013a) showed that partial unsealing is a common phenomenon for field roof shingles aged more than 6 years, with percentage of unsealed shingles as high as 79% for 20-year old roofs. They observed that the uplift strength decayed due to sealant degradation over the years, while the effects of other environmental stressors (i.e., ultraviolet light from the sun, temperature variation, and dry-thaw cycles from precipitations) were negligible. The weathering effect on sealant unseating of hip and ridge cap shingles appeared to be

uncorrelated with age and to depend on the installation method (Dixon et al. 2014b). This unseating can cause water leakage and can damage the roof sheathing.

The aging phenomena of wooden components can be identified as the irreversible changes in the mechanical, physical, and chemical properties of the material due to applied environmental and biological stressors, which generally induce a deterioration of the structural performance of the components (Kránitz et al. 2016). Sonderegger et al. (2015) investigated the natural aging of several types of wood under natural weathering conditions and observed high variation in both physical and mechanical properties for each species. In the absence of environmental and biological stressors, the mechanical properties of wood (e.g., compressive strength, Young's modulus, shear strength) do not change significantly during the service design life of a house, although some wood species might become more brittle (Kránitz et al. 2016). Biological stressors were identified as the main cause of strength degradation in wooden structures, which are generally described in terms of mass loss (Foliente G.C., Leicester R.H., Wang C., Mackenzie C., 2002; Viitanen et al. 2010). Persistent exposure to high humidity was identified as an important factor for biodeterioration of wood due to mold and fungi decay (Viitanen et al. 2010). Stirling et al. (2017) performed a detailed literature review on organisms that can affect western red cedar wood and identified fungi as one of the most damaging ones. Glass and Zelinka (2010) reported the moisture content of several wood species in equilibrium condition at various temperatures and different levels of humidity, and provided experimental evidence of moisture content effects on wooden physical properties. Witomski et al. (2016) investigated the changes in strength of Scots pine wood due to mass loss caused by brown rot and white rot fungi and observed an exponential trend between mass loss and changes in the bending strength. They found that the wood bending strength reduces in half as 7% and 20% of the wooden mass decays due to brown rot and white rot, respectively. Curling et al. (2002) showed that wood mass loss has significant effects on the modulus of rupture (MOR), modulus of elasticity (MOE), and work to maximum load of different woods. Research has shown that covering wooden components in light-frame house with paint, stucco, or other protective elements, can significantly reduce the effects of environmental and biological

stressors (Sekino et al. 2014). By contrast, even small damages to these protective layers can significantly increase the weathering of wooden components, e.g., by allowing water accumulation in vicinity of the wood, which significantly increases biological activities in the wood (Stirling et al. 2017, Droin et al. 1988), swelling due to changes in the equilibrium water content, and possible freeze-thaw cycles in cold weather, with potential propagation of cracks caused by the expansion of frozen water (Berdahl et al. 2008).

The mechanism of nail pull-out strength decay is quite complex and depends on nail corrosion, wood decay, and low-/high-cycle fatigue produced by cyclic loads like wind (Zelinka 2013; Prevatt et al. 2014; Rammer and Zelinka 2015). Zelinka and Rammer (2012) proposed a model for the lateral joint strength as a function of the nail corrosion rate. According to this model, fasteners are most likely to fail through a combination of wood-bearing failure and the formation of a plastic hinge in the fasteners. Strength loss is highly dependent on the corrosion rate, which can be described as time-dependent or moisture-dependent. They concluded that a moisture-dependent corrosion rate model used in conjunction with hygrothermal simulations provides the most accurate prediction of the corrosion rate and, thus, of the lateral strength loss of joints. Takanashi et al. (2017) investigated the withdrawal strength of nail joints considering nail corrosion and wood decay due to brown rot. They found that the rust formed around the nail can increase the withdrawal strength of the nail up to a 2% reduction of the nail shank diameter and can protect the nail from diameter reduction; by contrast, the wood decay can cause a significant reduction in the withdrawal strength of the nail, with an average strength decrease equal to 35% and 47% for joints nailed in the radial and tangential directions of the wood fibers, respectively, and mass loss contained between 0% and 20%. Wind-induced cyclic loads can have very different effects on different structural and cladding components, e.g., the mechanical properties of some structural roof timber elements were unaffected even after 85 years of service life (Fridley et al. 1996). Similarly, for the wooden shear walls, the dominant failure mode was identified as nail withdrawal rather than fatigue failure (Ming et al. 2001). Several studies have focused on the effects of cyclic loading on connection strength, as it was found that cyclic loading can cause a reduction of the contact surface between the fastener and the wooden material, thus reducing the pull-out strength of

the connection (Alhawamdeh and Shao 2021; Kent et al. 2005; Soltis and Mtenga 1985). Alhawamdeh and Shao (2021) investigated the effects of cyclic uplift loading on the roof-to-wall connections and concluded that the strength of the connection can decrease up to 60% after 1,000,000 cycles of loading and unloading. Datin et al. (2011) indicated that, although there is anecdotal evidence to suggest the roof sheathing panels experience fatigue-like failures under wind loads, they were not able to find any wind loading tests that have examined this type of failure.

The use of performance-based approaches in hurricane engineering has been shown to provide a rigorous and flexible framework to account for all uncertainties affecting the performance of structures (Barbato et al. 2013; Unnikrishnan and Barbato 2013, 2015, 2016a, 2016b, 2017). More recently, the performance-based hurricane engineering (PBHE) framework originally proposed by Barbato et al. (2013) was extended to account for the nonstationarity of both hurricane wind hazard, which is driven by climate change, and vulnerability, which is due to structural aging (Esmaeili and Barbato 2021b). This extended framework was applied to perform a hurricane-induced loss analysis and a cost-benefit analysis of hurricane mitigation strategies for single-family houses in the US Gulf and Atlantic coasts when considering the hurricane hazard's nonstationarity only. This study describes a proposed methodology that combines the extended PBHE framework developed in Esmaeili and Barbato (2021b), the predictive model for hurricane wind speed distributions under changing climate proposed in Esmaeili and Barbato (2021a), and several existing models for structural aging of different components of light-frame wooden houses. This investigation applies the proposed methodology to the analysis of hurricane-induced losses for a single-family light-frame wooden house located in Pinellas Park, FL. The individual and joint effects on hurricane-induced losses of nonstationarity in the hurricane wind hazard and in the structural vulnerability are investigated and quantified, including the case in which structural aging is modeled as dependent on climate change.

## 4.2. Novelty and Relevance

This study presents the first implementation of the extended PBHE framework to account for the nonstationarity of both hurricane wind hazard and structural aging. The implications of different assumptions on nonstationarity are investigated and quantified for a low-rise single-family light-frame wooden house.

The present study provides a simulation-based approach to assess the performance of structural systems under nonstationary hazards and vulnerability. The extended PBHE methodology used in this study is specialized for hurricane wind hazards and single-family light-frame wooden houses, which represent a significant contributor to societal losses due to hurricane events. In addition, the proposed framework can be further extended to other (individual and multiple) hazards and structural typologies, providing the blueprints for advancing performance-based design as a rigorous tool to address the societal needs for developing a climate resilient infrastructure.

## 4.3. Extended PBHE framework

The general methodology employed in this study was developed in Esmaeili and Barbato (2021b) as an extension of the original PBHE framework by Barbato et al. (2013). The performance of a target structure is described by a decision variable $(DV)$, which depends on damage measures $(DM)$, engineering demand parameters $(EDP)$, intensity measures $(IM)$, structural parameters $(SP)$, interaction parameters $(IP)$, and a vector of climatological parameters $(C)$. The probabilistic description of the selected $DV$ is given by:

$$\begin{aligned} G\left(DV_{t,\tau}\right) = \int\int\int\int\int\int G\left(DV_{t,\tau}\left|DM_{\tau}\right.\right)\cdot f\left(DM_{\tau}\left|EDP,C_{t}\right.\right) \\ \cdot f\left(EDP\left|IM,IP,SP_{\tau}\right.\right)\cdot f\left(IP\left|IM,SP_{\tau}\right.\right)\cdot f\left(IM\,|\,C_{t}\right) \\ \cdot f\left(SP_{\tau}\,|\,C_{t}\right)\cdot f\left(C_{t}\right)\cdot \mathrm{d}DM_{\tau}\cdot \mathrm{d}EDP\cdot \mathrm{d}IM\cdot \mathrm{d}IP\cdot \mathrm{d}SP_{\tau}\cdot \mathrm{d}C_{t} \end{aligned} \tag{4.1}$$

where a subscript $t$ denotes explicit dependence on the global time scale, generally corresponding to the calendar year; a subscript $\tau$ denotes explicit dependence on the structural time scale, i.e., the age in years of the structure of interest; $G(\bullet)$ = complementary cumulative distribution function (CDF); $G(\bullet|\bullet)$ = conditional complementary CDF; $f(\bullet)$ = probability density function (PDF); and $f(\bullet|\bullet)$ = conditional probability density function. The climatological parameters, $C_t$, depend explicitly on the global time scale to account for the effects of climate change. The structural parameters and damage measures, $SP_\tau$ and $DM_\tau$, dependent explicitly on the structural time scale, as they are changing as the structure ages. The decision variable, $DV_{t,\tau}$, depends explicitly on both global and structural time scales to account for the variability of costs and discount rates in time, as well as for effect of aging on the structure. All other parameters in Eq. (4.1) depend on one or both time scales implicitly (Esmaeili and Barbato 2021b). In this study, the solution of Eq. (4.1) is obtained using a multilayer Monte Carlo simulation approach (Barbato et al. 2013, Unnikrishnan and Barbato 2016, 2017).

## 4.4. Modeling of structural aging

This study adopts structural aging models available in or derived from the literature for low-rise light-frame wooden houses. For this specific structural typology, the structural parameters (i.e., wind exposure factor, external pressure coefficients, and internal pressure coefficients) can be considered as stationary, as they are affected more by breaching of the building envelopes induced by hazard chains (Barbato et al. 2013) than by structural aging. However, structural aging can significantly affect the strength associated with the different limit states (i.e., the damage measures) that control the performance of these structures. The limit states and the corresponding structural aging effects considered in this study are reported in Table 4-1.

Table 4-1. Limit states and corresponding structural aging effects considered in this study

| Component | Limit state | Degradation mechanism | Controlling parameter | Reference |
|---|---|---|---|---|
| Roof cover (shingles) | Separation | Sealant | Age | Dixon et al. (2014b) |

| | | | | |
|---|---|---|---|---|
| Roof sheathing (6d C6/12) | Separation | Nail strength | Mass loss | Takanashi et al. (2017) |
| Windows (unprotected) | Pressure failure | - | - | - |
| | Impact failure | - | - | - |
| Doors (unprotected) | Pressure failure | - | - | - |
| Roof-to-wall connection | Tension failure | Nail strength | Fatigue | Alhawamdeh & Shao (2021) |
| Wall | Uplift failure | - | - | - |
| | Lateral failure | - | - | - |
| Wall sheathing | Pressure failure | Nail strength | Mass loss | Takanashi et al. (2017) |
| | Impact failure | Wood decay | MOR | Curling et al. (2002) |

The pertinent limit states were identified from the literature (Unnikrishnan and Barbato 2016, Esmaeili and Barbato 2021b). The strength degradation models adopted in this study were derived by using data from the literature, as indicated in Table 4-1. The limit states corresponding to windows, doors, and walls were assumed to not undergo degradation, as the authors were unable to identify any studies that quantified their degradation in the literature. This assumption most likely underestimates the effects of structural aging and requires additional focused studies to quantify this underestimation and determine if the assumption is acceptable for engineering applications.

### 4.4.1. Strength degradation for asphalt shingles due to sealant aging

The model for the strength loss of shingles is derived by using the data in Dixon et al. (2014b), which reports the percentage of fully or partially unsealed shingles observed in field inspections of roofs as a function of the roof shingle age. The ratio of unsealed field shingles is given by:

$$R_{shingle}\left(\tau_s\right)=\begin{cases}0 & \tau_s \le 6 \text{ years}\\ 0.0 < 0.0257\cdot\tau_s - 0.1542 + \varepsilon_{shingle} \le 1.0 & \tau_s > 6 \text{ years}\end{cases} \tag{4.2}$$

where $\varepsilon_{shingle}$ is a random variable assumed to follow a normal distribution with zero mean and standard deviation equal to the regression error of the fitting function given in Eq. (4.2) and equal to 0.2, and $\tau_s$ the age of the shingles. In this study, the different behavior reported in Dixon et al. (2014b) for ridge and hip shingles is neglected, as they represent a relatively small portion of the roof and appear to be not affected by weathering. The non-stationary uplift strength of roof shingles is modeled as:

$$F_{shingle}\left(\tau_s\right)=F_{shingle,0}\cdot\left[1-R_{shingle}\left(\tau_s\right)\cdot R_{unsealing}\right] \tag{4.3}$$

in which $F_{shingle,0}$ represents the random variable describing the uplift strength of the shingles for the as-built structure, and $R_{unsealing}$ is random variable used to describe the relative portion of unsealing for all roof shingles. Due to lack of data on the statistics of $R_{unsealing}$, this quantity is modeled in this study as a standard uniform random variable.

### 4.4.2. rength degradation due to wood decay

The strength degradation due to wood decay is controlled by the mass loss of wood, which affects the MOR of the wood. This study employs the empirical mass loss decay model under variable conditions, which was developed by Viitanen et al. (2010) for brown rot in pine sapwood as a function of relative humidity, *RH*, air temperature in °C, *T*, and age of the wood in hours, $\tau_w$ . The decay process is described by an activation parameter, $\alpha(\tau_w)$, which assumes values between zero (before any weathering of the wood) and 1 (when mass loss is initiated). Both activation and mass loss processes occur only when $RH \geq 95\%$ and $T \geq 0$℃. The activation process is described as follows:

$$\alpha(\tau_w) = \sum_{i=1}^{n} \Delta\alpha_i \tag{4.4}$$

where

$$\tau_w = \sum_{i=1}^{n} \Delta\tau_{w,i}$$

$$\Delta\alpha_i = \begin{cases} \dfrac{\Delta\tau_{w,i}}{\tau_{w,crit}(RH,T)} & \text{if } T > 0\,^{\circ}\text{C},\ RH > 95\%, \text{ and } \alpha < 1 \\ 0 & \text{if } T > 0\,^{\circ}\text{C},\ RH > 95\%, \text{ and } \alpha = 1 \\ -\dfrac{\Delta\tau_{w,i}}{17520} & \text{otherwise} \end{cases} \tag{4.5}$$

$$\tau_{w,crit}(RH,T) = \frac{2.3T + 0.035RH - 0.024T \cdot RH}{-42.9 + 0.14T + 0.45RH} \cdot 720$$

The mass loss percentage, $ML(\tau_w)$, is given by:

$$ML(\tau_w) = \sum_{i=1}^{n} \left[ \left. \frac{dML(RH,T)}{d\tau} \right|_i \cdot \Delta\tau_{w,i} \right] \tag{4.6}$$

where

$$\left. \frac{dML(RH,T)}{d\tau} \right|_i = \begin{cases} -0.0596 + 1.96\times10^{-4} \cdot T + 6.25\times10^{-4} \cdot RH & \text{if } \alpha(\tau_w) = 1 \\ 0 & \text{if } \alpha(\tau_w) < 1 \end{cases} \tag{4.7}$$

In this study, the mass loss percentage is estimated through a simulation procedure that generates a time series of hourly air temperatures and relative humidity over a given year for a given average air temperature of the year under consideration. These time series are used to fit a distribution to the wood mass loss percentage for a given year and a given climate scenario, which is then used within the multilayer Monte Carlo simulation procedure for the total loss estimation. The detailed description of this simulation procedure is provided in the Appendix.

The wooden mass loss produces a relative reduction in the MOR, $R_{MOR}(\tau_w)$, which can be modeled as a random variable defined between zero and 1 by using the experimental data reported by Curling et al. (2002) for southern pine wood affected by brown rot. The following regression equation is proposed:

$$R_{MOR}(\tau_w) = \begin{cases} 0.01 \cdot \exp\left\{0.5453 \cdot \log\left[ML(\tau_w)\right] + 2.7375\right\} + \varepsilon_{\Delta F} \le 1 & 0 \le ML(\tau_w) \le 40 \\ 1 & ML(\tau_w) > 40 \end{cases} \tag{4.8}$$

where $\varepsilon_{\Delta F}$ is described by a normal random variable with zero mean and standard deviation equal to 0.011.

The impact strength of the wall sheathing, $F_{iws}(\tau_w)$, is assumed to be proportional to the MOR and given by:

$$F_{iws}(\tau_w) = F_{iws,0} \cdot \left[1 - R_{MOR}(\tau_w) \cdot R_{ws,rot}\right] \tag{4.9}$$

in which $F_{iws,0}$ represents the random variable describing the impact strength of the wall sheathing for the as-built structure, and $R_{ws,rot}$ is a random variable used to describe the relative portion of wall sheathing affected by rot.

### 4.4.3. Strength degradation due to nail pull-out strength decay

In this study, only the nail pull-out strength degradation mechanisms associated with wood decay and fatigue due to wind-induced cyclic loads were considered. In fact, a preliminary analysis of the rust formation on the nail perimeter based on the corrosion model proposed by Zelinka (2013) indicated that changes in the nail diameter are significantly smaller than 0.4% over the 50-year service design life of the structure.

The pull-out strength degradation due to wooden mass loss was modeled using the data presented in Takanashi et al. (2017), which reported the reduction in withdrawal strength for joints with nails in the radial and tangential direction to the annual rings (i.e., radial and tangential joints, respectively) as a function of $ML$. Based on the combined data from both radial and tangential joints, the withdrawal strength reduction due to wood decay, $R_{nail,w}(\tau_w)$, is given by:

$$R_{nail,w}(\tau_w) = \begin{cases} -0.0313 \cdot \tau_w + 1.0 + \varepsilon_{R_{nail,w}} & \text{if } 0 \le ML(\tau_w) \le 40 \\ 1 & ML(\tau_w) > 40 \end{cases} \tag{4.10}$$

where $\varepsilon_{R_{nail,w}}$ is the regression error, which is assumed to follow a normal distribution with mean equal to zero and standard deviations equal to 0.218.

The separation strength of the roof sheathing, $F_{rs}(\tau_w)$, and of the wall sheathing subject to pressure action, $F_{pws}(\tau_w)$, are assumed to be proportional to the residual withdrawal strength of the nails and are given by:

$$F_{rs}(\tau_w) = F_{rs,0} \cdot \left[1 - R_{nail,w}(\tau_w) \cdot R_{rs,rot}\right] \tag{4.11}$$

$$F_{pws}(\tau_w) = F_{pws,0} \cdot \left[1 - R_{nail,w}(\tau_w) \cdot R_{ws,rot}\right] \tag{4.12}$$

respectively, in which $F_{rs,0}$ and $F_{pws,0}$ represent the random variables describing the separation strength of the roof sheathing and of the wall sheathing subject to pressure action for the as-built structure, respectively, and $R_{rs,rot}$ is a random variable used to describe the relative portion of roof sheathing affected by rot.

The fatigue load-life model for the nail pull-out strength was taken from Alhawamdeh and Shao (2021) as:

$$R_{nail,f} = A \cdot N_f^B \tag{4.13}$$

in which $R_{nail,f}$ denotes the fatigue load normalized by the static capacity (also known as load reduction factor), $N_f$ is the number of constant amplitude cycles to failure, and *A* and *B* are regression constants that depend on the connection configuration, the nail material, and the wood material, and that for the case of Douglas Fir wood with no adhesive assume the values of 2.484 and -0.140, respectively. Miner's linear cumulative damage model (Miner 1945, Mahendran and Mahaarachchi 2002) was used to define the cumulative damage index $D_{nail}\left(\tau_f\right)$ as follows:

$$D_{nail}\left(\tau_f\right) = \sum_{j=1}^{m} \frac{N_j\left(\tau_f\right)}{N_{fj}} \tag{4.14}$$

where $N_j\left(\tau_f\right)$ denotes the number of applied cycles at the constant $j^{\text{th}}$ loading amplitude (corresponding in this study to the wind loads applied on the roof of a structure by an individual hurricane event), $N_{fj}$ denotes the number of cycles to failure under the constant $j^{\text{th}}$ loading amplitude, *m* is total number of loading amplitudes, and $\tau_f$ is the age of the nail subject to fatigue. The damage effects of load cycles with amplitudes smaller than 35% of the static strength were neglected (Alhawamdeh and Shao 2021). For simplicity, the cumulative damage to the roof-to-wall connection is assumed equal to the cumulative damage of the individual connection. In addition, in this work, the simplified approach proposed by Xu (1995) was utilized to estimate the number of applied cycles at a given amplitude as the number of cycles corresponding to the hourly wind speed of a hurricane hitting the structure at $\tau_f$, which is given by:

$$N_j\left(\tau_f\right) = \bar{n} \cdot V_j\left(\tau_f\right) \cdot \Delta t_j \tag{4.15}$$

where $\bar{n}$ is the number of cycles per hour per one m/s of the hourly mean wind speed (equal to 336, 225, and 652 for edge, center, and corner zones, respectively), $V_j\left(\tau_f\right)$, and $\Delta t_j$ denotes the duration of the

hurricane, which is modeled as a truncated normal random variable with mean equal to 2 hours and standard deviation equal to 0.5 hours with a lower truncation at 1 hour of duration. For simplicity, a single value of $\bar{n}$ was used for the entire roof as an average of the values for the different roof zones weighted by the areas of each zone. The corresponding wind load is calculated as (Unnikrishnan and Barbato 2016):

$$P_j = \frac{1}{2} \cdot \rho_a \cdot K_h \cdot K_{zt} \cdot V_j^2 \left( \tau_f \right) \cdot \sum_{r=1}^{n_c} G \cdot \left( C_{p,r} - C_{pi,r} \right) \cdot A_r \tag{4.16}$$

in which $\rho_a =$ air density, $K_h =$ wind pressure exposure factor evaluated at $h =$ height of the target building, $K_{zt}$ = topographic factor, $G =$ gust factor, $C_{p,r}$ = external pressure coefficient of for the *r*-th roof component, $C_{pi,r}$ = internal pressure coefficient of for the *r*-th roof component, $A_r$ = area of the *r*-th roof component, and $n_c =$ number of different roof components. By substituting Eq. (4.16) into Eq. (4.13)the corresponding number of cycles to failure is obtained as:

$$N_{fj} = \left( \frac{P_j}{A \cdot F_{rc}} \right)^{\frac{1}{B}} \tag{4.17}$$

in which $F_{rc}$ denotes the static strength of the roof-to-wall connection.

## 4.5. Multilayer Monte Carlo simulation procedure for aging structures

The distribution of the hurricane wind speed is altered by the effects of climate change. The model for the hurricane wind speed and changes over time due to climate change effect is adopted from Esmaeili and Barbato (2021a), where changes in the statistical properties of the hurricane winds is provided based on the location, year of interest, and the selected climate change scenario from AR5 RCP scenarios (Stocker et al. 2013). It is noted here that, when structural aging is considered, the proposed simulation methodology requires the simulation of the behavior of a sample structure for the entire duration of the period under consideration, as the progression of the damage due to structural aging is an irreversible process and creates a significant correlation between the damage and loss simulation at subsequent periods of time.

## 4.6. Case study

The performance of a target low-rise single family is investigated under different climate change scenarios and different structural aging conditions. The benchmark building is located in residential development in Pinellas Park, FL, as shown in Figure 3-2, where the building of interest is identified by a red circle. The unfolded view of the building is presented in Figure 3-3. It is assumed that the building was built in 2015, the value of the structure is $300,000, the value of its content is $150,000, and the design life is 50 years.

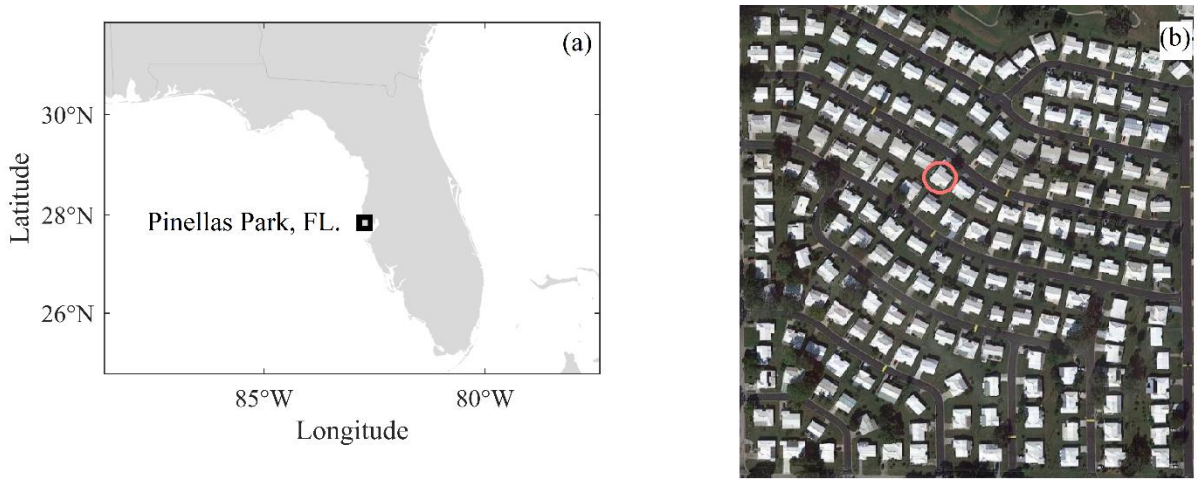


Figure 4-1. Benchmark building's location: (a) Pinellas Park, FL, and (b) plan view of the residential development with benchmark building identified by a red circle (map data © 2021 Google).

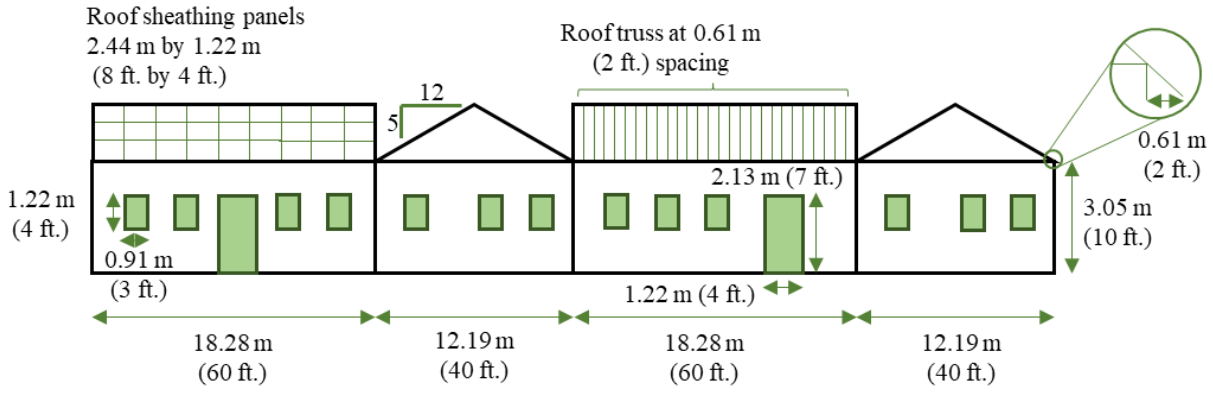


Figure 4-2. Unfolded view of the benchmark building

The statistical description of the different building components and corresponding limit states for the base structure is provided in Table 4-2 and is based on existing literature (Gurley et al. 2005; Datin et al. 2011; Dixon et al. 2014a; Masters et al. 2010; Stuckey and Carter 2001).

Table 4-2. Statistical description of limit state capacities for as-built structure

| Component | Limit state | Mean | COV | Distribution | Reference |
|---|---|---|---|---|---|
| Roof cover (shingles) | Separation | 1.96 kPa | 0.18 | Tr. Normal[(a)] | Dixon et al. (2014a) |
| Roof sheathing (6d C6/12) | Separation | 3.56 kPa | 0.22 | Lognormal | Datin et al. (2011) |
| Windows (unprotected) | Pressure failure | 3.33 kPa | 0.20 | Tr. Normal[(a)] | Gurley et al. (2005) |
| | Impact failure | 4.72 kg·m/s | 0.23 | Lognormal | Masters et al. (2010) |
| Doors (unprotected) | Pressure failure | 4.79 kPa | 0.20 | Tr. Normal[(a)] | Gurley et al. (2005) |
| Roof-to-wall connection | Tension failure | 16.68 kN | 0.20 | Lognormal | Gurley et al. (2005) |
| Wall | Uplift failure | 14.80 kN/m[(b)] | 0.25 | Tr. Normal[(a)] | Gurley et al. (2005) |
| | Lateral failure | 9.01 kN[(b)] | 0.25 | Tr. Normal[(a)] | Gurley et al. (2005) |
| Wall sheathing | Pressure failure | 6.03 kPa | 0.40 | Tr. Normal[(a)] | Gurley et al. (2005) |
| | Impact failure | 642 kg·m$^2$/s$^2$ | 0.07 | Lognormal | Stuckley & Carter (2001) |

[(a)] Truncated normal distribution with lower truncation at zero.

[(b)] Combination of toe-nail and sheathing nail connection strengths.

The sensitivity of the total losses experienced during the lifetime by the structure is quantified under different assumptions of exposure to wood mass loss and different combinations of increasing hazard due to climate change and increasing vulnerability due to structural aging. The hurricane wind hazard model for Pinellas Park, FL, under different AR5 RCP climate change scenarios is taken from Esmaeili and Barbato (2021a). The frequency of hurricanes is assumed to be stationary over time following a Poisson distribution with a frequency equal to 0.514 hurricanes per year. The duration of sustained peak wind speed for hurricanes is assumed to be normally distributed with a mean equal to 2.0 hours and a standard deviation of 30 minutes.

The historical data for air temperature and dew point temperature are collected for the period 2000-2020 from the Weather Underground website (Wunderground 2021). An example of generated time series for $T_{\mathrm{h}}$ and $RH_{\mathrm{h}}$ based on the procedure described in the Appendix is presented in Figure 4-3 for the year 2015.

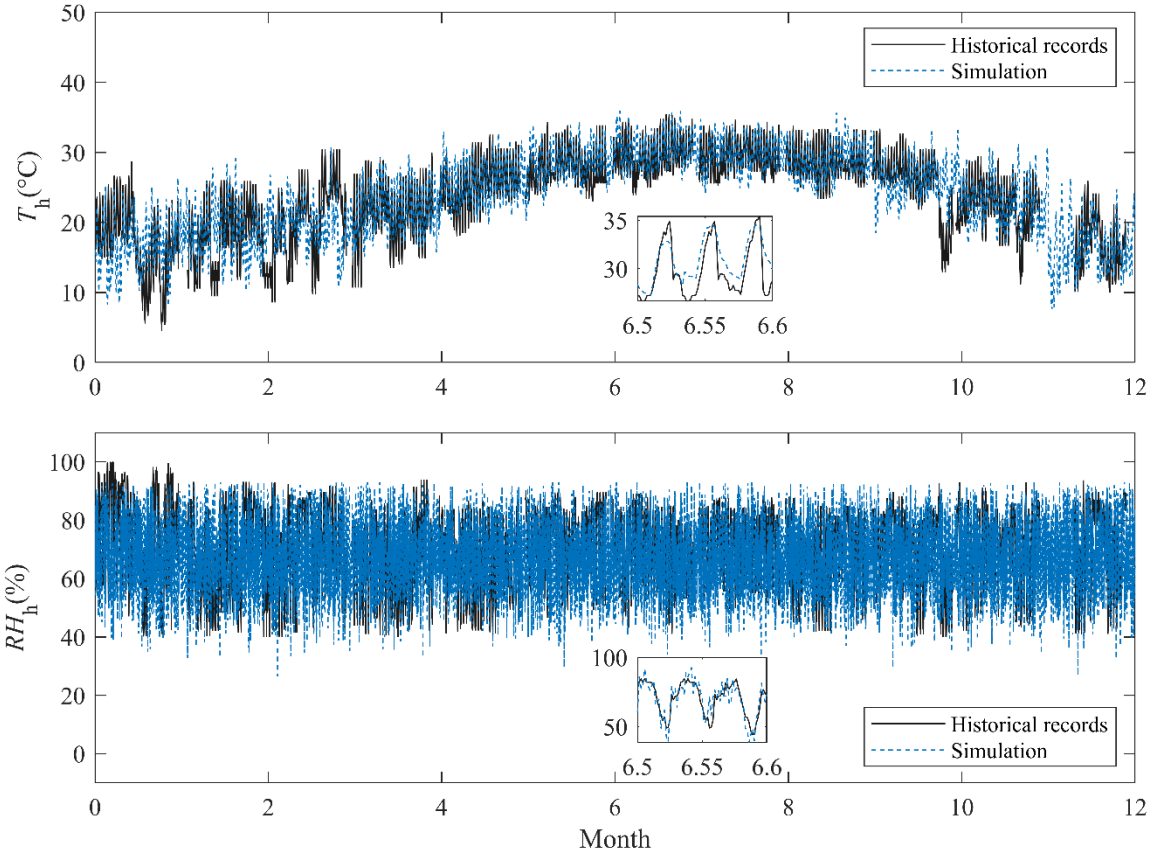


Figure 4-3. Historical records and sample realization of time histories corresponding to year 2015 for: (a) temperature and (b) relative humidity (with insets providing a zoomed view for a three-day interval.

The generated time series for $T_h$ and $RH_h$ are used in Eqs. (4.6) and (4.7) to calculate the wooden mass loss corresponding to the simulated data. The probability distributions of the wooden mass loss under different climate change scenarios at different times were estimated using 200 realizations for each year and each scenario. Figure 4-4 reports the mean wood mass losses and their 95% confidence interval at 10-year intervals during the period 2015-2065, which corresponds to the assumed service design life of the benchmark structure. The value of $\bar{n}$ to be used for the structure under consideration in Eq. (4.15) is equal to 291.

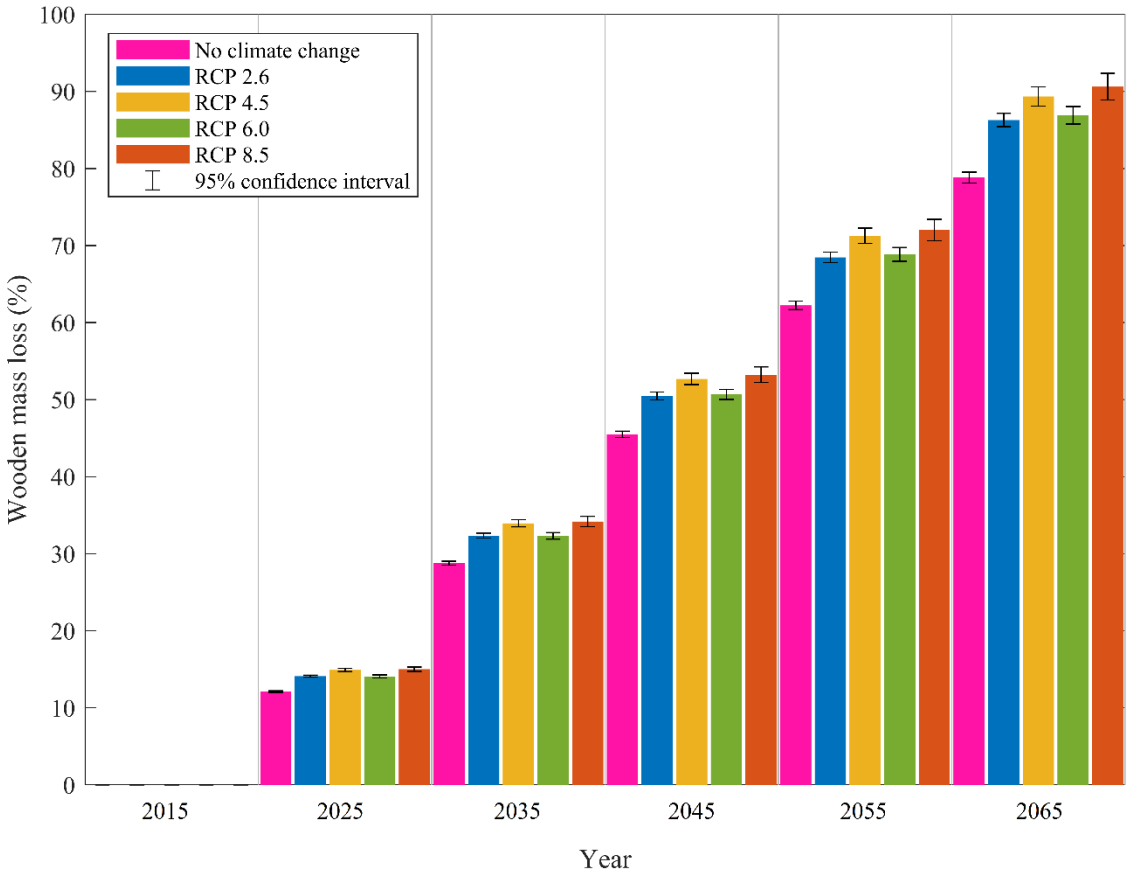


Figure 4-4. The average percentage of wooden mass loss for future climatological conditions along with 95% confidence intervals

At the beginning of the sampling procedure, the values of the strengths corresponding to the different limit states considered in this study are sampled together with 50 years of hurricane events according to the model presented in Esmaeili and Barbato (2021a). A constant discount rate equal to 3% is assumed for all loss analyses. Five conditions are considered for the loss analysis:

(1) No climate change and no structural aging: this case provides represent the baseline results corresponding to the original PBHE framework (Barbato et al. 2013). In this case, the climatological conditions are stationary and equal to those of 2015.

(2) Climate change and no structural aging: this case corresponds to analysis performed in Esmaeili and Barbato (2021b), where effects of different assumptions for climate change on the hurricane wind-induced losses were investigated but the damage measures were modeled as stationary over time.

(3) No climate change and structural aging: this case considers structural aging under stationary climatological conditions.

(4) Climate change and structural aging driven by stationary climate conditions: in this case, both nonstationary hazard and vulnerability are modeled, but the effects of nonstationary climate conditions are neglected when evaluating the structural aging.

(5) Climate change and structural aging driven by nonstationary climate conditions: this is the most realistic case, in which all nonstationarities are fully modeled and considered in the loss analysis.

When a structural component is damaged during the 50-year sample, it is assumed that the component is immediately replaced and the cost of replacement is immediately added to the losses. If structural aging is considered, the strength reduction and the damage index representing the fatigue effects are modeled as non-decreasing (i.e., the probability distributions at a given year are conditional to the current value being higher than the value in preceding years). However, when an aged component is damaged and replaced, it is assumed that the aging of the new component restarts from the beginning.

### 4.6.1. Results on the expected annual losses

Due to the lack of information to model the random variables describing the portion of a structure affected by rot (i.e., $R_{ws,rot}$ and $R_{rs,rot}$), three different conditions were considered: (1) low exposure, corresponding to $R_{ws,rot} = 0.10$ and $R_{rs,rot} = 0.20$; (2) medium exposure, corresponding to $R_{ws,rot} = 0.20$ and $R_{rs,rot} = 0.40$; and (3) high exposure, corresponding to $R_{ws,rot} = 0.30$ and $R_{rs,rot} = 0.50$;. The results of the all analyses are based on 100,000 samples and are reported in Table 4-3 in terms of the mean and standard deviations of the total losses..

Table 4-3. Mean and standard deviation of total losses under different assumptions

| Climate change scenario | No aging | | Aging | | | | |
|---|---|---|---|---|---|---|---|
| | | | | Independent aging | | Dependent aging | |
| | $m_{L_r}(\$)$ | $s_{L_r}(\$)$ | Exposure level | $m_{L_r}(\$)$ | $s_{L_r}(\$)$ | $m_{L_r}(\$)$ | $s_{L_r}(\$)$ |
| No climate change | 52738 | 54919 | | | | | |
| | | | Low | 52,804 | 55,405 | | |
| | | | Medium | 61,401 | 62,416 | | |
| | | | High | 69,957 | 65,386 | | |
| RCP 2.6 | 60650 | 57831 | Low | 60,911 | 59,464 | 61,112 | 59,392 |
| | | | Medium | 74,261 | 66,544 | 74,531 | 66,179 |
| | | | High | 85,623 | 72,003 | 85,585 | 72,660 |
| RCP 4.5 | 65460 | 59156 | Low | 67,316 | 62,099 | 67,287 | 62,247 |
| | | | Medium | 80,264 | 69,866 | 80,236 | 69,185 |
| | | | High | 92,844 | 75,000 | 93,144 | 75,134 |
| RCP 6.0 | 59678 | 56298 | Low | 60,250 | 58,255 | 60,029 | 58,176 |
| | | | Medium | 72,216 | 65,347 | 72,225 | 65,204 |
| | | | High | 83,998 | 70,546 | 84,163 | 70,180 |
| RCP 8.5 | 72831 | 61714 | Low | 75,755 | 64,992 | 75,574 | 64,603 |
| | | | Medium | 90,495 | 73,120 | 90,877 | 73,096 |
| | | | High | 103,360 | 78,070 | 103,956 | 78,175 |

The reported results show that the effects of the nonstationarity induced by climate change and structural aging are substantial. The expected total losses suffered by the benchmark structure when considering both climate change and structural aging increase between 15.50% (RCP 2.6) and 43.64% (RCP 8.5) for the case of low exposure when compared to the baseline case corresponding to no climate change and no aging during the 2015-2065 period. For the case of high exposure, the expected total losses increase between 62.35% (RCP 2.6) and 95.99% (RCP 8.5). The effects of climate change alone are also significant, with increases in the expected total losses contained between 15.00% (RCP 2.6) and 38.10% (RCP 8.5). As expected, the effects of structural aging alone are highly dependent on the level of exposure, with increases

contained between 0.13% for low exposure and 32.65% for high exposure. By contrast, the differences between the case considering climate change and structural aging driven by stationary climate conditions and the case considering climate change and structural aging driven by nonstationary climate conditions are always smaller than or equal to 0.58%.

## 4.7. Conclusions

In this chapter, the generalized performance-based hurricane engineering framework was utilized to investigate the combined effects of climate change and structural aging for a single-family house located in Pinellas Park, FL, during a 50-year service design life of the structure corresponding to the 2015-2065 period. The model for nonstationarity of hurricane wind hazard under climate change scenario is adopted from a previous study by Esmaeili and Barbato (2021a), where climate change scenarios were based on the 5$^{th}$ Assessment Report of the Intergovernmental Panel on Climate Change. The models for aging of different components utilized in this work are empirical models developed using experimental and survey data available in the literature. In order to account for the uncertainties for the future climatological conditions, a multi-layer Monte Carlo simulation approach is utilized. Due to the lack of information on the exposure of a wooden structure to rot, three different levels of exposure are considered. Five different cases are investigated: (1) no climate change and no structural aging; (2) climate change and no structural aging; (3) no climate change and structural aging; (4) climate change and structural aging driven by stationary climate conditions; and (5) climate change and structural aging driven by nonstationary climate conditions. It is found that the effects of both climate change and structural aging are significant, and their interaction can substantially increase the expected total losses for the considered structure, with increase as high as 95.99% for RCP 8.5 and high exposure when compared to the case in which both climate change and structural aging are neglected. By contrast, the effects of climate change on the structural aging are negligible.

# Chapter 5. Research Summary and Conclusion

Hurricanes are among the costliest natural hazards causing severe economic losses and loss of life. The large majority of climate scientists agrees that climate change has an intensifying effect on the hurricane-related hazards and resulting losses. In this work, a methodology is presented to account for the effects of climate change on hurricane hazards, which is fully probabilistic, computationally efficient, easy to use, and sufficiently accurate for structural engineering purposes. The methodology can be used to simulate the hurricane wind hazard under any climatological condition of interest in the past, present, or future provided the projections of climatological conditions. The performance-based hurricane engineering framework is extended to account for non-stationarity in the hurricane hazard, due to climate change, and vulnerability, due to structural aging, during the lifetime of the structure. The sensitivity of the results to many assumptions is investigated. In the following sections, the major conclusions of this research work are summarized and some future research ideas are proposed.

## 5.1. Conclusions

In chapter 2, an efficient and accurate simulation methodology for predicting the hurricane wind speed statistics is proposed. This model is based on historical records and can predict the hurricane wind speeds for any location along the US Gulf and Atlantic coasts under any climate change scenario. The model is validated against historical data from the NIST database and the design wind speeds in ASCE 7-16. The model results are also compared to those obtained from existing procedures that require full-track modeling of hurricanes. The comparison of the results shows that the model is highly accurate in terms of simulating the historical data and produces results that are very close to those obtained from more computationally expensive models. Based on the results obtained using this new model, by 2060, the design wind speed is projected to increase by approximately 14% for risk category II under the representative concentration pathway (RCP) 2.6 scenario and by approximately 26% for risk category IV under the RCP 8.5 scenario, which correspond to an increase in design wind forces acting on a structure by approximately 30% and 59%, respectively.

In chapter 3, an extended version of the PBHE framework is presented to account for the effects of climate change on intensity measures and of aging on structural parameters and damage measures. This model is used in conjunction with the predictive model for hurricane wind speed derived in chapter 2 to evaluate the hurricane-induced losses for a low-rise single-family building located in the US Gulf and Atlantic Coast region. The sensitivity of the results to different assumptions for climate change, discount rates, time integration, location, and variability of the repair costs is investigated. The performance of several retrofit scenarios for reducing the hurricane-induced losses to the building and benefits obtained from each of them is also investigated for a RCP 8.5 climate change scenario. The methodology is found to be little sensitive to modeling assumptions, with the exception of the discount rate, which can have a significant influence on the loss analysis results. It is concluded that the hurricane wind losses could increase between 15% in the best-case scenario and 38% in the worst-case scenario for the 50-years lifetime of the structure between 2015 and 2065. The proposed methodology can also be used to find the optimal storm hardening strategies for given climatological and location conditions.

In chapter 4, the effect of aging on structural components is investigated. Aging models are derived for roof sheathing, wall sheathing, connections, and roof cover and are used in conjunction with the predictive models of hurricane wind speed distribution from chapter 3 and the extended PBHE framework from chapter 4 to estimate hurricane-induced losses under future climatological conditions for an aging structure. A residential building is selected as the target structure to evaluate the effects of aging, which are based on the simulated time history of climate data. The sensitivity of the results to whether structural aging is dependent or independent of climate change is also investigated. The effects of different assumptions on the structural aging are also analyzed. The results of this study shows that the total expected losses for the benchmark structure can increase by a fraction of percent and up to 44%, depending on the level of exposure to aging stressors, when compared to the hurricane-induced losses obtained by neglecting the effects of climate change and structural aging during the 50-year service design life of the structure. This value can increase by 46% in the best-case scenario and by approximately 108% in the worst-case scenario. It is further concluded that the dependence of aging on climate change is a secondary effect and has little effects on the wind loss estimates for the target house.

## 5.2. Future research work

Based on the research results presented in this dissertation, some ideas for further work are proposed in the following areas:

1. The newly-developed fully-probabilistic model for hurricane wind hazard presented in this study has been validated only for locations near the coast. Additional research is needed to extend the proposed model to inland locations to properly include the effects on wind speed distributions produced by hurricanes after they have reached landfall and propagate inland.
2. The effects of climate change for hurricane related hazards in this work is limited to wind and windborne debris hazard. Further research is required to model and quantify the climate change effects on hurricane rain and flood hazards associated with hurricane events.
3. The extended performance-based hurricane engineering framework is a general-purpose framework and can be applied to any structural system. Further research should be performed to apply this methodology to engineered structures such as tall and large buildings, bridges, industrial plants, etc.
4. The loss analysis results reported in this study for single-family houses are based on the unrealistic assumption that a damaged structure is immediately repaired after a hurricane event. This assumption does not affect the loss results when the damage is produced by a single hurricane event in a given year. However, in the less common (but not unrealistic) situation in which a given structure is affected by more than a hurricane in a given year, or when losses due to lack of use are also included, a more advanced model of repair time is needed.
5. The aging models considered in this study are limited to only some components and materials. Further research is required to investigate structural aging for other materials and components and its effects on the expected losses.

# References


Adams, C., Hernandez, E., and Cato, J. C. (2004). "The economic significance of the Gulf of Mexico related to population, income, employment, minerals, fisheries and shipping." *Ocean & Coastal Manag.*, 47(11–12): 565–580.

Alhawamdeh, B., and Shao, X. (2021). "Fatigue performance of wood frame roof-to-wall connections with elastomeric adhesives under uplift cyclic loading." *Eng. Struct.*, Elsevier Ltd, 229(January 2020), 111602.

Alphonso, T. C., and Barbato, M. (2014). "Experimental fragility curves for aluminum storm panels subject to windborne debris impact." *J. Wind Eng. Ind. Aerodyn.,* 134, 44-55

Amini, M., and Memari, A. M. (2020). "Review of literature on performance of coastal residential buildings under hurricane conditions and lessons learned." *J. Perform. Constr. Facil.*, 34(6), 04020102.

Angus, J. E. (1994). "Probability integral transform and related results." *SIAM Review*, 36(4), 652–654.

ASCE (2016). *ASCE/SEI 7: Minimum Design Loads and Associated Criteria for Buildings and Other Structures.* American Society of Civil Engineers, Reston, VA, USA.

Ballesteros-Pérez, P., Sanz-Ablanedo, E., Soetanto, R., González-Cruz, M. C., Larsen, G. D., and Cerezo-Narváez, A. (2020). "Duration and cost variability of construction activities: an empirical study." *J. Constr. Eng. Manag.*, 146(1), 04019093.

Barbato, M., Petrini, F., Unnikrishnan, V. U., and Ciampoli, M. (2013). "Performance-based hurricane engineering (PBHE) framework." *Struct. Saf.,* 45, 24-35.

Batts, M. E., Simiu, E., and Russell, L. R. (1980). "Hurricane wind speeds in the United States." *J. Struct. Eng.,* 106(10): 2001-2016.

Berdahl, P., Akbari, H., Levinson, R., and Miller, W. A. (2008). "Weathering of roofing materials - An overview." *Constr. Build. Mater.,* 22(4), 423–433.

Bisadi, V., and Padgett, J. E. (2015). "Explicit time-dependent multi-hazard cost analysis based on

parameterized demand models for the optimum design of bridge structures." *Comput-aided CIV inf.*, 30(7), 541–554.

Bjarnadottir, S., Li, Y., and Stewart, M. G. (2011). "A probabilistic-based framework for impact and adaptation assessment of climate change on hurricane damage risks and costs." *Struct. Saf.*, 33(3), 173–185.

Bjarnadottir, S., Li, Y., and Stewart, M. G. (2014). "Regional loss estimation due to hurricane wind and hurricane-induced surge considering climate variability." *Struct. Infrastruct.*, 10(11): 1369–1384.

Bradley, B. A., Lee, D. S., Broughton, R., and Price, C. (2009). "Efficient evaluation of performance-based earthquake engineering equations." *Struct. Saf.*, 31(1), 65–74.

Ciampoli, M., Petrini, F., and Augusti, G. (2011). "Performance-based wind engineering: towards a general procedure." *Struct. Saf.*, 33(6), 367–378.

Conte, J. P., and Zhang, Y. (2007). "Performance Based Earthquake Engineering : Application to an actual bridge-foundation-ground system." *12th Italian National Conference on Earthquake Engineering*, Pisa, Italy, 1–18.

Crossett, K., Ache, B., Pacheco, P., and Haber, K. (2013). *National Coastal Population Report: Population Trends From 1970 to 2010*. NOAA State of the Coast Report Series, US Department of Commerce, Washington, DC, USA.

Cui, W., and Caracoglia, L. (2016). "Exploring hurricane wind speed along US Atlantic coast in warming climate and effects on predictions of structural damage and intervention costs." *Eng. Struct.*, 122: 209–225.

Curling, S. F., Clausen, C. A., and Winandy, J. E. (2002). "Relationships between mechanical properties, weight loss, and chemical composition of wood during incipient brown-rot decay." *For. Prod. J.*, 52(7/8), 34–39.

Datin, P. L., Prevatt, D. O., and Pang, W. (2011). "Wind-uplift capacity of residential wood roof-sheathing panels retrofitted with insulating foam adhesive." *J. Archit. Eng.*, 17(4), 144–154.

Decò, A., and Frangopol, D. M. (2011). "Risk assessment of highway bridges under multiple hazards." *J. Risk Res.*, 14(9), 1057–1089.

Dixon, C. R., Masters, F. J., Prevatt, D. O., and Gurley, K. R. (2014a). "Wind uplift resistance of artificially and naturally aged asphalt shingles." *J. Archit. Eng.*, 20(4), 1–14, B4014003.

Dixon, C. R., Masters, F. J., Prevatt, D. O., Gurley, K. R., Brown, T. M., Peterka, J. A., and Kubena, M. E. (2014b). "The influence of unsealing on the wind resistance of asphalt shingles." *J. Wind. Eng. Ind.*, Elsevier, 130, 30–40.

Dixon, C. R., Prevatt, D. O., Masters, F. J., and Gurley, K. R. (2013a). "The unsealing of naturally aged asphalt shingles: an in-situ survey." *Resid. Build. Des. Constr. Conf*, 202–211.

Dixon, C. R., Masters, F. J., Prevatt, D. O., and Gurley, K. R. (2013b). "Investigation of the wind resistance of asphalt shingles." *ATC & SEI Conf. on Advances in Hurricane Engineering 2012*, 24(4), 53–66.

Dong, Y., and Frangopol, D. M. (2016). "Probabilistic time-dependent multihazard life-cycle assessment and resilience of bridges considering climate change." *J. Perform. Constr. Facil.* 30(5), 1–12.

Dong, Y., and Li, Y. (2016). "Reliability of roof panels in coastal areas considering effects of climate change and embedded corrosion of metal fasteners ." *ASCE-ASME J. Risk Uncertain. Eng. Syst. A: Civ. Eng.*, 2(1), 04015016.

Droin, A., Taverdet, J. L., and Vergnaud, J. M. (1988). "Modeling the kinetics of moisture adsorption by wood." *Wood Sci. Technol*., 22(1), 11–20.

Elsner, J. B, Lewers, S. W., Malmstadt, J. C. and Jagger, T. H. (2011). "Estimating contemporary and future wind-damage losses from hurricanes affecting Eglin Air Force Base, Florida". *J. Appl. Meteorol. Climatol.*, 50(7): 1514-1526.

Elsner, J. B., Trepanier, J. C., Strazzo, S. E., and Jagger, T. H. (2012). "Sensitivity of limiting hurricane intensity to ocean warmth". *Geophys. Res. Lett.*, 39: L17702.

Emanuel, K. (1999). "Thermodynamic control of hurricane intensity." *Nature*, 401: 665–669.

Emanuel, K. (2005). “Increasing destructiveness of tropical cyclones over the past 30 years.” *Nature*, 436, 686–688.

Emanuel, K. (2011). “Global warming effects on U.S. hurricane damage.” *Weather Clim. Soc.*, 3(4): 261–268.

Emanuel, K. (2013). “Downscaling CMIP5 climate models shows increased tropical cyclone activity over the 21st century.” *Proc. of the National Academy of Sciences*, 110(30), 12219–12224.

Emanuel, K. (2013). “Downscaling CMIP5 climate models shows increased tropical cyclone activity over the 21st century.” *Proc. of the National Academy of Sciences*, 110(30), 12219–12224.

Emanuel, K., Sundararajan, R., and Williams, J. (2008). “Hurricanes and global warming: results from downscaling IPCC AR4 simulations.” *Bull. Amer. Meteor.*, 89(3): 347–367.

Esmaeili, M., and Barbato, M. (2021a). “Predictive model for hurricane wind hazard under changing climate conditions.” *Nat. Hazards Rev.*, 22(3), 04021011.

Esmaeili, M., and Barbato, M. (2021b). “Performance-based hurricane engineering under changing climate conditions: general framework and performance of single-family houses in the US” *Under Review*.

Estrada, F., Botzen, W. J. W., and Tol, R. S. J. 2015. “Economic losses from US hurricanes consistent with an influence from climate change.” *Nat. Geosci.*, 8(11), 880–884.

Foliente, G. C., Leicester, R. H., Wang C., Mackenzie C., Cole. I., (2002). “Durability design of wood construction.” *For. Prod. J.*, 52(1):10-19

Fridley, K. J., Mitchell, J. B., Hunt, M. O., and Senft, J. F. (1996). “Effect of 85 years of service on mechanical properties of timber roof members. Part 2. Cumulative damage analysis.” *For. Prod. J.*, 46(6), 85–90.

Galhano, C. (2013). “Effect of coastal environment in clay facing bricks and roof tiles.” *Proc. of 1st Annual International Interdisciplinary Conference*, AIIC2013, Azores, Portugal, Vol. 3 pp. 414-422.

Georgiou P. N., Davenport A. G., and Vickery B. J. (1983). "Design wind speeds in regions dominated by tropical cyclones."*J. Wind Eng. Ind. Aerodyn.*, 13(1-3): 139-152.

Ghosh, J., and Padgett, J. E. 2010. "Aging considerations in the development of time-dependent seismic fragility curves." *J. Struct. Eng.*, 136(12), 1497–1511.

Glass, S. V., and Zelinka, S. L. (2010). "Chapter 4: moisture relations and physical properties of wood," in *Forest Products Laboratory. Wood Handbook: Wood as an Engineering Material*, Centennial, Vol. 2010, ed. General Technical Report FPL-GTR-190 (Madison, WI: U.S. Dept. of Agriculture, Forest Service, Forest Products Laboratory), 4.1–4.19.

Grinsted, A., Moore, J. C., and Jevrejeva, S. (2013). "Projected Atlantic hurricane surge threat from rising temperatures." *Proc. of the National Academy of Sciences*, 110(14): 5369–5373.

Gurley, K., Pinelli, J. P., Subramanian, C., Cope, A., Zhang, L., and Murphree, J. (2005). "Predicting the Vulnerability of Typical Residential Buildings to Hurricane Damage." *Florida Public Hurricane Loss Projection Model (FPHLPM) Engineering Team Final Rep.*, I.H.R. Center, Florida International Univ., Miami.

Hallegatte, S. (2007). "The use of synthetic hurricane tracks in risk analysis and climate change damage assessment." *J. Appl. Meteorol. Climatol.*, 46(11): 1956–1966.

He, M., Magnusson, H., Lam, F., & Prion, H. G. (1999). "Cyclic performance of perforated wood shear walls with oversize OSB panels." *J. Struct. Eng.*, 125(1), 10-18.

Huang, Z., Rosowsky, D. V., and Sparks, P. R. (2001). "Hurricane simulation techniques for the evaluation of wind-speeds and expected insurance losses." *J. Wind Eng. Ind. Aerodyn.*, 89(7–8): 605–617.

Huang, Z., Rosowsky, D. V., and Sparks, P. R. (2001). "Long-term hurricane risk assessment and expected damage to residential structures." *Reliab. Eng. Syst.*, 74(3), 239–249.

Jagger, T. H., and Elsner, J. B. (2012). "Hurricane clusters in the vicinity of Florida". *J. Appl. Meteorol. Climatol.*, 51(5): 869-877.

Jagger, T. H., Elsner, J. B., and Niu, X. (2001). "A dynamic probability model of hurricane winds in coastal counties of the United States". *J. Appl. Meteorol. Climatol.,* 40(5): 853-863.

Jalayer, F., and Cornell, C. A. (2003). "A technical framework for probability-based demand and capacity factor design (DCFD) seismic formats." *PEER Report 2003/8,* 122.

Kent, S. M., Leichti, R. J., Rosowsky, D. V., and Morrell, J. J. (2005). "Effects of decay on the cyclic properties of nailed connections." *J. Mater. Civ. Eng.*, 17(5), 579–585.

Klotzbach, P. P. J., Bowen, S. G., PielKe, R. G. R., and Bell, M. (2018). "Continental U.S. hurricane landfall frequency and associated damage: Observations and future risks." *Bull. Amer. Meteor.,* 99(7), 1359–1376.

Knutson, T. R., McBride, J. L., Chan, J., Emanuel, K., Holland, G., Landsea, C., Held, I., Kossin, J. P., Srivastava, A. K., and Sugi, M. (2010). "Progress article: tropical cyclones and climate change." *Nat. Geosci.*, 3(3): 157–163.

Knutson, T. R., Sirutis, J. J., Garner, S. T., Held, I. M., and Tuleya, R. E. (2007). "Simulation of the recent multidecadal increase of Atlantic hurricane activity using an 18-km-grid regional model." *Bull. Amer. Meteor.*, 88(10): 1549–1565.

Knutson, T. R., Sirutis, J. J., Vecchi, G. A., Garner, S., Zhao, M., Kim, H. S., Bender, M., Tuleya, R. E., Held, I. M., and Villarini, G. (2013). "Dynamical downscaling projections of twenty-first-century atlantic hurricane activity: CMIP3 and CMIP5 model-based scenarios." *J. Clim.,* 26(17): 6591–6617.

Kránitz, K., Sonderegger, W., Bues, C. T., and Niemz, P. (2016). "Effects of aging on wood: a literature review." *Wood Sci. Technol.*, 50(1), 7–22.

Landsea, C., Franklin, J., and Beven, J. (2015). "The revised Atlantic hurricane database (HURDAT2)." Accessed March 17, 2018. http://www.aoml.noaa.gov/hrd/hurdat/hurdat2.html.

Lawrence, M. G. (2005). "The relationship between relative humidity and the dewpoint temperature in moist air: A simple conversion and applications." *Bull. Amer. Meteor.,* 86(2), 225–233.

Lee, C., and Lee, E. B. (2017). “Prediction method of real discount rate to improve accuracy of life-cycle cost analysis.” *Energy Build.*, 135, 225–232.

Lee, J. Y., and Ellingwood, B. R. (2017). “A decision model for intergenerational life-cycle risk assessment of civil infrastructure exposed to hurricanes under climate change.” *Reliab. Eng. Syst. Saf.*, 159:100-107.

Li, Q., Wang, C., and Ellingwood, B. R. (2015). “Time-dependent reliability of aging structures in the presenceof non-stationary loads and degradation.” *Struct. Saf.*, 52, 132–141.

Li, Y., and Ellingwood, B. R. (2006). “Hurricane damage to residential construction in the US: Importance of uncertainty modeling in risk assessment.” *Eng. Struct.*, 28(7): 1009–1018.

Li, Y., and Stewart, M. G. (2011). “Cyclone damage risks caused by enhanced greenhouse conditions and economic viability of strengthened residential construction.” *Nat. Hazards Rev.*, 12(1), 9–18.

Liang, Z., and Lee, G. C. (2012). “Towards multiple hazard resilient bridges: A methodology for modeling frequent and infrequent time-varying loads Part II, Examples for live and earthquake load effects.” *J. Earthq. Eng. Eng. Vib.*, 11(3), 303–311.

Liel, A. B., and Deierlein, G. G. (2013). “Cost-benefit evaluation of seismic risk mitigation alternatives for older concrete frame buildings.” *Earthq.*, 29(4), 1391–1411.

Liu, P. L., and Der Kiureghian, A. (1986). “Multivariate distribution models with prescribed marginals and covariances.” *Probabilistic Eng. Mech.*, 1(2), 105–112.

Lombardo, F. T. and Ayyub, B. M. (2015). “Analysis of Washington, DC, wind and temperature extremes with examination of climate change for engineering applications.” *ASCE-ASME J. Risk Uncertain. Eng. Syst. A: Civ. Eng.*, 1(1): 04014005.

Lopez, J. M., Roueche, D. B., and Prevatt, D. O. (2020). “Wind resistance and fragility functions for wood-framed wall sheathing panels in low-rise residential construction.” *J. Struct. Eng.*, 146(8), 04020139.

Mahendran, M., Mahaarachchi, D. (2002). “Cyclic pull-out strength of screwed connections in steel roof and wall cladding systems using thin steel battens.” *J. Struct. Eng.*, 128(6):771–778.

Malmstadt, J. C, Elsner, J. B., and Jagger, T. H. (2010). "Risk of strong hurricane winds to Florida cities". *J. Appl. Meteorol. Climatol.*, 49(10): 2121-2132.

Masters, F. J., Gurley, K. R., Shah, N., and Fernandez, G. (2010). "The vulnerability of residential window glass to lightweight windborne debris." *Eng. Struct.*, 32(4), 911–921.

Miner, M.A. (1945). "Cumulative damage in fatigue." *J. Applied Mech*.,12(3):159–164.

Mudd, L., Wang, Y., Letchford, C., and Rosowsky, D. (2014). "Assessing climate change impact on the U.S. East Coast hurricane hazard: Temperature, frequency, and track." *Nat. Hazards Rev.*, 15(3), 04014001.

National Hurricane Center. (2020). "Costliest U.S. tropical cyclones tables updated." *NOAA Tech. Memo. NWS NHC-6*, 3.

NIST. (2016). "Extreme wind speed data sets: hurricane wind speeds." Accessed March 17, 2018. http://www.itl.nist.gov/div898/winds/hurricane.htm

NOAA. 2021. "Billion-dollar weather and climate disasters." Accessed August 20, 2021. https://www.ncdc.noaa.gov/billions/

NOAA/OAR/ESRL-PSD. (2015). "NOAA high resolution SST data." Accessed March 25, 2018. http://www.esrl.noaa.gov/psd/.

Oxenyuk, V., Gulati, S., Kibria, B. M. G., and Hamid, S. (2017). "Distribution fits for various parameters in the Florida Public Hurricane Loss model." *J. Mod. Appl. Stat. Methods*, 16(1): 481-497.

Pant, S., and Cha, E. J. (2018). "Effect of climate change on hurricane damage and loss for residential buildings in Miami-Dade County." *J. Struct. Eng.*, 144(6), 04018057.

Pant, S., and Cha, E. J. (2019). "Wind and rainfall loss assessment for residential buildings under climate-dependent hurricane scenarios." *Struct. Infrastruct. Eng.*, 5(6): 771–782.

Peng, X., Yang, L., Gavanski, E., Gurley, K., and Prevatt, D. (2014). "A comparison of methods to estimate peak wind loads on buildings." *J. Wind. Eng. Ind.*, 126: 11–23.

Peterka, J.A., Cermak, J.E., Cochran, L.S., Cochran, B.C., Hosoya, N., Derickson, R.G., Jones, J., Metz, B. (1997). "Wind uplift model for asphalt shingles." *J. Archit. Eng.*, 3(4):147-155.

Pielke, R. A., Gratz, J., Landsea, C. W., Collins, D., Saunders, M. A., and Musulin, R. (2008). "Normalized hurricane damage in the United States: 1900–2005." *Nat.l Hazards Rev.*, 9(1): 29–42.

Plotner, S. C., Babbitt, C., Charest, A. C., Elsmore, C., and Gomes, J. (2017). *Building Construction Costs with RSMeans Data*. Gordian RSMeans Data.

Porter, K. A. (2003). "An overview of PEER's performance-based earthquake engineering methodology." *9th International Conf. on Applications of Statistics and Probability in Civil Engineering*, 1-8.

Porter, K. A., Kiremidjian, A. S., and LeGrue, J. S. (2001). "Assembly-based vulnerability of buildings and its use in performance evaluation." *Earthq.*, 17(2), 291–312.

Prevatt, D. O., McBride, K. E., Roueche, D. B., and Masters, F. J. (2014). "Wind uplift capacity of foam-retrofitted roof sheathing panels subjected to rainwater intrusion." *J. Archit. Eng.*, 20(4), 1–9.

Prevatt, D. O., Shreyans, S., Kerr, A., and Gurley, K. R. 2014. "In situ nail withdrawal strengths in wood roof structures." *J. Struct. Eng.*, 140(5), 1–8.

Rammer, D. R., and Zelinka, S. L. 2015. "Withdrawal strength and bending yield strength of stainless steel nails." *J. Struct. Eng*., 141(5), 04014134.

Rizzo, F., Barbato, M., and Vincenzo, S. (2018). "Peak factor statistics of wind effects for hyperbolic paraboloid roofs." *Eng. Struct.*, 173: 313-330

Sackey, S., and Kim, B.-S. (2018). "Environmental and economic performance of asphalt shingle and clay tile roofing sheets using life cycle assessment approach and TOPSIS." *J. Constr. Eng. Manag.*, 144(11), 04018104.

Sekino, N., Sato, H., and Adachi, K. (2014). "Evaluation of particleboard deterioration under outdoor exposure using several different types of weathering intensity." *J. Wood Sci.*, 60(2), 141–151.

Seldén, R., Nyström, B., and Långström, R. (2004). "UV aging of poly(propylene)/wood-fiber composites." *Polym. Compos.*, 25(5), 543–553.

Shdid, C. A., Mirmiran, A., Wang, T.L., Jimenez, D., and Huang, P. (2011). "Uplift capacity and impact resistance of roof tiles." *Pract. Period. Struct. Des. Constr.*, 16(3), 121–129.

Soltis, L., and Mtenga, P. (1985). "Strength of nailed wood joints subjected to dynamic load." *For. Prod. J.*, 35(11/12).

Sonderegger, W., Kránitz, K., Bues, C. T., and Niemz, P. (2015). "Aging effects on physical and mechanical properties of spruce, fir and oak wood." *J. Cult. Herit.*, 16(6), 883–889.

Soong, T. T. (2004). *Fundamentals of Probability and Statistics for Engineers*. John Wiley & Sons, West Sussex, UK.

Stewart, M. G., Rosowsky, D. V., and Huang, Z. (2003). "Hurricane risks and economic viability of strengthened construction." *Nat. Hazards Rev.*, 4(1), 12–19.

Stirling, R., Sturrock, R. N., and Braybrooks, A. (2017). "Fungal decay of western redcedar wood products–a review." *Int. Biodeterior*, 125, 105–115.

Stocker, T. F., Qin, D., Plattner, G.-K., Tignor, M., Allen, S. K., Boschung, J., Nauels, A., Xia, Y., Bex, V., Midgley, P. M., and Others. (2013). *Climate Change 2013 - The Physical Science Basis. Contribution of Working Group I to the Fifth Assessment Report of the Intergovernmental Panel on Climate Change*, Cambridge University Press, Cambridge, UK, and New York, NY, USA.

Stuckley, A., and Carter, R. (2001). "Perforation threshold speeds of windborne debris for various wall and above ground shelter concepts." *Internal Rep.*, Wind Engineering Research Center, Texas Tech Univ., Lubbock, TX.

Sutter, D., DeSilva, D., and Kruse, J. (2009). "An economic analysis of wind resistant construction." *J. Wind. Eng. Ind.*, 97(3–4), 113–119.

Takanashi, R., Sawata, K., Sasaki, Y., and Koizumi, A. (2017). "Withdrawal strength of nailed joints with decay degradation of wood and nail corrosion." *J. Wood Sci*., 63:192-198.

Tofallis, C. (2015). "A better measure of relative prediction accuracy for model selection and model estimation." *J. Oper. Res. Soc.*, 66(8), 1352–1362.

Tonoli, G. H. D., Santos, S. F., Savastano, H., Delvasto, S., Mejía De Gutiérrez, R., and Lopez De Murphy, M. D. M. (2011). "Effects of natural weathering on microstructure and mineral composition of cementitious roofing tiles reinforced with fique fibre." *Cem. Concr. Compos.*, 33(2), 225–232.

Unnikrishnan V. U and Barbato, M. (2013). "Performance-based hurricane risk assessment with application to wind and windborne debris hazards." *Proc. of 11th International Conference on Structural Safety and Reliability (ICOSSAR 2013)*, June 16-20, 2013, Columbia University New York, NY (USA).

Unnikrishnan, V. U., and Barbato, M. (2015). "Cost-benefit assessment of different storm mitigation techniques for residential buildings using the PBHE framework." *Proc. of 12th International Conference on Applications of Statistics and Probability in Civil Engineering (ICASP12)*, July 12-15, 2015, Vancouver, British Columbia (Canada).

Unnikrishnan, V. U., and Barbato, M. (2016). "Performance-based comparison of different storm mitigation techniques for residential buildings." *J. Struct. Eng.*, 10.1061/(ASCE)ST.1943-541X.0001469, 04016011, 142(6), June 2016.

Unnikrishnan, V. U., and Barbato, M. (2016). "Chapter 16: Performance-based hurricane engineering: A multi-hazard approach." In *Multi-hazard Approaches to Civil Infrastructure Engineering*, Gardoni, P., LaFave, J.M., Editors, Springer, ISBN: 978-3-319-29713-2.

Unnikrishnan, V. U., and Barbato, M. (2017). "Multi-hazard interaction effects on the performance of low-rise wood-frame housing in hurricane-prone regions." *J. Struct. Eng.*, 143(8), August 2017. https://doi/10.1061/(ASCE)ST.1943-541X.0001797

van de Lindt, J. W., and Dao, T. N. (2009). "Performance-based wind engineering for wood-frame buildings." *J. Struct. Eng.*, 135(2), 169–177.

Van Dyke, J., and Hu, P. (1989). "Determinants of variation in calculating a discount rate." *Energy*, 14(10), 661–666.

Vickery, P. J., Masters, F. J., Powell, M. D., and Wadhera, D. (2009). "Hurricane hazard modeling: The past, present, and future." *J. Wind. Eng. Ind.*, 97(7–8): 392–405.

Vickery, P. J., Skerlj, P. F., and Twisdale, L. A. (2000). "Simulation of hurricane risk in the US using empirical track model." *J. Struct. Eng.*, 126(10): 1222-1237.

Viitanen, H., Toratti, T., Makkonen, L., Peuhkuri, R., Ojanen, T., Ruokolainen, L., and Räisänen, J. (2010). "Towards modelling of decay risk of wooden materials." *Eur. J. Wood Prod.*, 68(3), 303–313.

Wang, C., Li, Q., Pang, L., Zou, A., and Zhang, L. (2016). "Hurricane damage assessment for residential construction considering the non-stationarity in hurricane intensity and frequency." *Acta Oceanol. Sin.*, 35(12), 110–118.

Webster, P. J., Holland, G. J., Curry, J. A., and Chang, H. R. (2005). "Atmospheric science: Changes in tropical cyclone number, duration, and intensity in a warming environment." *Science*, 309 (5742): 1844-1846

Willoughby, H. E., Darling, R. W. R., Rahn, M. E. (2006). "Parametric representation of the primary hurricane vortex. Part II: A new family of sectionally continuous profiles." *Mon. Weather Rev.*, 134(4), 1102–1120.

Witomski, P., Olek, W., and Bonarski, J. T. (2016). "Changes in strength of Scots pine wood (Pinus silvestris L.) decayed by brown rot (Coniophora puteana) and white rot (Trametes versicolor)." *Constr. Build. Mater.*, Elsevier Ltd, 102, 162–166.

Xu, Y. L. (1995). "Determination of wind-induced fatigue loading on roof cladding." *J. Eng. Mech.*, 121(9), 956–963.

Zelinka, S. L. (2013). “Corrosion of embedded metals in wood: An overview of recent research with implications for building moisture design.” *ASHRAE Trans*, 119 (PART 2), 442–448.

Zelinka, S. L., and Rammer, D. R. (2012). “Modeling the effect of nail corrosion on the lateral strength of joints.” *For. Prod. J.*, 62(3), 160–166.

# Appendix: Simulation procedure for wood mass loss

The simulation procedure to assess the wood mass loss is broken down into two main steps: (1) the simulation of time series of the hourly temperatures and relative humidity under different climate change scenarios, and (2) the development of the wood mass loss distribution as a function of time and its use within the PBHE framework to estimate the change in strength of the components affected by the wooden mass.

## A.1. Simulation of temperature and relative humidity time series

The simulation of the hourly temperature time series for the future years under a given climate change assumption requires to build the probability distributions of the hourly temperatures as a function of the yearly average temperature. These distributions are based on historical temperature records collected for the location of the target house. In particular, hourly temperature data were collected from weather underground website (wunderground) for a duration of 20 years corresponding to the 2000-2020 period at Pinellas Park, FL. These data were used to fit a normal distribution to: (1) the differences between the hourly temperatures and the average temperature of a given day (hourly deviations), (2) the differences between the daily average temperatures and the average temperature of a given month (daily deviations), and (3) the differences between the average monthly temperatures and the average temperature of a given year (monthly deviations).

The temperature $T$, dew point temperature $D_T$, and relative humidity $RH$ time series are described by the symbol $X_p^t$, where $X = T, D, RH$ is the random process of interest, the subscript $p = y, m, d, h$ indicates the averaging period ($y$: yearly, $m$: monthly, $d$: daily, and $h$: hourly). Once the distributions of the deviations are derived from local temperature data, the time series can be sampled for a given climate change scenario by using the distribution of the projected change in the yearly temperature, $\Delta T_y$, which is assumed to follow a normal distribution. These distributions were obtained following the same approach

used for the sea surface temperature and described in Esmaeili and Barbato (2021a), by fitting a normal distribution to the increases in average yearly air temperature corresponding to the projection scenarios provided by IPCC AR5 (Stocker et al. 2013). Figure A-1 shows the mean and 95% confidence intervals for the increases in average yearly air temperature when compared to the reference year 2005. Once the projected temperature change due to climate change is sampled, the sampled average yearly temperature for the future years, $T_y$, can be obtained by adding $\Delta T_y$ to $T_{2005} = 23.44\,°\text{C}$, which is the average yearly temperature for the reference year 2005 that is used by IPCC AR5 scenarios. The sample for the monthly temperature, $T_m$, can be obtained by sampling the $\Delta T_m$ from its distribution and adding that to the sampled $T_y$. A similar procedure is used to sample the daily temperatures and hourly temperatures. The distributions of the monthly, daily, and hourly deviations are assumed to be stationary and are given in Table A-1 through Table A-3. The sampling procedure is described by the flowchart given in Figure A-2.

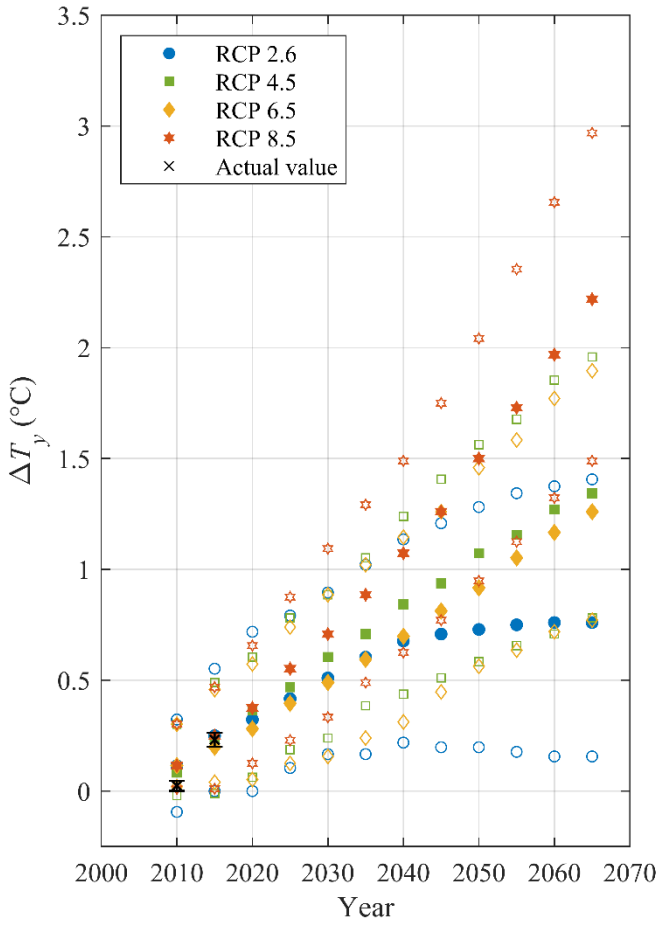


Figure A-1. IPCC AR5 projections for increases in the average yearly temperature

- Select the climate change scenario
- Select the number of time series samples, $n_s$.
- Select the year of interest: $y$.
- For $i = 1:n_s$
    - Sample $\Delta T_y^{(i)}$ from a normal distribution based on IPCC AR5 projections.
    - Calculate $T_y^{(i)} = T_{2005} + \Delta T_y^{(i)}$.
    - For $m = 1:12$
        - Sample $\Delta T_m^{(i)}$ from its fitted normal distribution
        - Calculate $T_m^{(i)} = T_y^{(i)} + \Delta T_m^{(i)}$.
        - For $d = 1:d_m$
            - Sample $\Delta T_d^{(i)}$ from its fitted normal distribution
            - Calculate $T_d^{(i)} = T_m^{(i)} + \Delta T_d^{(i)}$.
            - For $h = 1:24$
                - Sample $\Delta T_h^{(i)}$.
                - Sample $T_h^{(i)} = T_d^{(i)} + \Delta T_h^{(i)}$
            - End for (*h*)
        - End for (*d*)
    - End for (*m*)
- End for (*i*)

Figure A-2. Flowchart to generate the temperature time series.

Table A-1. Probability distributions for monthly temperature deviations (°C) for Pinellas Park, FL, based on historical data corresponding to the period 2000-2020

| month | $\mu_{\Delta T_m}$ | $\sigma_{\Delta T_m}$ | Lower limit | Upper limit |
|---|---|---|---|---|
| Jan | -5.72 | 2.97 | -8.99 | -2.45 |
| Feb | -5.06 | 2.92 | -10.46 | 0.35 |
| Mar | -3.17 | 2.95 | -7.20 | 0.87 |
| Apr | -0.39 | 2.97 | -6.25 | 5.47 |
| May | 2.56 | 2.89 | -2.51 | 7.62 |
| Jun | 4.61 | 2.65 | 1.01 | 8.22 |
| Jul | 5.28 | 2.52 | 0.89 | 9.66 |
| Aug | 5.28 | 2.53 | 1.96 | 8.60 |
| Sep | 4.50 | 2.50 | 0.89 | 8.11 |
| Oct | 1.39 | 2.74 | -3.99 | 6.77 |
| Nov | -3.00 | 2.93 | -6.38 | 0.38 |
| Dec | -5.44 | 2.92 | -8.39 | -2.50 |

Table A-2. Probability distributions for daily temperature deviations (°C) for Pinellas Park, FL, based on historical data corresponding to the period 2000-2020

| day | $\mu_{\Delta T_d}$ | $\sigma_{\Delta T_d}$ |
|---|---|---|
| 1 | 0 | 1.75 |
| 2 | 0 | 1.24 |
| 3 | 0 | 1.18 |
| 4 | 0 | 1.20 |
| 5 | 0 | 1.40 |
| 6 | 0 | 1.79 |
| 7 | 0 | 1.78 |
| 8 | 0 | 1.63 |
| 9 | 0 | 1.40 |
| 10 | 0 | 1.03 |
| 11 | 0 | 1.59 |
| 12 | 0 | 1.46 |
| 13 | 0 | 1.56 |
| 14 | 0 | 1.12 |
| 15 | 0 | 1.02 |
| 16 | 0 | 1.25 |
| 17 | 0 | 1.31 |
| 18 | 0 | 1.67 |
| 19 | 0 | 1.80 |
| 20 | 0 | 1.15 |
| 21 | 0 | 1.46 |
| 22 | 0 | 1.29 |
| 23 | 0 | 1.61 |
| 24 | 0 | 1.52 |
| 25 | 0 | 1.21 |
| 26 | 0 | 1.78 |
| 27 | 0 | 1.70 |
| 28 | 0 | 1.51 |
| 29 | 0 | 1.07 |
| 30 | 0 | 1.79 |
| 31 | 0 | 1.32 |

Table A-3. Probability distributions for hourly temperature deviations (°C) for Pinellas Park, FL, based on historical data corresponding to the period 2000-2020

| hour | $\mu_{\Delta T_h}$ | $\sigma_{\Delta T_h}$ |
|---|---|---|
| 1 | -3.18 | 1.28 |
| 2 | -3.64 | 1.26 |
| 3 | -4.14 | 1.21 |
| 4 | -4.39 | 1.18 |
| 5 | -4.72 | 1.19 |
| 6 | -4.96 | 1.14 |
| 7 | -5.12 | 1.08 |
| 8 | -4.11 | 0.94 |
| 9 | -2.16 | 0.94 |
| 10 | 0.05 | 0.97 |
| 11 | 2.08 | 1.06 |
| 12 | 3.86 | 1.07 |
| 13 | 5.19 | 1.15 |
| 14 | 6.13 | 1.21 |
| 15 | 6.45 | 1.35 |
| 16 | 6.49 | 1.36 |
| 17 | 5.82 | 1.38 |
| 18 | 4.26 | 1.41 |
| 19 | 2.16 | 1.28 |
| 20 | 0.38 | 1.11 |
| 21 | -0.71 | 1.01 |
| 22 | -1.34 | 0.92 |
| 23 | -1.94 | 0.96 |
| 24 | -2.47 | 1.13 |

where $\mu_{\Delta T_p}$ and $\sigma_{\Delta T_p}$, $p = y, m, d, h$ indicate the mean and standard deviation of the distribution of $\Delta T_p$.

The hourly time series of the dew point temperature, $D_{T,h}$, are also collected for the same period as that for $T_h$. The following linear relation is developed:

$$\begin{aligned} D_{T,h} &= a_0 + a_1 \cdot T_h + \varepsilon_{D_T} \le T_h \\ \varepsilon_{D_T} &\sim N\left(0.0, \sigma_{\varepsilon_{D_T}}\right) \end{aligned} \tag{1}$$

where $a_0$ and $a_1$ are location-dependent regression constants, $\varepsilon_{D_T}$ is the regression error, and $\sigma_{\varepsilon_{D_T}}$ is the standard deviation of the error, and the regression error is assumed to follow a truncated normal distribution so that the dew point is contained between 0 °C and $T_h$. For Pinellas Park, FL, these quantities are given by:

Table A-4. Parameters describing the relationship between temperature and dew point temperature

| Regression parameter | value |
|---|---|
| $a_0$ | 0.86 |
| $a_1$ | -0.77 |
| $\sigma_\varepsilon$ | 6.15 |

The time series of $RH_h$ are then simulated using the methodology presented in Lawrence (2005). The wooden mass loss corresponding to the sampled temperature and relative humidity time series is finally calculated using the model developed by Viitanen et al. (2010).

## A.2. Development of the wood mass loss probability distribution as a function of time

Generating the time series data for temperature and relative humidity needed to calculate the sample wooden mass loss is computationally expensive. Therefore, a wood mass loss distribution for each year and each climate change scenario is developed based on the previously described simulation procedure for temperature and relative humidity. This wood mass loss distribution is obtained by fitting 200 samples for each year and each climate change scenario obtained as described in Figure A-2. The obtained distributions are given in Table A-5.

Table A-5. Wood mass loss probability distributions for Pinellas Park, FL, during the period 2015-2065

| year | No climate change | | RCP 2.6 | | RCP4.5 | | RCP 6.0 | | RCP 8.5 | |
|---|---|---|---|---|---|---|---|---|---|---|
| | $\mu_{ML}$ | $\sigma_{ML}$ | $\mu_{ML}$ | $\sigma_{ML}$ | $\mu_{ML}$ | $\sigma_{ML}$ | $\mu_{ML}$ | $\sigma_{ML}$ | $\mu_{ML}$ | $\sigma_{ML}$ |
| 2015 | 0.00 | 0.00 | 0.00 | 0.00 | 0.00 | 0.00 | 0.00 | 0.00 | 0.00 | 0.00 |
| 2016 | 0.01 | 0.00 | 0.00 | 0.00 | 0.00 | 0.00 | 0.00 | 0.00 | 0.00 | 0.00 |
| 2017 | 0.04 | 0.00 | 0.10 | 0.01 | 0.08 | 0.01 | 0.09 | 0.01 | 0.10 | 0.01 |
| 2018 | 0.59 | 0.04 | 1.24 | 0.09 | 1.47 | 0.15 | 1.25 | 0.12 | 1.55 | 0.21 |
| 2019 | 2.14 | 0.14 | 3.03 | 0.22 | 3.37 | 0.34 | 3.05 | 0.29 | 3.48 | 0.48 |
| 2020 | 3.83 | 0.25 | 4.87 | 0.35 | 5.27 | 0.53 | 4.88 | 0.46 | 5.39 | 0.75 |
| 2021 | 5.49 | 0.36 | 6.70 | 0.49 | 7.22 | 0.72 | 6.73 | 0.64 | 7.30 | 1.01 |
| 2022 | 7.14 | 0.46 | 8.55 | 0.62 | 9.15 | 0.92 | 8.55 | 0.81 | 9.22 | 1.28 |
| 2023 | 8.83 | 0.57 | 10.42 | 0.75 | 11.07 | 1.11 | 10.37 | 0.98 | 11.16 | 1.55 |
| 2024 | 10.49 | 0.68 | 12.26 | 0.89 | 12.99 | 1.30 | 12.24 | 1.16 | 13.08 | 1.82 |
| 2025 | 12.10 | 0.79 | 14.10 | 1.02 | 14.91 | 1.50 | 14.06 | 1.33 | 15.01 | 2.08 |
| 2026 | 13.72 | 0.89 | 15.94 | 1.15 | 16.82 | 1.69 | 15.89 | 1.50 | 16.93 | 2.35 |

| | | | | | | | | | | |
|---|---|---|---|---|---|---|---|---|---|---|
| 2027 | 15.37 | 1.00 | 17.77 | 1.29 | 18.74 | 1.88 | 17.72 | 1.67 | 18.84 | 2.62 |
| 2028 | 17.07 | 1.11 | 19.63 | 1.42 | 20.65 | 2.07 | 19.52 | 1.84 | 20.78 | 2.89 |
| 2029 | 18.80 | 1.22 | 21.45 | 1.55 | 22.57 | 2.26 | 21.35 | 2.02 | 22.68 | 3.15 |
| 2030 | 20.44 | 1.33 | 23.28 | 1.69 | 24.45 | 2.45 | 23.19 | 2.19 | 24.59 | 3.42 |
| 2031 | 22.11 | 1.44 | 25.11 | 1.82 | 26.38 | 2.65 | 25.00 | 2.36 | 26.51 | 3.68 |
| 2032 | 23.74 | 1.54 | 26.87 | 1.95 | 28.27 | 2.84 | 26.81 | 2.53 | 28.45 | 3.95 |
| 2033 | 25.46 | 1.65 | 28.69 | 2.08 | 30.17 | 3.03 | 28.64 | 2.71 | 30.37 | 4.22 |
| 2034 | 27.17 | 1.76 | 30.52 | 2.21 | 32.06 | 3.22 | 30.49 | 2.88 | 32.27 | 4.48 |
| 2035 | 28.76 | 1.87 | 32.35 | 2.34 | 33.95 | 3.41 | 32.31 | 3.05 | 34.17 | 4.75 |
| 2036 | 30.43 | 1.98 | 34.14 | 2.47 | 35.82 | 3.59 | 34.14 | 3.23 | 36.07 | 5.01 |
| 2037 | 32.10 | 2.08 | 35.98 | 2.61 | 37.71 | 3.78 | 35.96 | 3.40 | 38.01 | 5.28 |
| 2038 | 33.82 | 2.20 | 37.79 | 2.74 | 39.58 | 3.97 | 37.81 | 3.57 | 39.93 | 5.55 |
| 2039 | 35.51 | 2.30 | 39.61 | 2.87 | 41.46 | 4.16 | 39.65 | 3.75 | 41.84 | 5.81 |
| 2040 | 37.21 | 2.42 | 41.42 | 3.00 | 43.35 | 4.35 | 41.52 | 3.92 | 43.74 | 6.08 |
| 2041 | 38.87 | 2.52 | 43.21 | 3.13 | 45.24 | 4.54 | 43.34 | 4.09 | 45.64 | 6.34 |
| 2042 | 40.62 | 2.64 | 44.98 | 3.26 | 47.09 | 4.73 | 45.20 | 4.27 | 47.53 | 6.60 |
| 2043 | 42.24 | 2.74 | 46.81 | 3.39 | 48.95 | 4.91 | 47.04 | 4.44 | 49.43 | 6.87 |
| 2044 | 43.88 | 2.85 | 48.62 | 3.52 | 50.81 | 5.10 | 48.86 | 4.62 | 51.30 | 7.13 |
| 2045 | 45.48 | 2.95 | 50.44 | 3.65 | 52.67 | 5.29 | 50.67 | 4.79 | 53.21 | 7.39 |
| 2046 | 47.16 | 3.06 | 52.26 | 3.79 | 54.54 | 5.47 | 52.49 | 4.96 | 55.12 | 7.66 |
| 2047 | 48.83 | 3.17 | 54.06 | 3.92 | 56.45 | 5.67 | 54.31 | 5.13 | 57.00 | 7.92 |
| 2048 | 50.54 | 3.28 | 55.88 | 4.05 | 58.32 | 5.85 | 56.13 | 5.30 | 58.88 | 8.18 |
| 2049 | 52.22 | 3.39 | 57.69 | 4.18 | 60.18 | 6.04 | 57.95 | 5.47 | 60.79 | 8.44 |
| 2050 | 53.91 | 3.50 | 59.50 | 4.31 | 62.03 | 6.23 | 59.75 | 5.64 | 62.67 | 8.71 |
| 2051 | 55.57 | 3.61 | 61.30 | 4.44 | 63.89 | 6.41 | 61.59 | 5.82 | 64.51 | 8.96 |
| 2052 | 57.23 | 3.72 | 63.09 | 4.57 | 65.71 | 6.59 | 63.38 | 5.99 | 66.39 | 9.22 |
| 2053 | 58.90 | 3.82 | 64.90 | 4.70 | 67.55 | 6.78 | 65.19 | 6.16 | 68.28 | 9.48 |
| 2054 | 60.58 | 3.93 | 66.68 | 4.83 | 69.40 | 6.97 | 67.02 | 6.33 | 70.12 | 9.74 |
| 2055 | 62.23 | 4.04 | 68.45 | 4.96 | 71.26 | 7.15 | 68.82 | 6.50 | 71.98 | 10.00 |
| 2056 | 63.92 | 4.15 | 70.23 | 5.09 | 73.13 | 7.34 | 70.64 | 6.67 | 73.86 | 10.26 |
| 2057 | 65.58 | 4.26 | 72.01 | 5.22 | 74.94 | 7.52 | 72.47 | 6.85 | 75.69 | 10.51 |

| | | | | | | | | | | |
|---|---|---|---|---|---|---|---|---|---|---|
| 2058 | 67.20 | 4.36 | 73.83 | 5.35 | 76.75 | 7.70 | 74.28 | 7.02 | 77.55 | 10.77 |
| 2059 | 68.86 | 4.47 | 75.61 | 5.48 | 78.57 | 7.89 | 76.07 | 7.19 | 79.41 | 11.03 |
| 2060 | 70.48 | 4.58 | 77.41 | 5.61 | 80.40 | 8.07 | 77.88 | 7.36 | 81.31 | 11.30 |
| 2061 | 72.08 | 4.68 | 79.20 | 5.74 | 82.20 | 8.25 | 79.68 | 7.53 | 83.19 | 11.56 |
| 2062 | 73.77 | 4.79 | 80.98 | 5.87 | 84.00 | 8.43 | 81.49 | 7.70 | 85.06 | 11.82 |
| 2063 | 75.49 | 4.90 | 82.75 | 6.00 | 85.82 | 8.61 | 83.30 | 7.87 | 86.92 | 12.07 |
| 2064 | 77.13 | 5.01 | 84.53 | 6.12 | 87.59 | 8.79 | 85.09 | 8.04 | 88.76 | 12.33 |
| 2065 | 78.81 | 5.12 | 86.27 | 6.25 | 89.34 | 8.97 | 86.89 | 8.21 | 90.60 | 12.59 |

where $\mu_{ML}$ and $\sigma_{ML}$ is the mean and standard deviation of the mass loss.

In order to account for the fact wood loss mass is an irreversible phenomenon, the probability distributions of wood loss mass for a given sample are conditional to the value of wood loss mass simulated in previous years, so that the wood loss mass for any given sample is a non-decreasing random process, unless a damaged component is substituted with a new one, for which the wood loss mass process is restarted.